EBF3GLWingOpt: A Framework for Multidisciplinary Design Optimization of Wings Using *SpaRibs*

Qiang Liu

Dissertation submitted to the Faculty of the
Virginia Polytechnic Institute and State University
in fulfillment of the requirements for the degree of

Doctor of Philosophy
in
Engineering Mechanics

Rakesh K. Kapania (Committee Chair)
Scott W. Case
Mark S. Cramer
Muhammad R. Hajj
Mayuresh J. Patil

June 05, 2014
Blacksburg, Virginia

Keywords: Structural Optimization, Global-local Optimization, Wing Optimization, Multidisciplinary Design Optimization, SpaRibs, Stiffened Panel Optimization

EBF3GLWingOpt: A Framework for Multidisciplinary Design Optimization of Wings Using *SpaRibs*

Qiang Liu

ABSTRACT

A global/local framework for multidisciplinary optimization of generalized aircraft wing structure has been developed. The concept of curvilinear stiffening members (spars, ribs and stiffeners) has been applied in the optimization of a wing structure. A global wing optimization framework ***EBF3WingOpt***, which integrates the static aeroelastic, flutter and buckling analysis, has been implemented for exploiting the optimal design at the wing level. The wing internal structure is optimized using curvilinear spars and ribs (*SpaRibs*). A two-step optimization approach, which consists of topology optimization with shape design variables and size optimization with thickness design variables, is implemented in ***EBF3WingOpt***. A local panel optimization framework ***EBF3PanelOpt***, which includes stress and buckling evaluation criteria, is performed to optimize the local panels bordered by spars and ribs for further structural weight saving. The local panel models are extracted from the global wing finite element model. The boundary conditions are defined on the edges of local panels using the displacement fields obtained from the global model analysis. The local panels are optimized to satisfy the stress and buckling constraints. Stiffened panel with curvilinear stiffeners is implemented in the

EBF3PanelOpt to improve the buckling resistance of the local panels. The optimization of stiffened panels has been studied and integrated in the local panel optimization. The global wing optimization ***EBF3WingOpt*** has been applied for the optimization of the wing structure of the Boeing N+2 supersonic transport wing and NASA common research model (CRM). The optimization results have shown the advantage of curvilinear spars and ribs concept. The local panel optimization ***EBF3PanelOpt*** is performed for the NASA CRM wing. The global-local optimization framework ***EBF3GLWingOpt***, which incorporates global wing optimization module ***EBF3WingOpt*** and local panel optimization module ***EBF3PanelOpt***, is developed using MATLAB and Python programming to integrate several commercial software: MSC.PATRAN for pre and post processing, MSC.NASTRAN for finite element analysis. An approximate optimization method is developed for the stiffened panel optimization so as to reduce the computational cost. The integrated global-local optimization approach has been applied to subsonic NASA common research model (CRM) wing which proves the methodology's application scaling with medium fidelity FEM analysis. Both the global wing design variables and local panel design variables are optimized to minimize the wing weight at an acceptable computational cost.

Dedication

This dissertation is dedicated to my beloved family

for their endless love, invaluable guidance, relentless support and encouragement.

Acknowledgements

I am grateful to all people who encouraged me and supported me throughout my life. I have a number of individuals to thank for helping me to pursue my dream and

I would like to express my deepest gratitude to my supervisor, Professor Rakesh K. Kapania, for his encouragement, patient guidance and support throughout my PhD research. Without him, I would not have the opportunity of working with some of the greatest experts in aerospace sciences. He was a true mentor and guided me along the path toward my doctorate. I cannot thank him enough for all he taught me.

I would like to thank my dissertation committee members, Dr. Scott Case, Dr. Mark Cramer, Dr. Muhammad R. Hajj, Dr. Mayuresh Patil, for their precious time, sharing their knowledge and experience with me.

I would like to thank Karen M. Brown Taminger of NASA Langley Research Center, as the technical monitor of the project funded under NASA's Fundamental Subsonic Aeronautics Program through a subcontract from the National Institute of Aerospace, Hampton, Virginia. I would like to thank Carol D. Wieseman, Bret K. Stanford, James B. Moore, and Christine V. Jutte of NASA Langley Research Center for substantial technical discussions and inputs. The

original research on the *SpaRibs* concept was funded under the NASA's Fundamental Aeronautics Program for Supersonic Aircraft with Marcia Domack as the project monitor.

I would like to express my sincere thanks to Dr. Sameer B. Mulani. Discussing technical matters with him is always a pleasure and an enriching experience. I would like to thank other members in our research group, Dr. Davide Locatelli, Wei Zhao, Mohamed Jrad, and Shuvodeep De, for their valuable help throughout my studies.

I would like to thank all my friends at Virginia Tech. My life in Blacksburg would not have been so wonderful and memorable without them.

Contents

List of Figures

List of Tables

Nomenclature

MDO	Multidisciplinary Design Optimization
PSO	Particle Swarm Optimization
GBO	Gradient Based Optimization
GA	Genetic Algorithm
σ_{cr}	Critical Buckling Stress
x	Design Variables
$KS_{\sigma}(\sigma)$	Kreisselmeier-Steinhauser Stress Coefficient
ρ	Kreisselmeier-Steinhauser Parameter
σ_y	Yield Stress
σ_{vmi}	i^{th} Finite Element von Mises Stress
A_i	i^{th} Finite Element Area
BF	Buckling Factor
SF	Safety Factor
u_z	Vertical Displacement
t_{opt}	Local Panel Optimized Thickness
λ_p	Fundamental Buckling Eigenvalue
OML	Outer Mold Line
Q_{cr}	Critical Flutter Dynamic Pressure

Q_{fl}	Flight Condition Dynamic Pressure
$F_{subsonic}$	Subsonic Flutter Constraint Coefficient
$F_{supersonic}$	Supersonic Flutter Constraint Coefficient
t_{skin}	Skin Panel Thickness
b_{skin}	Spacing between Two Adjacent Stiffeners
DV	Design Variables

Chapter 1

Introduction

1.1 Background

Multidisciplinary Design Optimization (MDO) has been used in a number of fields, particularly in the aircraft design process. Because of the emergence of innovative aircraft design concepts, the aircraft design process using the empirical structural and aerodynamic equations based on databases obtained from past experience may not be reliable or efficient for a non-conventional aircraft structure design. The aircraft design needs to consider different disciplines, such as the aerodynamics, structural analysis, propulsion, control and dynamics, and the manufacturing and operating costs. The design of aircraft wing structure consists of the internal structural layout, the size of the structural components, the aerodynamic loads and the aeroelastic response of the structure. In particular, the study of the interaction between the structure and the aerodynamics is critical for designing transport aircraft and must be considered in an optimization framework that aims to devise more efficient wing structures.

In the multidisciplinary design, there are many conflicting objectives that need to be considered. Reducing the weight is often one of the most important objectives in aircraft structural optimization, while various additional constraints should be imposed on the aircraft. Therefore, design engineers need to take into account multidisciplinary constraints using appropriate fidelity during the conceptual and preliminary design stages and they need optimization tools to accomplish this complex task.

A MDO problem is usually decomposed into multiple sub-systems so as to reduce the complexity and computational cost of the optimization process. In the optimization problem of an aircraft wing with local panels bordered by spars and ribs, the design variables can be divided into two groups: global wing design variables which define the topology of wing internal structure; local panel design variables which define the details of local panel models, like the panel thickness and stiffeners. Therefore, the wing variables and local panel variables can be optimized in global wing optimization and local panel optimization, respectively. Based on this idea, a global-local optimization framework is developed for the transport aircraft wing design to integrate the wing and panel optimization.

One of the most important challenges of the global-local optimization is the high computational cost due to multidisciplinary analyses of the complex wing structure. In the previous research about the global-local optimization of aircraft wing, the local panels are usually modeled as un-stiffened panels, or using surrogate models to substitute the stiffened panels to save computational cost. This research represents the first time a global-local optimization framework is implemented with medium fidelity tools for the aircraft wing with stiffened panels.

Another important aspect of this research is the application of the new concept of curvilinear stiffening members to improve the efficiency of the structure load bearing mechanism and to

enlarge the design space. In this research, the use of curvilinear spars and ribs (*SpaRibs*), and stiffened panel with curvilinear stiffeners have been integrated in the global-local optimization framework.

In the MDO study, a general optimization tool needs to be developed, not only designed for a particular aircraft wing, but also can be applied for other wing designs. Therefore, the geometry parameterization of the wing structure is very important for the MDO research.

This dissertation is structured as follows: firstly, the literature review about previous work which is closely related to this research is presented. The details about multidisciplinary analyses, geometry parameterization of wing stiffening members, and the global-local multidisciplinary optimization framework are described in Chapter 2. In Chapter 3, the global wing optimization has been applied to two aircraft wing structures: the Boeing high speed commercial transport aircraft concept (Boeing HSCT) and a public-domain NASA wing structure, commonly referred to as the Common Research Model (CRM Wing). Chapter 4 discusses the local panel optimization and presents the application on the NASA CRM wing with un-stiffened panels. The stiffened panel optimization and the application of integrated global-local optimization are discussed in Chapter 5. Finally, Chapter 6 concludes the current research and discusses the future work.

1.2 Literature Review

1.2.1 Multidisciplinary Design Optimization

The aim of a multidisciplinary design optimization (MDO) study is to find an efficient approach to incorporate all relevant disciplines and analytical tools simultaneously in a single optimization problem.

The study of MDO originates in structural optimization, which can be traced back to Schmit's innovative paper published in 1960 [1]. In his work [1-3], the numerical optimization technique was coupled with finite element analysis, in order to search the optimum design in an efficient way. Motivated by the success of structural optimization, the MDO approach has been widely applied in the aircraft structural design since the 1970s thanks to the improvement of the computer technology. Haftka [4-6], Sobieszczanski-Sobieski [7] and their collaborators studied the optimization of aircraft wing including the interaction of multiple disciplines, such as strength, aeroelasticity, and buckling.

In the mathematical view, MDO problem is a constrained nonlinear programming problem to maximize or minimize a particular objective function, subject to the constraints for multiple disciplines. According to the number of objectives, the aircraft design optimization problem can be classified into single objective problems and multi-objective problems. For the single objective problem, the most common objective, in structural optimization, is minimizing the structural weight. Multi-objective optimization which involves two or more objectives can be solved by calculating a set of Pareto optimal solutions [8-10]. In the multidisciplinary optimization, penalty method is widely used to describe the values of multiple constraints [11].

One of the major challenges in MDO study is how to manage the coupling of the multiple disciplines in the constraints. In most MDO problems, the discipline analyses are mutually

interdependent. The results of one analysis may depend on the output of other analyses. The interdisciplinary coupling in the MDO increases the complexity of the problem. A large number of design variables are required for all disciplines in the MDO, which cause more computational and organizational challenges. Because of the interaction of different disciplines, MDOs typically cost much more than the sum of costs of the sequential single discipline optimizations [12]. For the complex MDO problem, it is a very important to find a proper procedure to organize the optimization and reduce the computational cost. Rabeau [13] classified the MDO methodologies into hierarchical decomposition or non-hierarchical decomposition:

(1) Hierarchical decomposition: complex optimization problem is decomposed into multilevel sub-systems. For instance, the aircraft structure is divided into wingbox, fuselage, control surfaces, tail and engine in the first level. Then in the second level, the wingbox can be divided into top skin, bottom skin, spars and ribs. The wing skins can be decomposed into a number of panels in the third level. A complex system can be optimized using a combination of basic sub-systems through the multilevel decomposition.

(2) Non-hierarchical decomposition: all the sub-systems are in the same level, in other words there is no reason to optimize one sub-system before another.

In a recent review, Martines [14] classified all the MDO procedures into two types: monolithic architecture and distributed architecture. The monolithic architecture means that the researchers solved the MDO problem as a single optimization problem. Distributed architectures can be implemented by decomposing the structure or design variables into multiple sub-systems, then optimizing the sub-systems subject to local constraints.

In the monolithic architectures, a widely used MDO procedure is the All-at-Once optimization [12, 14], which means the optimization is considered as an integrated system, all design variables

and all constraints of various disciplines are included in one single optimization process. The All-At-Once optimization procedure is easier to understand and implement. However, for the problems with complex mathematical model and interaction between multiple disciplines, this method may be inefficient because it requires too many design variables and constraints to describe the whole problem. For the optimization problems with a large number of design variables or constraints, the optimization process can be improved using a sequential multiple-step optimization approach [15, 16]. Only a part of design variables or constraints are included in each step of the optimization process. Locatelli *et al.* [15] implemented a two-step optimization for a supersonic wing structure, in which all the design variables are classified as shape design variables or size design variables. The first step optimization focuses on optimizing the shape design variables. The second step optimization is based on the results of the first step optimization, to refine the size design variables.

In the distributed MDO architectures, the complex optimization problem of engineering system is decomposed into multiple smaller tasks to improve the overall optimization efficiency. Numerous decomposition strategies have been proposed to reduce the complexity and computational cost of MDO. Kroo and his collaborators studied collaborative optimization [24, 25]. Collaborative optimization is designed to allow each discipline to solve its sub-system problem in parallel with the others. Sobieszczanski-Sobieski *et al.* [17, 18] divided the optimization problem into two sub-levels: system level and subsystem level. The design variables of the entire structure are optimized in the system level optimization. The subsystem design variables and constraints are evaluated in the subsystem level optimization. The smaller subsystems can be executed simultaneously and are compatible with parallel computing using multiprocessors. For some MDO problems with a complex structure, the global structure is

usually decomposed into smaller local structures. This kind of decomposition scheme is also named as global/local design optimization. Some authors have applied the global/local design optimization in the aircraft wing design [19-21]. Ciampa and Nagel [20] studied the global/local optimization for a cantilever wing. In their research, a global level optimization which includes both shape and size design variables of the wing structure was performed. Then the global optimal design was decomposed into many local panels. The thicknesses of local panels were refined in local panel optimization by optimizing the stiffened local panels to minimize the structural mass. Considering that the optimal results of local optimization need to be fed back to the global model for updating the properties of local models, the global wing optimization and local panel optimization need to be integrated into an iterative global-local optimization framework [20, 21].

The interaction between sub-systems increases the complexity of MDO problems. If the design variables of one sub-system are not independent to the design variables of other sub-systems, or the output responses of one sub-system are needed for several other sub-systems as input variables, the optimization problem will become more difficult to solve. The quasi-separable decomposition, as discussed by Haftka *et al.* [22], means the subsystem consists of local design variables and global system variables, but no variables from other subsystems. The idea of solving this kind of problem is to give each subsystem a local model, and then ask each subsystem to independently search the optimum in the constraint margins. Gürdal *et al*. [23] studied the multidisciplinary design optimization of a composite wing considering strength, buckling, aerodynamic twist and aileron effectiveness constraints. In their finite element model, each wing panel bordered by the stringers and ribs was represented using one element. The

thicknesses of the wing panels were independent in the global-local optimization therefore they can be optimized simultaneously.

1.2.2 Optimization Algorithm

Optimization methods play a major role in solving the MDO problems by searching through the design space to minimize or maximize the objection function. For the complex optimization problem with a large number of design variables, a considerably high-dimensional design space is required, which creates an exponential challenge for optimization.

The optimization algorithms essentially can be classified into two groups: gradient-based methods and non-gradient-based methods. The origins of gradient methods are nearly as old as calculus, dating back to Isaac Newton, Leonhard Euler, Daniel Bernoulli, and Joseph Louis Lagrange. The gradient-based methods determine the optimal design using the gradient information from a first-order design sensitivity analysis. The recursive formulas of gradient-based methods are derived based on the Karush–Kuhn–Tucker (KKT) necessary conditions for an optimal design [26]. Sequential quadratic programming (SQP) was developed for nonlinear gradient optimization. SQP methods are used for the problems where the objective function and the constraints are twice continuously differentiable. Approximation concepts were constructed by Fleury and Schmit [27]. In combination with other techniques, such as constraint deletion, reciprocal approximation and design variable linking, they have been successfully applied in structural optimization. Canfield [28] developed a Rayleigh Quotient approximation to improve the accuracy of eigenvalue approximations. The gradient-based methods normally find the optimal point close to the starting design point, in other words it is possible to get a local optimum but not the global optimum.

The non-gradient methods do not need gradient information at the design points. These methods include nature-inspired evolutionary methods and the related swarm algorithm, such as, genetic algorithm (GA) [29], particle swarm optimization (PSO) [30, 31], that have recently demonstrated their success as well as popularity in MDO applications. Both the GA [32] and PSO [33] methods have been extensively applied in transport aircraft wing optimization. Those methods are successful applications with the philosophy of bounded rationality and decentralized decision making for exploiting the optimal design in the global design space.

The Genetic Algorithms (GA) have become one of the most employed solution methods in engineering problems since they can handle integer, binary, discrete and continuous variables and is effective with nonlinear functions and non-convex design spaces. The method is based on Darwin's theory of natural adaptation and biological evolution, which is translated into algorithmic terms through the computational operators of selection, crossover and mutation. Marin *et al.* [34] developed a two-step optimization framework using neural networks and genetic algorithms for a composite stiffened panel, showing a reduction of the computational cost of about 90% with suitable accuracy. Zingg *et al.* [35] compared the efficiency of genetic algorithm and gradient based methods in aerodynamic shape optimization. In their conclusion, the genetic algorithm is more suited to preliminary design where low-fidelity models are used. However, the gradient based methods are more appropriate for detailed design where high-fidelity models and tight convergence tolerances are needed.

A number of advantages with respect to other evolutionary algorithms are attributed to PSO making it a prospective candidate for optimum structural design. The PSO-based algorithm is robust and well suited to handle nonlinear, non-convex design spaces with discontinuities, exhibiting fast convergence characteristics. Nevertheless, those algorithms cannot fully satisfy

the MDO problem need for the complex and computationally expensive problems so that some minor/major modifications are demanded depending on the nature of difficulty. Hybrid algorithms can integrate the advantages of the PSO and gradient methods. Plevris *et al.* [36] present an enhanced PSO algorithm combined with a gradient-based sequential quadratic programming (SQP) method for solving structural optimization problems. The modified PSO incorporates the exploiting the whole design space and searching the neighborhood of the global optimum. Then the mathematical optimizer, starting from the best estimate of the PSO and using gradient information, accelerates convergence toward the global optimum. Hajikolaeil *et al.* [37] introduced a self-accelerated PSO method to improve the velocity updating process. The idea is to build a metamodel from all previous particles from the beginning of the optimization process until the current step. Then, the algorithm updates new velocities using the parameters obtained from the metamodel.

A focus of current research on optimization methods is to improve the quality of approximations and reduce the number of iterations and thus the total optimization time and cost. Surrogate models are widely used in the computationally expensive optimizations, such as response surfaces optimization [38], neural networks method, and kriging [39]. It uses computationally cheap hierarchical surrogate models to replace the exact computationally expensive objective functions to reduce the computational cost.

Tradeoff between accuracy and computational cost is an important topic in the study of MDO. Approximation technique that helps to eliminate the computational challenge has been extensively studied, especially for the engineering problems with complex structures. For most complex problems, design variables and response quantities are used to improve the accuracy of the approximate optimization. Response surface method (RSM) was introduced by Box and

Wilson in 1951 [40] to explore the relationships between several explanatory variables and response variables. The main idea of RSM is to implement a sequence of designed experiments with approximated model to obtain an optimal response. As shown in Eq. (1.1), the approximate response quantity y can be evaluated by variables in a k-dimensional design space, and error ε.

$$y = f(x_1, x_2, x_3, \dots x_k) + \varepsilon \tag{1.1}$$

Response surface methods evaluate the responses at selected design points using easy-to-calculate surrogate models. The response values of the design points in the k-dimensional design space can be adequately represented by a polynomial of degree *d*. All the coefficients in the d^{th} degree polynomial can be estimated using the data generated at the design points. Box and Wilson [40] searched the optimum using the second order polynomial curves, which are fitted to the response quantities at design points. For the global/local optimization of aircraft wing structure, previous decomposition schemes focused on the use of response surface approximations, fit to the values of multiple lower level optima, as a way to integrate the various design levels [41].

Reliability-based optimization (RBO) [42] attempts to find the optimum design with allowance of a specific risk and target reliability level which accounts for the various sources of uncertainty. The method integrates the probability of failure in the optimization using approximation concepts.

The study of complex optimization problems is the driving force for the development of massively parallel systems for high performance computing. The parallel computing has been applied in the response surface method [43], kriging [39, 44], and population-based optimization such as PSO and GA [45]. PSO has been effectively implemented on massively parallel processing architectures using Graphics Processing Units (GPU) [46]. The parallel computing

toolbox has been integrated in commercial software such as MATLAB, and optimization software such as VisualDOC and DAKOTA, which can be easily implemented by the users.

1.2.3 Instability of Local Panel

The structural instability of wing skins, which consist of smaller local panels bordered by spars and ribs, is a crucial concern in aircraft structural design. The panel may buckle in a variety of modes depending upon its loading, boundary conditions and panel sizes. Lundquist and Stowell [47] studied the buckling of a flat rectangular plate supported along all edges. The critical buckling stress of that plate with compressive loads applied on two opposite edges can be given as following formula

$$\sigma_{CR} = \frac{k\pi^2 E}{12(1-\nu^2)}\left(\frac{t_{plate}}{b_{plate}}\right)^2 \tag{1.2}$$

where k is a constant depends upon the particular shape of the panel being investigated. t_{plate} is the panel thickness, and b_{plate} is the length of the panel edge that is perpendicular to the compressive loads.

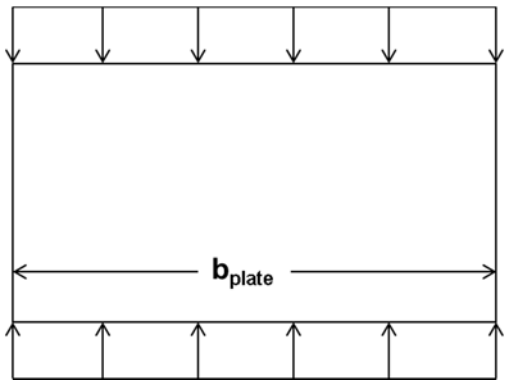

Figure 1.1: Buckling Analysis of Flat Plate

An effective method to improve the buckling performance of plates is to place stiffeners on the plates, whereby the aim of the stiffeners is to increase the panels overall flexural rigidity and in-plane stiffness and act as structural supports and panel breakers, forcing the panel skin to buckle in the small pockets between those stiffeners. The buckling of stiffened panels has received considerable attention dating back to Timoshenko [48] who studied the instability of isotropic longitudinally and transversely stiffened plates subject to compression, shear and bending. As shown in Figure 1.2, stiffened panels with lightweight configurations have been commonly used in aerospace [49, 50]. A typical configuration of a stiffened panel consists of a plate braced by longitudinal stiffeners to resist the compressive stress.

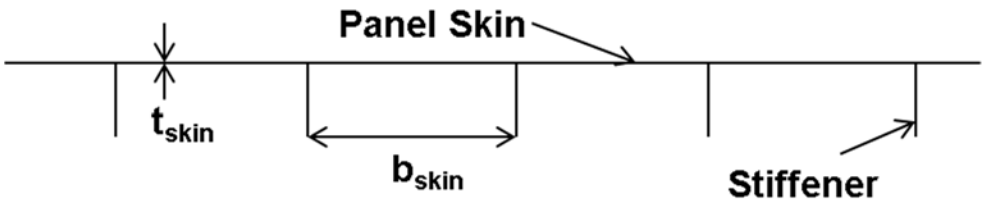

Figure 1.2: Stiffened Panel

The prediction of critical stresses for the stiffened panels with a large number of stiffeners is difficult and relies heavily on energy and semi-empirical methods [51]. Ratzersdorfer [52] studied the buckling of a rectangular plate with simply supported edges, which is reinforced by longitudinal stiffeners at equal spacing and is submitted to the action of uniformly distributed compressive forces.

The critical buckling stress of a thin stiffened panel with evenly distributed stiffeners, and compressive loads applied on the two opposite edges, is given by Eq. 1.3 [53].

$$\sigma_{CR} = \frac{k\pi^2 E}{12(1-\nu^2)}\left(\frac{t_{skin}}{b_{stiff}}\right)^2 \tag{1.3}$$

where k is a constant depends upon the particular shape of the panel being investigated. t_{skin} is the panel thickness, and b_{stiff} is the spacing between two adjacent stiffeners. This analytic solution shows the critical buckling stress is related to the ratio of plate thickness and spacing between stiffeners.

The design optimization of stiffened panel has been exhaustively studied to identify the lightest-weight stiffening configuration subject to stress and buckling constraints. Design variables can be the stiffener spacing, stiffener height and thickness, skin thickness, and stiffening configuration.

The panel stiffened by blade stiffeners was studied by many researchers [54, 55, 56]. Herencia *et al.* studied the optimization of composite panel with T-shape stiffeners [57]. Vitali optimized the stiffener spacing, panel thickness, and thickness of stiffener components of hat stiffeners.

The most common design of stiffened panels is that the panel is stiffened by longitudinal stiffeners [58, 59, 60, 61]. Jaunky *et al.* studied the buckling of grid-stiffened composite panel with both axial and transverse stiffeners [62].

A number of optimization methods have been applied in the optimization of stiffened panel. Gradient based method and particle swarm method are compared in the stiffened panel optimization [63]. Parallel computing is implemented with genetic algorithm [59, 62, 63] or response surface method [60, 64].

In the finite element analysis, as compared to the un-stiffened panels, much smaller size of elements are required for meshing the panel with a large number of stiffeners. In order to avoid the high computational cost, buckling analysis can be approached with two methods: smearing the properties of the stiffener elements over the skin or treating the stiffeners as beam elements with an effective flexural rigidity. Walch *et al.* [65] developed a tool S4WING to efficiently

predict stiffness, spanwise and chordwise mass distribution in a wingbox at conceptual design stages. It uses a physics-based simplification process for a finite element wing box model in which the stiffeners are smeared in the skin to reduce the number of elements of the model.

1.2.4 Curved Stiffening Members

Classic structural design for aircraft wingbox uses simple components such as straight spars and ribs, quadrilateral wing skin panels with straight stiffeners. The components are connected using bolts and rivets or by welding. A new design philosophy, using curvilinear spars and ribs (*SpaRibs*), pioneered by Kapania and his group at VT (Locatelli, Mulani and Kapania [66, 67]), has been introduced based on emerging manufacturing technologies such as Friction Stir Welding(FSW) [68, 69] and Electron Beam Free Form Fabrication (EBF3) [70]. In these innovative technologies, the structure is manufactured as an integrated part instead of using mechanically fastened structural components. Based on the new technology, the concept of curvilinear stiffening members with non-uniform thickness have been implemented in design of wing internal structure ([66, 67, 71]). Compared with the conventional straight spars, ribs and stringers, the advantage of curved stiffening members resides in the coupling between bending and torsional rigidity. That means bending and torsional deformation can be reduced by suitably placing curvilinear *SpaRibs* and stiffeners. The concept of curvilinear stiffening members enlarges the design space and provides possibility for a more efficient aircraft design.

Multidisciplinary optimization of stiffened panel with curvilinear stiffeners is studied [66, 72, 73, 74] with an objective of minimizing the mass of panels and subject to constraints on buckling, von Mises stress, and crippling or local failure of the stiffener.

1.3 Research Objectives

The aim of this research is to develop a multidisciplinary design optimization framework for transport aircraft wing design. Static aeroelastic, flutter and buckling analyses are integrated in the optimization framework, all in an effort to reduce structural weight, when subjected to stress, displacement, flutter and buckling constraints for multiple flight conditions. The optimization framework is integrated by wing optimization ***EBF3WingOpt*** and panel optimization ***EBF3PanelOpt***.

In the ***EBF3WingOpt***, a new design concept curvilinear spars and ribs (*SpaRibs*) has been introduced to take advantage of the structural deformation couplings provided by the curvature and to design more efficient and lighter structures. The use of curvilinear internal structures allows for an enlarged design space which gives the designers more flexibility to tailor the structure according to the stress distribution. In this research, geometry parameterization of *SpaRibs*, aeroelasticity analysis and topology/sizing optimization have been integrated into global wing optimization framework ***EBF3WingOpt***.

The wing skins are divided into local panels by the *SpaRibs*. A framework ***EBF3PanelOpt*** is developed for the optimization of un-stiffened or stiffened panels considering buckling and stress constraints. In this research, a global-local multidisciplinary design optimization procedure has been developed to incorporate ***EBF3WingOpt*** and ***EBF3PanelOpt*** for the optimization of aircraft wing. The commercial software MSC.NASTRAN, which incorporates the static, buckling and aeroelasticity module, is selected as finite element analysis tool. The optimization framework is developed using Python and MATLAB programming to integrate the geometry and mesh generation, finite element analysis and optimization algorithms.

The objectives of this research can be summarized as:

- Developing a multidisciplinary design framework for the optimization of aircraft wing structure which includes the use of curvilinear stiffening members (*SpaRibs*).
- Developing an efficient global wing optimization framework to optimize the size and topology of the wing internal structure.
- Developing a local panel optimization framework for optimizing the un-stiffened or stiffened panels.
- Implementing the integration of global-local multidisciplinary optimization framework using commercially available analysis software as MSC. PATRAN, MSC. NASTRAN.

Chapter 2

Global-Local Optimization Framework

The global-local MDO framework ***EBF3GLWingOpt***, which integrates the global wing optimization module ***EBF3WingOpt*** and local panel optimization module ***EBF3PanelOpt***, is discussed in this chapter. The integration of multidisciplinary analyses, such as static aeroelastic, flutter, and buckling analyses, is introduced in the first section. The second section presents the geometry parameterization of wing structure that consists of curvilinear spars, ribs or stiffeners. Then the optimization procedure of global wing optimization and local panel optimization is described.

2.1 Multidisciplinary Analyses

In this research, the design objective is to minimize structural weight subject to multiple constraints, such as stress, flutter and the buckling constraints. The interaction of aerodynamic loads and the structural deformation of aircraft is the concern of structural analyst in aerospace engineering. The static aeroelastic, flutter and buckling analyses are discussed in this section.

2.1.1 Static Aeroelastic Analysis

In the MDO of aircraft design, the interaction of aerodynamics and structure is one of the most important problems concerned by many researchers. Higher fidelity aerodynamic loads can be obtained using the aerodynamic methods such as Euler, Navier-Stocks CFD. However these high order methods are not suitable in the MDO because the computational cost is too high for the complex optimization problems with large numbers of design variables and constraints. The aerodynamic analysis in most MDO problems is performed by aerodynamic panel method based on potential flow theory [12].

In the aeroelasticity problems, the aerodynamic loads are related to the outer shape and the internal build-up of the wing structure, the airspeed and the air density. Meanwhile, the aerodynamic load causes structural deformation and stress redistribution which leads to the interaction of aerodynamic forces and structural deformation on a flexible aircraft. In this research, the flight loads and the structural deformation calculation is performed by integrating MSC.NASTRAN solution sequence SOL144 and by retrieving the aerodynamic loads data to use for the structural analysis. The equation for static aeroelastic analysis is given as follows:

$$[K_{aa} - q_d Q_{aa}]\{u_a\} + [M_{aa}]\{\ddot{u}_a\} = q_d[Q_{ax}]\{u_x\} \tag{2.1}$$

where K_{aa} and M_{aa} are structural stiffness matrix and structural mass matrix, respectively. u_a is the vector of structural displacements. u_x is the vector of displacements of aerodynamic extra points, such as aerodynamic control surface deflections and rigid body motions. q_d is dynamic pressure. Q_{aa} is aerodynamic influence coefficient matrix, which is used to calculate the aerodynamic forces due to structural deformation. Q_{ax} is the aerodynamic matrix due to the deflections of aerodynamic extra points.

MSC.NASTRAN provides the Doublet Lattice Method (DLM) [75, 76] and ZONA51 [77] method for the computation of the aerodynamic loads at subsonic and supersonic regimes, respectively. Both methods are based on the linearized aerodynamic potential theory, which neglects both the thickness of the wingbox and the viscous effects. The two methods are panel methods which represent lifting surfaces by flat panels. In the MSC.NASTRAN aerodynamic analysis, the aero elements are boxes in regular arrays with sides that are parallel to the airflow. The deflection of the wing structure is the combination of rigid body motions and the flexible structural deformation of the wing with the applied aerodynamic loading.

The aerodynamic grid points for DLM are located at the centers of the aerodynamic boxes. The flat plate aerodynamic methods solve for the pressures at a discrete set of point contained within these boxes. Doublets are assumed to be concentrated uniformly across the one quarter chord line of each box. The control point in each box is located on the three-quarter chord line of the box. The doublet magnitudes are determined so as to satisfy the surface normal-wash boundary condition at all of these control points. As in the DLM, the interfering lifting panels are divided into small trapezoidal lifting boxes which are arranged in strips parallel to the free flow with box edges. There is one control point in each box, centered spanwise on the 95 percent chord line of the box.

Aeroelasticity problems are solved by studying the interconnection of the structure with aerodynamics. There are two transformations: the relationship between the structural deformation and the aerodynamic deformation and the interpolation from aerodynamic loads to the structural loads acting on the structural grid nodes. A group of spline nodes is defined for each aerodynamic panel. The splining methods lead to an interpolation matrix [G_{kg}] for determining the relationship between structural grid nodes deflections $\{u_a\}$ and aerodynamic grid nodes deflections $\{u_k\}$.

$$\{u_k\} = [G_{ka}]\{u_a\} \tag{2.2}$$

The aerodynamic forces $\{F_a\}$ are transferred onto the structure as structurally equivalent forces $\{F_s\}$. That means the two force systems cause a same structural deflection and do a same virtual work.

$$\{\delta u_a\}^T\{F_a\} = \{\delta u_k\}^T\{F_k\} \tag{2.3}$$

Substituting the Eq. (2.2) into Eq. (2.3), the relationship between the aerodynamic forces and structural equivalent forces can be given as following equation:

$$\{F_a\} = [G_{ka}]^T\{F_k\} \tag{2.4}$$

In this research, the aerodynamic grid for the aeroelasticity analysis is automatically generated by global wing optimization package ***EBF3WingOpt***. The structural and the aerodynamic grids are connected by surface splining method, which has been implemented in MSC.NASTRAN. The structural nodes corresponding to the *SpaRibs* caps were selected as spline nodes. Static aeroelastic trim analysis and flight loads computation are performed using MSC.NASTRAN solution SOL144 to determine the structural deformation and stress.

2.1.2 Modal Analysis

The dynamic properties of aircraft structure are studied in modal analysis. The equation of motion in the aeroelastic system is given in Eq. (2.5)

$$[\mathrm{M}]\ddot{X}(t) + [D]\dot{X}(t) + [K]X(t) = F_a(t) \tag{2.5}$$

where [M] is the mass matrix, [D] is structural damping matrix, [K] is the stiffness matrix, X is the vector of physical displacements. $F_a(t)$ is the aerodynamic forces applied on the structure grid points. In the undamped free vibration problem, Eq. (2.5) can be reduced to

$$[\mathrm{M}]\ddot{X}(t) + [K]X(t) = 0 \tag{2.6}$$

The vector of physical displacements X can be represented by a combination of its normal modes

$$X(t) = \sum_i \phi_i \, q_i = [\phi]q \tag{2.7}$$

where $[\phi]$ is the structural modal matrix, q is vector of modal displacements. The generalized mass and stiffness matrices are $\bar{M} = [\phi]^T M[\phi]$, $\bar{K} = [\phi]^T K[\phi]$, respectively.

Equation 2.7 can be rewritten as

$$-\omega^2 \bar{M} + \bar{K} = 0 \tag{2.8}$$

The eigenvalues and eigenvectors can be obtained by solving Eq. (2.8).

2.1.3 Flutter Analysis

Flutter is a dynamic instability phenomenon of an elastic structure in a fluid flow, caused by positive feedback between the body's deflection and the force exerted by the fluid flow. Many engineering structures exposed to aerodynamic forces, such as aircraft wings, wind turbine blades, and bridges, are designed carefully to avoid failure caused by flutter. Flutter analysis is critical for large supersonic transport aircrafts since the flexibility of the structure and the severe load conditions can lead to flutter instability.

Flutter velocity prediction is a process of determining the flutter boundary for a structure that is moving in a fluid when the vibration amplitude starts increasing infinitely. In complex structures where both the aerodynamics and the mechanical properties of the structure are not fully understood, even changing the mass distribution of an aircraft or the stiffness of one structural component can induce flutter in an apparently unrelated aerodynamic component.

In flutter analysis, aerodynamic force $F_a(t)$ can be given by the following formula

$$F_a(t) = q_d G_{ka}^T Q(k, M_\infty) G_{ka} X \tag{2.9}$$

where the reduced frequency k is determined by $k = \omega \bar{c}/2V$. Equation (2.9) can be transferred into the modal coordinate system, as shown in Eq. (2.10)

$$\bar{M}\ddot{q} + \bar{D}\dot{q} + \bar{K}q = q_d Q(k, M_\infty) q \tag{2.10}$$

where $\bar{M}$, $\bar{D}$ and $\bar{K}$ are the modal mass matrix, modal damping matrix and modal stiffness matrix, respectively. q_d is the dynamic pressure of the air flow. q is the modal coordinate vector.

Flutter speed can be computed by solving an eigenvalue equation of modal flutter analysis. In a linear system 'flutter point' is the point at which the structure is undergoing simple harmonic motion - zero net damping - and so any further decrease in net damping will result in a self-growing oscillation and eventual failure. MSC.NASTRAN implements several flutter analysis methods, such as the K-method and the PK-method [78]. The K-method computes eigenvalues and eigenvectors for user specified reduced frequencies. PK-method solves the eigenvalue problem for user specified velocities. The flutter equation of PK-method is given in the following equation:

$$\left[\bar{M}p_c^2 + \left(\bar{D} - \frac{\frac{1}{4}\rho_a c_{ref} V Q_I(k, M_\infty)}{k}\right) p_c + \left(\bar{K} - \frac{1}{2}\rho_a V^2 Q_R(k, M_\infty)\right)\right] q = 0 \tag{2.11}$$

where V is the velocity, M_∞ is the Mach number of free airflow, ρ_a is the density of air. p_c is the eigenvalue, q is the eigenvector. $Q_R(k, M_\infty)$ and $Q_I(k, M_\infty)$ are the real and imaginary parts of aerodynamic matrix $Q(k, M_\infty)$.

In both the PK and K-methods, the flutter velocity can be determined using the velocity-damping (v-g) diagram. Flutter will occur if the damping value becomes positive. The PKNL method is the PK-method without looping on all combinations of density, Mach number, and velocities. Thus only the matched points are analyzed. The PKNL method was selected in MSC.NASTRAN solution sequence SOL 145 to solve the flutter problem in this particular case.

The global wing optimization module ***EBF3WingOpt*** offers two schemes to search the critical flutter points. The first scheme is solving the flutter velocity at a certain altitude and a series of velocities. As shown in Figure 2.1, the flutter velocity is determined by the crossing point of damping curve and velocity axis. The second flutter point searching scheme is finding the flutter dynamic pressure at a certain Mach number and various air densities, in which the flutter dynamic pressure is computed using the velocity and the air density at the matched points. The flutter analysis in subsonic or supersonic regime has been integrated in ***EBF3WingOpt.***

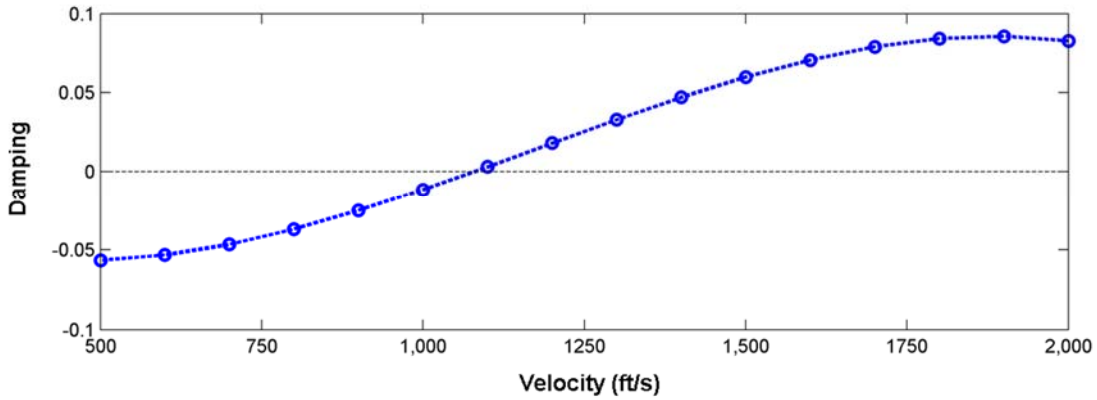

Figure 2.1: Flutter Velocity of Jet Transport Wing

In MSC.NASTRAN solution SOL145 module, flutter analysis is carried out using the unstressed mode shapes and natural frequencies to transform the equations of motion to generalized coordinates. Both the mode shapes and the corresponding natural frequencies of aircraft structure have significant effect on the flutter speed. If there is large structural deformation caused by high structural loads, the changes of natural frequencies and mode shapes cannot be ignored. Therefore the pre-stressed mode shapes and natural frequencies have been introduced in flutter analysis [79]. Both global modes and local modes of aircraft structure are possible to be found through modal analysis. In order to obtain more reliable flutter result, enough number of global modes should be included in flutter analysis.

2.1.4 Buckling Analysis

Buckling behavior is another important problem for this research. The buckling analysis is implemented for a global wing or local panel and is integrated in the global-local multidisciplinary design optimization framework. In global wing buckling analysis, the aerodynamic loads are calculated for the global wing model and applied on the structural grids through splining interpolation.

In the local panel optimization framework ***EBF3PanelOpt***, the buckling analysis is carried out for each local panel. The boundary conditions are defined using the displacements of the global wing grid points and applied on the edges of the local panels. An interpolation program has been developed for transferring the displacements of global coarse structural grid nodes to the local fine grid.

2.2 Geometry Parameterization

The generation of the wing geometry with curvilinear spars and ribs, based on a parametric approach is described in this section. The 3D representation of the aircraft structure, with all its material properties and thicknesses, should be created as a finite element model in a very simple and effective way. Geometry parameterization of all the details of the wingbox structure, such as the shape and size of spars and ribs, has been fundamental in order to implement the structural optimization. The advantage of geometry parameterization can be seen in the fast generation of the finite element model, without having to redesign the structure manually every time after the change of any major layout parameters, like wing skin thickness, sweep angle, number of spars or ribs. In the aircraft optimization, the generation of the parametric model is an automated design process using a set of design variables to specify the topology and size of aircraft structure.

2.2.1 Geometry Parameterization of Curvilinear *SpaRibs*

A new geometry parameterization method for the *SpaRibs* has been introduced by Locatelli *el al.* [71, 80]. This method is called *linked shape method*, since each curve has its unique shape but is not totally independent. This type of parameterization method allows for a unique shape of the *SpaRibs* limiting the number of design variables required in the geometry definition. The curves defining the shape of the *SpaRibs* are placed in the normalized space and subsequently transformed in the physical space as presented in Figure 2.2. Each element of a set is characterized by its own curvature. However, the shapes of the *SpaRibs* belonging to the same set are coupled together.

The shape of each curvilinear spar or rib is parameterized using B-spline method. B-splines are the standard parameterization implemented in MSC.PATRAN. In this research, the B-spline curve is parameterized in third order B-splines, which are second degree piecewise continuous polynomial functions and can be implemented using three points: the start point, end point and control point. More details about B-splines can be found in reference [81].

The details of the *linked shape method* have been discussed in reference [80]. In the *linked shape method* for geometry parameterization, a total of six parameters or design variables are required to describe one set of *SpaRibs* placed in a quadrilateral wing box. As shown in Table 2.1, the first parameter defines the number of *SpaRibs* in that space. Then two parameters are used to define the control point line that includes the control points of all the *SpaRibs*. The other three parameters define the spacing of the start, end and control points. The spacing is computed by partitioning the edges of the normalized square space and the control point line using a geometric progression. The three parameters define the ratio of the first interval to the last interval on the two edges or control point line.

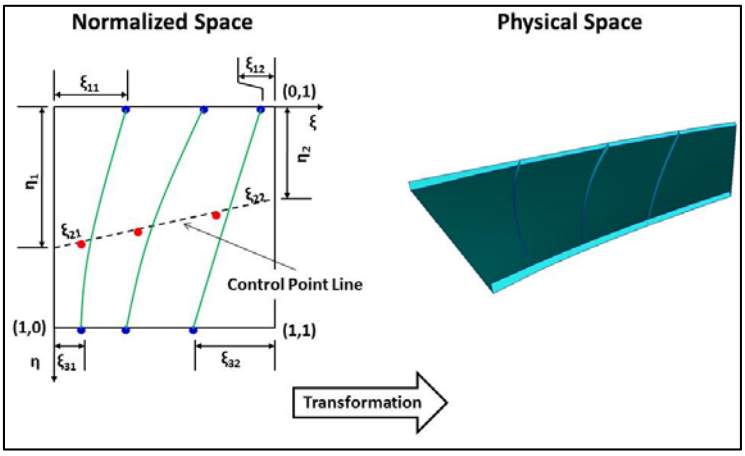

Figure 2.2: Linked Shape Parameterization. (Locatelli *et al*. [80])

Table 2.1: Parameters Description in Linked Shape Method. (Locatelli *et al.* [80])

Parameter	Description
P_1	Number of *SpaRibs*
P_2	η_1
P_3	η_2
P_4	ξ_{11}/ ξ_{12}
P_5	ξ_{21}/ ξ_{22}
P_6	ξ_{31}/ ξ_{32}

The parameterization has been implemented in the ***EBF3WingOpt*** framework using MSC.PATRAN geometry generation routines. An example of internal *SpaRibs* layout automatically generated using MSC.PATRAN session file is presented in Figure 2.3.

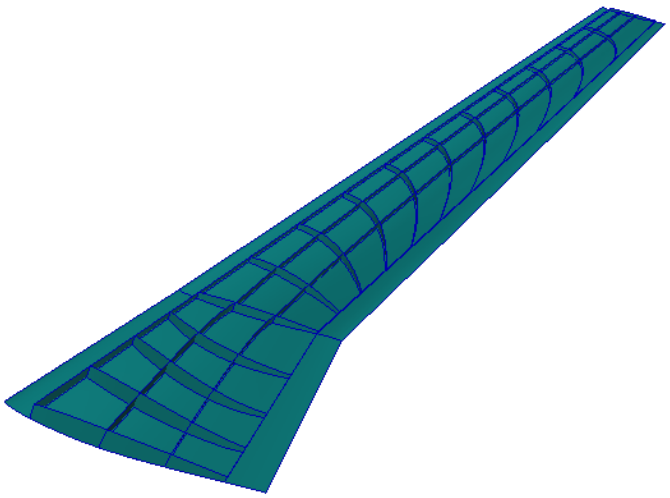

Figure 2.3: Example of NASA CRM Wing with Curvilinear *SpaRibs*

2.2.2 Geometry Parameterization of Curvilinear Stiffeners

In this research, stiffened panels with curvilinear stiffeners are studied to improve the local buckling performance of the structure. As similar as the parameterization of *SpaRibs*, the curves of stiffeners are defined using third order B-splines. The shape of each B-splines curve is determined by three points: starting point, control point and ending point. Since the starting point and ending point are located on two panel edges, only one parameter is required to define each point. The control point which locates inside of the panel is defined using two parameters. Six parameters are needed to define the start, control, end points, height and thickness of one stiffener, as presented in Figure 2.4 and Table 2.2.

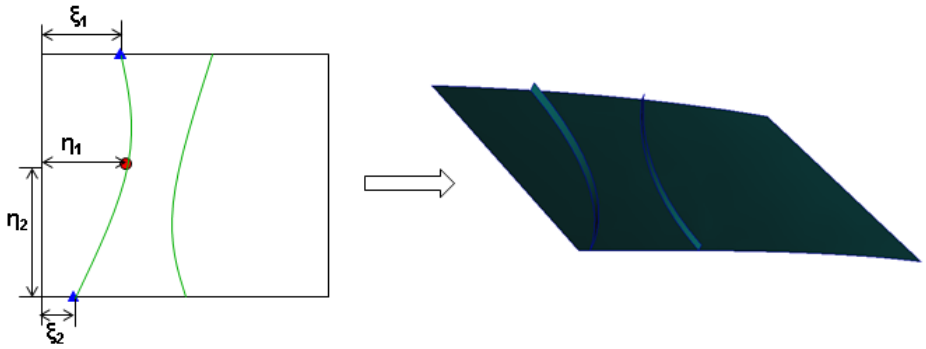

Figure 2.4: Parameterization of Curvilinear Stiffeners.

Table 2.2: Parameters of Curvilinear Stiffeners

Parameter	Description
P_1	Start Point ξ_1
P_2	η_1
P_3	η_2
P_4	End Point ξ_2
P_5	Height of Stiffener
P_6	Thickness of Stiffener

2.3 Global-Local Optimization Framework

The MDO problem of aircraft wing structure can be defined mathematically as minimizing the objective function $f(x)$, which is usually the structural weight, with respect to the design variable vector x under the multidisciplinary constraints $g_i(x)$.

$$\min_x f(x)$$

$$\text{Subject to } g_i(x_1,x_2,\ldots,x_n) \le g_i$$

$$x_{j\_L} \le x_j \le x_{j\_U} \tag{2.12}$$

In Eq. 2.12, x_{j_L} and x_{j_U} are the lower and upper bounds on each of the design variables.

In this research, the objective of multidisciplinary optimization is to minimize the structural weight subjected to constraints from several disciplines. The optimization problem is divided into two coupled sub-systems: global wing optimization and local panel optimization. The global-local multidisciplinary optimization framework, which consists of global wing optimization module ***EBF3WingOpt*** and local panel optimization module ***EBF3PanelOpt***, is presented in Figure 2.5.

2.3.1 Global Wing Optimization

In the global wing optimization, both the topology of *SpaRibs* and the thicknesses of the wing structural panels are optimized considering multidisciplinary constraints such as von Mises stress, maximum displacement, flutter speed and buckling eigenvalue. A two-step optimization approach is developed to reduce the complexity and improve the efficiency of global wing optimization. The design variables are decomposed into two groups: shape variables that determine the shape of *SpaRibs,* size variables that define the thickness of wing components. Considering some shape variables, such as the number of spars or ribs, are not continuous, non-

gradient optimization methods are more suitable for searching the optimal topology design in the global design space. In the first step of the optimization process, both the shape and size design variables are optimized using particle swarm optimization (PSO), to minimize the weight of wing structure. The wing topology design with minimum weight, which is obtained in the first step optimization, is selected as the baseline design for the second step optimization. The second step optimization with fixed wing internal topology design is carried out to optimize only the size design variables. In this stage, gradient based optimization (GBO) method is used to refine the thicknesses of wing skins and *SpaRibs*.

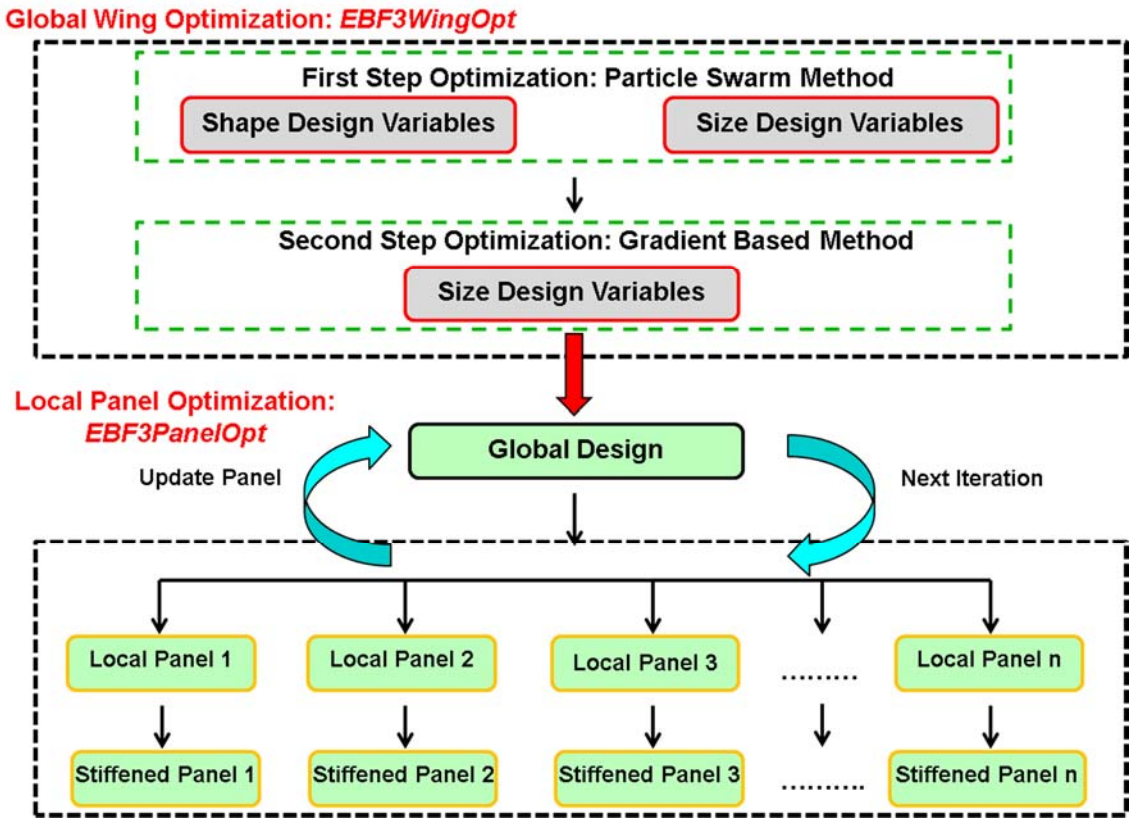

Figure 2.5: Global-Local Optimization Framework

In this research, MSC.PATRAN is utilized to create the geometry and finite element model of the wing structure. The aerodynamic model is created using MSC.FlightLoads. The structural and aerodynamic models are output as input files of MSC.NASTRAN for the aeroelasticity analysis. The particle swarm optimization and gradient base optimization have been implemented using MATLAB. The mentioned software are incorporated in the global optimization framework ***EBF3WingOpt***.

2.3.2 Local Panel Optimization

The goal of local panel optimization is to obtain a more precise structural design with minimum weight by optimizing each panel bordered by spars and ribs, based on the design obtained through global wing optimization. Static and linear buckling analyses are carried out for the local panels using MSC.NASTRAN solution SOL105 that gives the first buckling eigenvalue as well as the von Mises stress distribution in each panel.

Local panel optimization is implemented in ***EBF3PanelOpt***. The flow diagram of local panel optimization is presented in Figure 2.6. The aerodynamic forces applied on the wing structural grid points are computed in static aeroelastic analysis using MSC.NASTRAN solution sequence SOL144. The force fields are applied in the global static and buckling analysis, which generates the displacement fields of the global model. The local panel models are defined by the intersections of wing skins, spars and ribs. The finite element model of local panel and global displacement fields are extracted from the global model. The applied loads in static and buckling analysis of local panel are defined as enforced displacements applied at the edges of each panel. Then static and buckling analyses are performed for the local panels to obtain the stress and buckling results. Local panel design is optimized to satisfy the constraints applied on the first

buckling eigenvalue and the maximum von Mises stress. The global model is updated using the optimized thicknesses of local panels. The new global displacement fields are computed using the updated global model and applied on the local panels as enforced displacements to start the next iteration of local panel optimization.

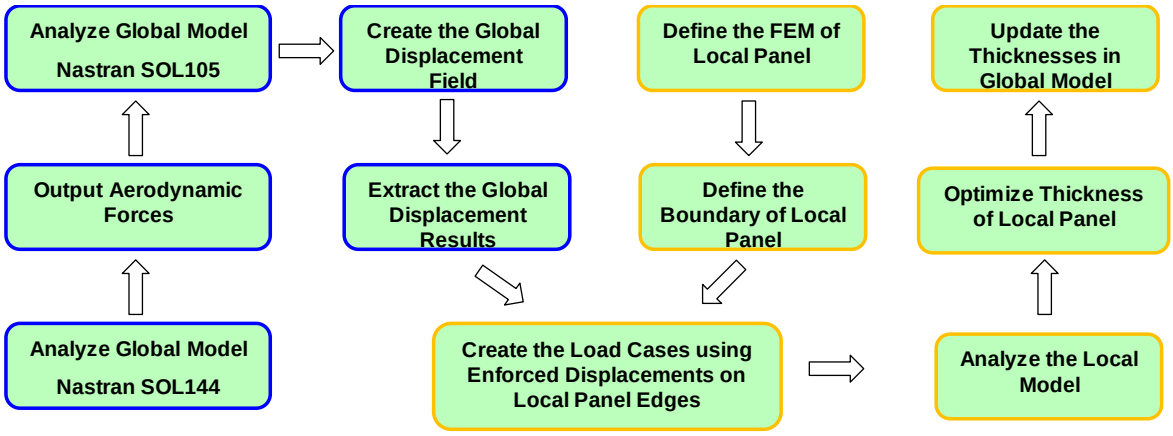

Figure 2.6: Flow Diagram of Local Panel Analysis.

Stiffened panel optimization with straight or curvilinear stiffeners has been integrated to improve the buckling performance of local panels. Since buckling constraint is the critical constraint for many local panels, there is significant potential to save the weight of local panels by adding proper stiffeners. ***EBF3PanelOpt*** generates the geometry of stiffeners and meshes the stiffened panel using a fine grid. The boundary conditions are defined using the displacements on the grid nodes of panel edges. The fine grid of stiffened panel does not match with the grid of global model. In order to solve that problem, a linear interpolation technology has been developed for interpolating the displacements of global structural nodes onto the local panel edges. Static and buckling analyses are included in the stiffened panel analysis. The panel is also optimized to

minimize the panel weight subject to stress and buckling constraints. Shape optimization of stiffeners has been implemented to optimize the curvilinear stiffeners.

2.3.3 Integration of Global Wing and Local Panel Optimization

As shown in Figure 2.5, this global-local optimization procedure is an iterative process. After local panel optimization, the optimized thicknesses of panels are substituted into the global wing model. Then multidisciplinary analysis of the global wing model considering stress, displacement, flutter and buckling constraints is carried out to generate the new displacement results. The new global displacement fields are interpolated onto the edges of local panels as boundary conditions to start the next iteration of the local panel optimization. The details of the integrated global-local optimization procedure will be discussed in Chapter 5.

The global-local optimization framework has been implemented by incorporating ***EBF3WingOpt*** for global wing optimization and ***EBF3PanelOpt*** for local panel optimization. The framework is developed using MATLAB programming to integrate MSC.PATRAN for pre/post processing, MSC.NASTRAN for finite element analysis, and Python code of ***EBF3PanelOpt.***

2.4 Summary

In this chapter, the integration of multidisciplinary analysis and geometry parameterization are discussed for the global wing optimization and local panel optimization. The global wing optimization is implemented in ***EBF3WingOpt***. The local panel optimization procedure ***EBF3PanelOpt*** is also described. The global-local optimization framework has been developed to integrate the optimization software package ***EBF3WingOpt*** and ***EBF3PanelOpt***. Multiple disciplines like static aeroelasticity, buckling, and dynamic flutter are considered in the optimization process. The geometry of curvilinear spars, ribs, and stiffeners are parameterized and constructed automatically by the optimization software package. The optimization framework is not only developed for a particular aircraft wing but also can be easily generalized for the design of other aircraft wings by changing the geometry parameters.

Chapter 3

Global Wing Optimization: *EBF3WingOpt*

In this chapter, the details of the global wing optimization framework ***EBF3WingOpt*** are discussed. The aircraft wing optimization has been applied to a concept supersonic wing Boeing High Speed Commercial Transport aircraft (Boeing HSCT) and subsonic wing NASA Common Research Model (NASA CRM). The advantages of using curvilinear spars and ribs, termed *SpaRibs*, are investigated to design aircraft wing-box in comparison to the use of classic design concepts that employ straight spars and ribs. This optimization scheme performs both the sizing and the shaping of the wing internal structure, connecting the geometry modeling software MSC.PATRAN and finite element analysis software MSC.NASTRAN.

3.1 Optimization of Boeing N+2 HSCT Wing

3.1.1 Boeing N+2 HSCT Wing Description

The Boeing HSCT aircraft is characterized by an 86.1 ft wing span and a fuselage length of about 154 ft; 30 passengers can be transported at a cruise velocity equivalent to Mach 1.6 at an altitude of 50,000 ft for a maximum range of 3200nm. The baseline aircraft layout is presented in Figure 3.1 [82]. The wing, tail and fuselage structures are specified as fabricated from a titanium alloy material, while the secondary structures and control surfaces are fabricated from honeycomb and composite materials. The yield stress of the titanium alloy chosen for the design is 110,000 psi. Titanium alloy physical characteristics widely change depending on the alloy composition and thermal treatments. In particular, the yield stress can vary from about 100,000 psi to over 200,000 psi. In absence of more precise indications, a lower grade alloy has been chosen as reference for the design to avoid contamination of the results due to the "optimistic" estimation of the material properties. In the baseline aircraft design, straight spars and ribs are used for the wing and tail internal structure which is outlined in Figure 3.2.

Figure 3.3 shows the flight envelope of Boeing N+2 HSCT aircraft [83]. The aircraft cruises at a subsonic velocity Mach 0.836 if the altitude is between 20,000 ft and 35,000 ft, or at a supersonic velocity Mach 1.6 if the altitude is above 40,000ft. In this research, two flight conditions are concerned in the optimization: Mach 0.836 at 20,000 ft and Mach 1.6 at 40,000 ft.

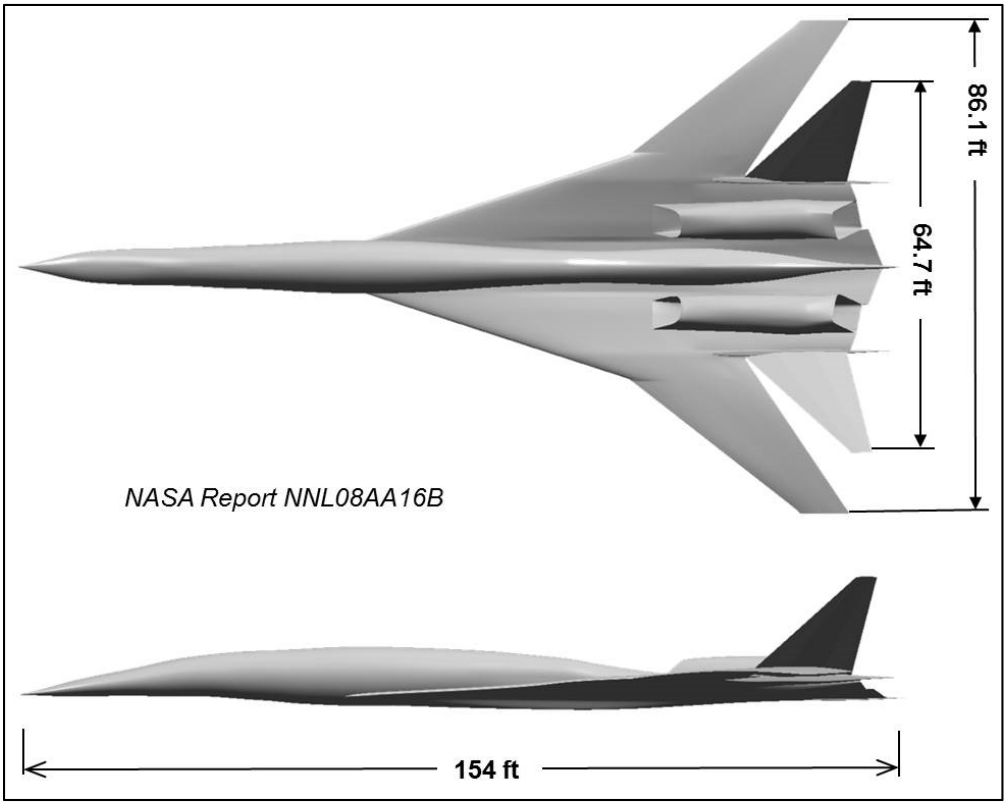

Figure 3.1: Boeing N+2 HSCT Aircraft Concept.

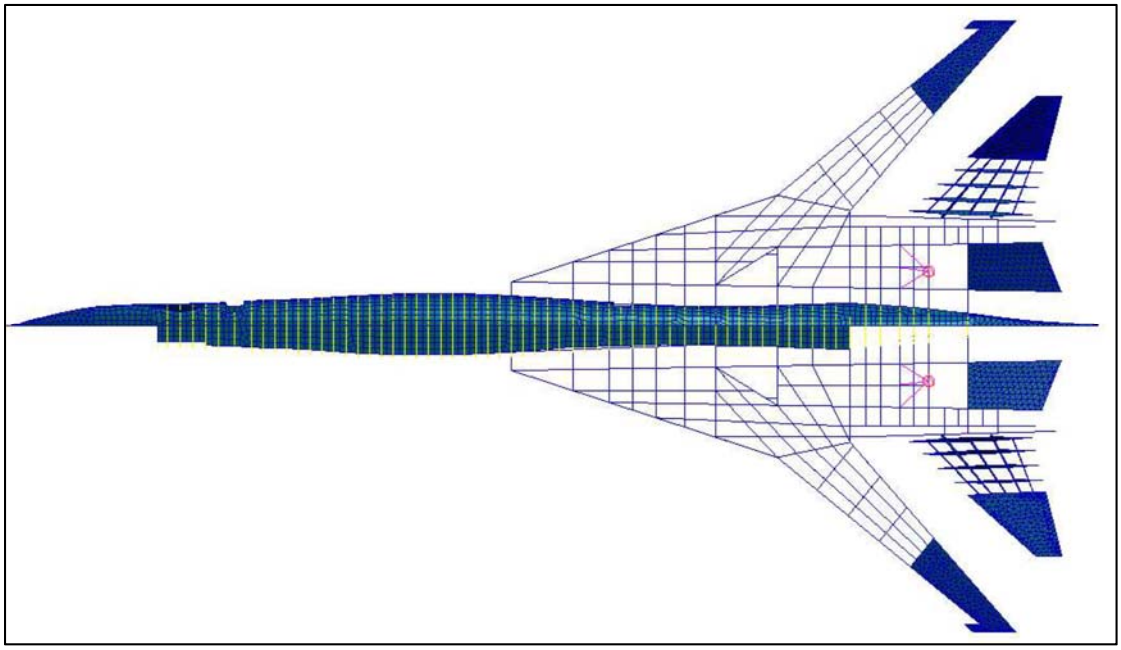

Figure 3.2: Boeing N+2 HSCT Aircraft Structural Configuration. (Chen *et al.* 2010 [83])

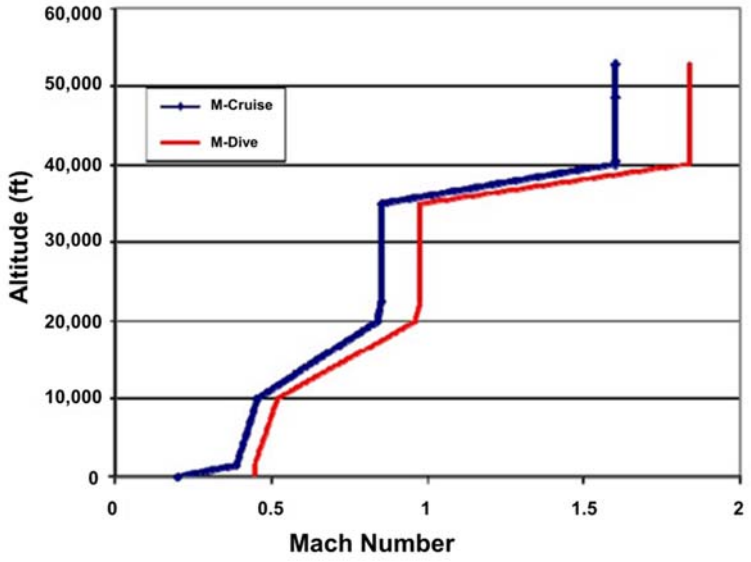

Figure 3.3: Flight Envelop of Boeing HSCT Aircraft Concept. (Chen *et al.* 2010 [83])

3.1.2 Optimization Procedure of Boeing N+2 HSCT Wing

The N+2 supersonic aircraft concept developed by Boeing was optimized using ***EBF3WingOpt*** framework by Virginia Tech unitized structures group. The internal structure layout is replaced by a new layout characterized by curvilinear *SpaRibs*. The optimization of the structural weight was conducted under structural stress and subsonic and supersonic flutter constraints. The optimization includes the re-design of the load bearing structure of the wing and of the tail; the fuselage structure, the control surfaces and the wing and tail tips are not optimized using ***EBF3WingOpt*** and are kept fixed throughout the process. The optimization framework ***EBF3WingOpt*** developed for Boeing N+2 wing includes a geometry modeling module, a static aeroelastic analysis module, an flutter analysis module and an optimization module.

The geometry parameterization has been implemented in the ***EBF3WingOpt*** optimization framework using MSC.PATRAN session file. The geometry and finite element model of Boeing HSCT wing internal structure are defined by a set of design variables. An example of wing

internal *SpaRibs* layout automatically generated using MSC.PATRAN is presented in Figure 3.4. The wing internal topology is divided into 14 smaller wingboxes. *SpaRibs* layout is defined by *Linked Shape Method* in each wingbox. Therefore the wing internal *SpaRibs* layout is defined using 53 shape variables. The details of the geometry definition of Boeing HSCT wing has been presented in *Ref.* [84].

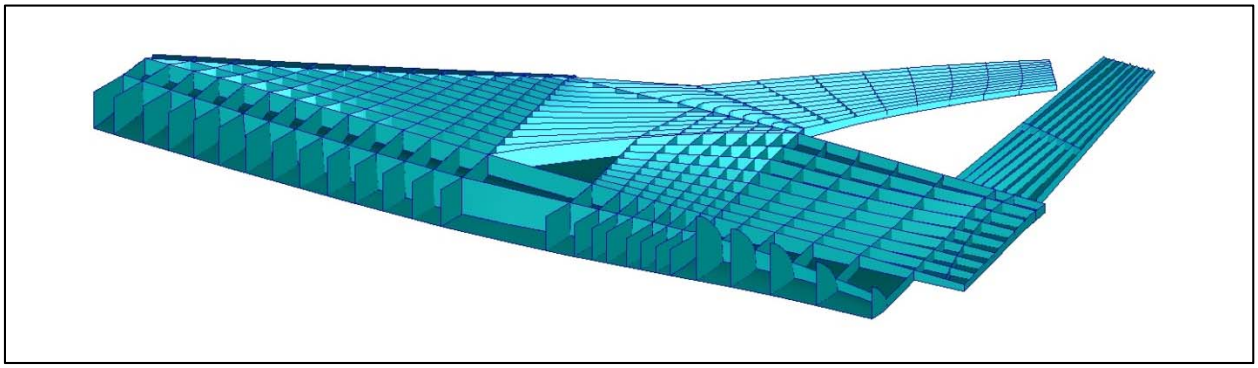

Figure 3.4: Example of Internal Wing Structure Configuration Generated with *EBF3WingOpt*

The static aeroelastic analysis module computes the flight loads and the associated stresses for multiple flight conditions. The flight loads and structural stress calculation are carried out by MSC.Nastran. There are five maneuvers concerned in the optimization: 2.5g pull up, -0.5g push over and roll at Mach 0.836 and 20,000 ft altitude, 1.2 g pull up and 1.5g pitch up at Mach 1.6 and 40,000 ft altitude.

The stress response of the wing structure is evaluated using an aggregated stress approximation. The stress constraint is formalized using the modified Kreisselmeier-Steinhauser criterion, following the relation:

$$KS_{\sigma}(\sigma) = \frac{1}{\rho}\ln\left(\frac{1}{\sum_{i=1}^{N} A_i}\sum_{i=1}^{N} A_i e^{\rho\left(\sigma_{vmi}/\sigma_y\right)^{1/2}}\right) < 1 \tag{3.1}$$

where ρ is the aggregation parameter defined by user, A_i is the area of the i^{th} finite element in the model, σ_{vmi} is the von Mises stress in the i^{th} finite element of the model and σ_y is the yield stress of the material. The parameter ρ determines the difference between the original maximum von Mises stress and the KS approximation. The KS function becomes a better approximation of the maximum von Mises stress for greater values of ρ. A machine-zero error could be achieved by choosing a large enough ρ. However, in order to avoid that the stress response is determined by the maximum von Mises stress only in a couple of finite elements, a value of $\rho = 5$ is a recommended value for aggregation parameter in this research. For more information about the Kreisselmeier-Steinhauser stress criterion and its application please see *Ref*. [82] and *Ref*. [85].

In this research, a sequence of matched points with a same Mach number but various air densities has been analyzed in the flutter analysis. Flutter velocity is calculated using PKNL method in SOL 145 of MSC.NASTRAN for two flight conditions: Mach 0.836 at 20,000ft and Mach 1.6 at 40,000ft. SOL 145 available in MSC.NASTRAN is incorporated in ***EBF3WingOpt*** framework in order to calculate the supersonic and subsonic flutter speeds.

Two flutter constraints are used during the optimization process, one for subsonic cruise regime and one for supersonic cruise regime. The constraints are formulated as follow:

$$F_{Subsonic} = 1.2\frac{Q_{fl_{Subsonic}}}{Q_{cr_{Subsonic}}} < 1 \tag{3.2}$$

$$F_{Supersonic} = 1.2\frac{Q_{fl_{Supersonic}}}{Q_{cr_{Supersonic}}} < 1 \tag{3.3}$$

where Q_{cr} is the critical dynamic pressure computed using MSC.NASTRAN and Q_{fl} is the dynamic pressure at the two flight conditions. A safety factor of 1.2 is also applied on the flutter velocities. If the flutter analysis shows that the critical dynamic pressure value is outside the range investigated the flutter constraint value is considered to be zero. From *Ref.* [83] the velocities for subsonic and supersonic flight conditions are chosen to be 867 ft/sec at 20,000 ft (M = 0.836) and 1782 ft/sec at 40,000 ft (M = 1.6), respectively. The corresponding dynamic pressure values are 3.31 psi and 6.19 psi respectively.

The aerodynamic model of Boeing HSCT wing is defined using MSC.FlightLoads. As shown in Figure 3.5, the aerodynamic surface consists of 840 aerodynamic boxes. The aerodynamic loads are interpolated onto the spline nodes, which locate at the intersection of upper wing skin and *SpaRibs*, to compute the structural deformation and stress. Some grid points in the control surfaces, wing tip and tail tip, are also selected as spline nodes for transforming the aerodynamic loads onto those regions. The spline nodes are shown in Figure 3.6.

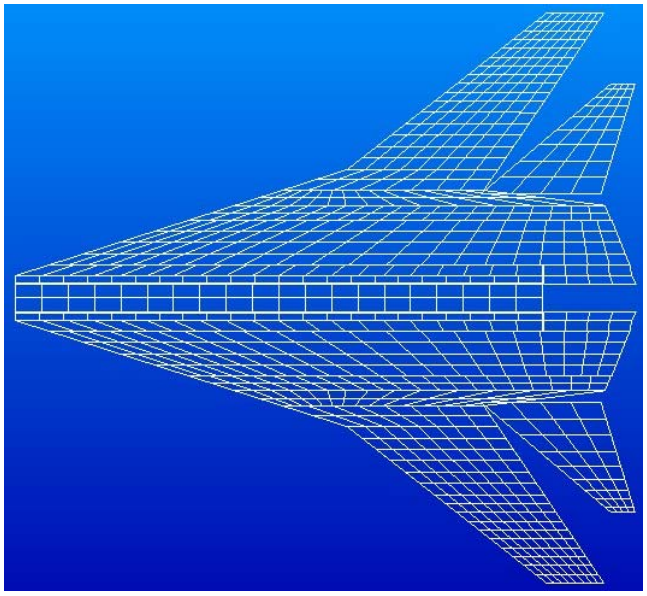

Figure 3.5: Aerodynamic Elements of Boeing HSCT Wing

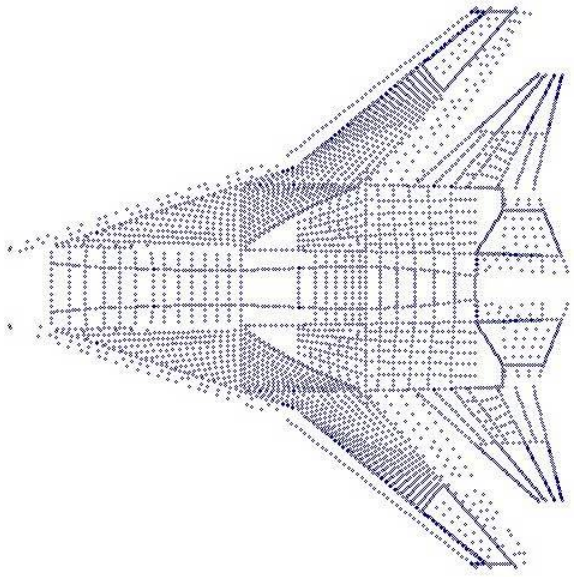

Figure 3.6: Spline Nodes in Boeing HSCT Wing

In order to reduce the complexity of the optimization problem, the design variables of the Boeing N+2 wing are decomposed into two groups: topology variables that define the topology of wing internal structure, and size variables which determine the thicknesses of wing components. The ***EBF3WingOpt*** framework incorporates both topology optimization and size optimization for the Boeing N+2 supersonic wing. The optimal topology configuration of wing internal structure is computed in the first optimization step; the optimal thicknesses of the wing skin panels and *SpaRibs* are computed with the fixed optimal topology of wing internal structure in the second optimization step. The structural weight is minimized in each step of the optimization subject to the strength and flutter constraints. The optimization framework is presented in Figure 3.7. The topology optimization requires both topology and size design variables to be specified for computing the stress and flutter responses of the aircraft structure. At this stage, the topology design variable vector and two thickness variables are used to generate an aircraft configuration, including the geometry definition of the *SpaRibs* and wing skins and the finite element model for

aerodynamic and structural analysis. Constraints are prescribed on the number and shape variables of *SpaRibs* to be placed in the wing structure. If the number of *SpaRibs* is determined, the value of the corresponding design variables could be fixed and the optimizer would find the best shape of the *SpaRibs* for that particular requirement.

The wing components are decomposed into 31 groups. The thickness of the structural components is optimized using the 31 size variables in the second step with the given topology configuration obtained in the first step. The details of the wing components decomposition is discussed in the chapter 3.1.4.

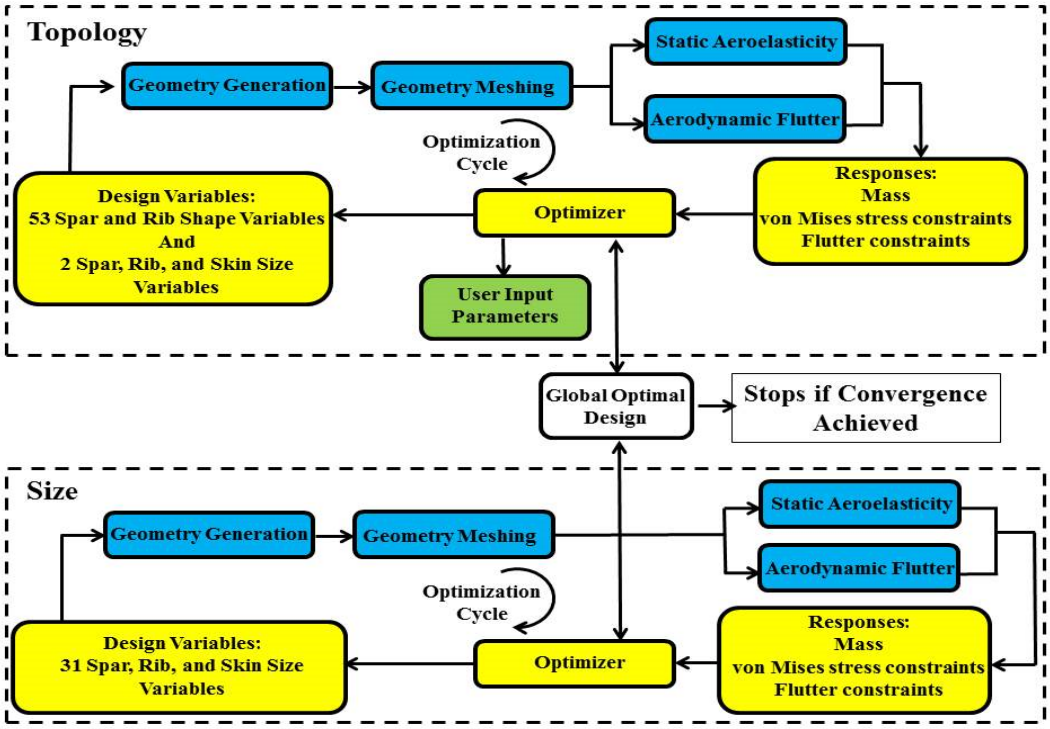

Figure 3.7: Global Optimization Framework for Boeing N+2 HSCT Wing

The optimization of topology and size design variables is carried out using particle swarm optimization method. Once the responses are computed the optimizer checks the convergence

criterion of the optimization method used and eventually restarts the process with a new design variables vector, if the convergence in not achieved. The topology and size loops are executed sequentially and convergence must be achieved in both steps separately. The final output of the optimization process is a wing structure with optimal topology and optimal thickness, for that particular configuration of *SpaRibs*, and that satisfies both strength and flutter constraints.

3.1.3 Baseline Boeing N+2 HSCT Configuration

This baseline aircraft configuration was optimized under strength and flutter constraints by the Boeing Company. The results are summarized in Chen *et al.* 2010 [83]. As shown in Table 3.1, the weight of the load bearing structure optimized to satisfy only the strength constraint is 39,305 lbs. If the flutter constraint is considered, the weight of the structure increases by 18.5%.

Table 3.1: Weight Summary for Boeing N+2 Aircraft Concept (Chen *et al.* 2010 [83]).

	Strength Optimization	**Strength and Flutter Optimization**
Wing Structural Weight (lb)	39,305	46,587
Weight of Re-Design Portion (lb)	12,780	16,050

The wing structural weight presented in reference paper [83] refers to the whole structure of the aircraft concept developed by Boeing. This includes the wing, the tail and the fuselage. The weight of baseline design is subdivided as follow: wing-tail assembly 25,560 lbs, fuselage assembly 13,745 lbs. The ***EBF3WingOpt*** optimization framework is only applied to re-design part of the wing and the tail structure. For consistency the data relative to the half portion of the structure re-designed during the optimization process are also presented in Table 3.1. The weight of re-design portion refers to the half structure presented in Figure 3.4. The mass of the

structure subjected only to the strength constraint is computed from the finite element model provided by Boeing, using MSC.PATRAN mass estimator. The weight of a half re-design portion was increased from 12,780 lb to 16,050 lb in strength and flutter optimization.

3.1.4 Optimization Results of Boeing N+2 HSCT Aircraft

This aircraft configuration is optimized and subjected to strength and flutter constraints in ***EBF3WingOpt***. The strength constraints are computed for different flight conditions as prescribed by Boeing. The optimal weight of the portion of the structure that was actually optimized is presented in Table 3.2. The mass refers to the half structure presented in Figure 3.8.

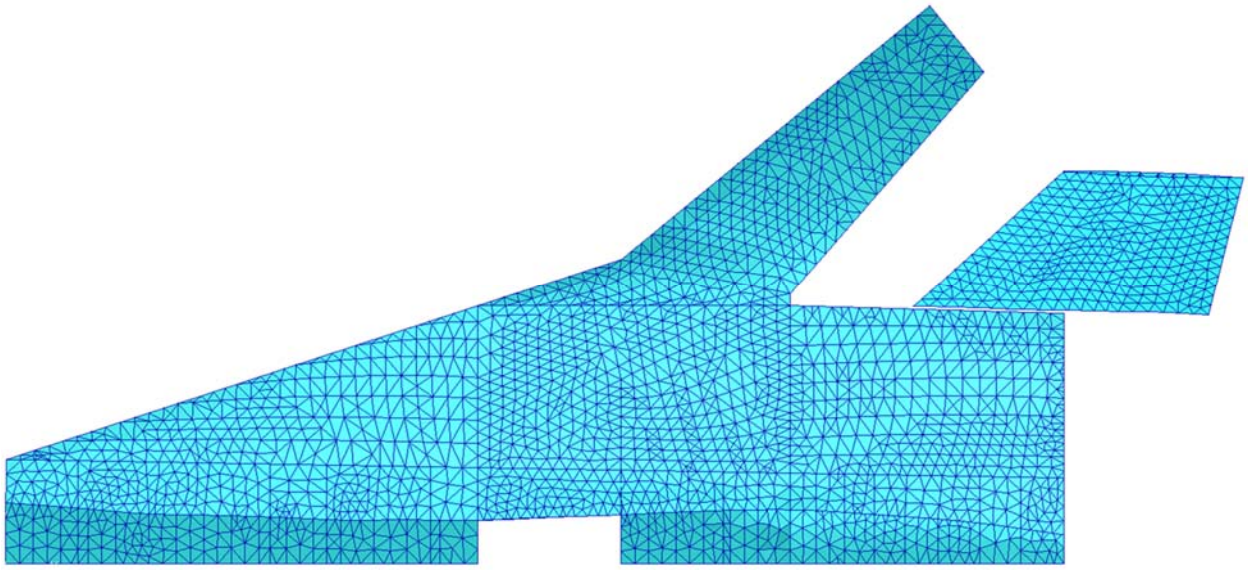

Figure 3.8: Finite Element Mesh of the Portion of the Re-designed Structure

Table 3.2: Mass Summary for Boeing N+2 Aircraft Concept Optimized with *SpaRibs*.

	Strength and Flutter Optimization
Optimal Weight (lb)	12,340

Table 3.3 and Table 3.4 present the constraint coefficients computed according to the relations presented above. The coefficients refer to the configuration shown in Figure 3.8. The stress constraints are satisfied in all of the five flight conditions. Flutter does not occur in the flight range investigated therefore the flutter constraint coefficients are zero. This means that the structure actually flutters outside the flight envelope and the flutter velocity and critical dynamic pressure requirements are satisfied.

Table 3.3: Kreisselmeier-Steinhauser Coefficients for Different Flight Conditions

Maneuver	**KSσ(σ)**
2.5G Pull Up at M = 0.836	0.89
1.2G Pull Up at M = 1.6	0.34
-0.5G Push Over at M = 0.836	0.17
Roll at M = 0.836	0.53
1.5G Pitch Up at M = 1.6	0.33

Table 3.4: Flutter Constraint Coefficients of Optimal Configuration.

$F_{Subsonic}$	0.0
$F_{Supersonic}$	0.0

The first step of the optimization process is to find the optimal topology design of the *SpaRibs*. This task involves the use of 53 design variables which define number of *SpaRibs* required and their curvilinear shape. The optimum topology configuration computed at this stage is shown in

Figure 3.9 along with the baseline structure for comparison. The optimized structure is characterized by a higher number of internal elements in every section of the wing.

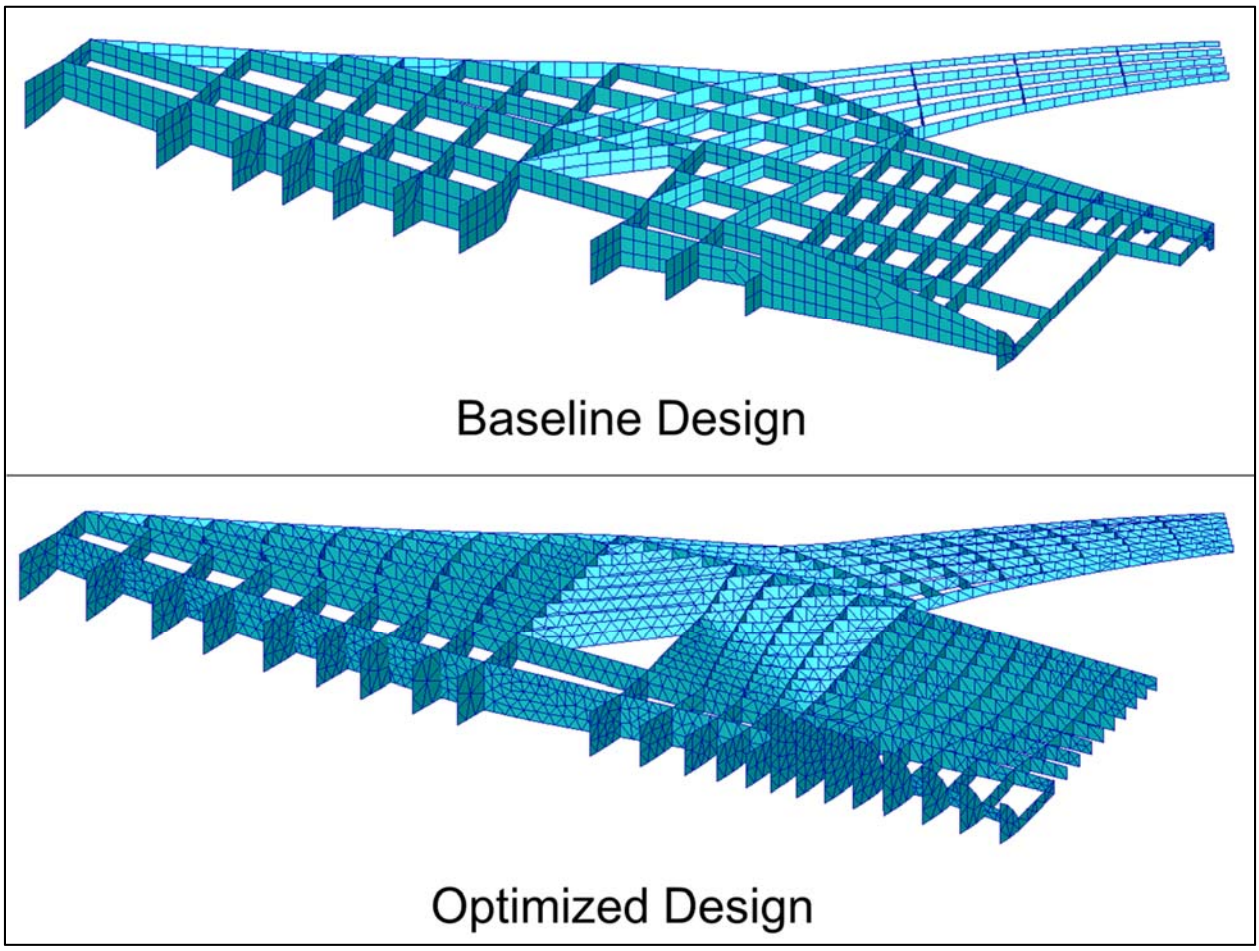

Figure 3.9: Optimum Topology Computed at the First Optimization Step.

The second phase of the optimization process is the sizing of the internal components and the skin panels. This task includes 31 size design variables to define the thickness of wing structure. The optimal size of re-designed wing components is presented in Figure 3.10. The maximum component thickness is reduced to about 0.3 inches from the 1.1 inches of the baseline. In general a significant thickness reduction of the skin panels is observed. The reduction is more

pronounced in the outer, center and forward portion of the wing structure. The forward wing is characterized by thicker *SpaRibs*.

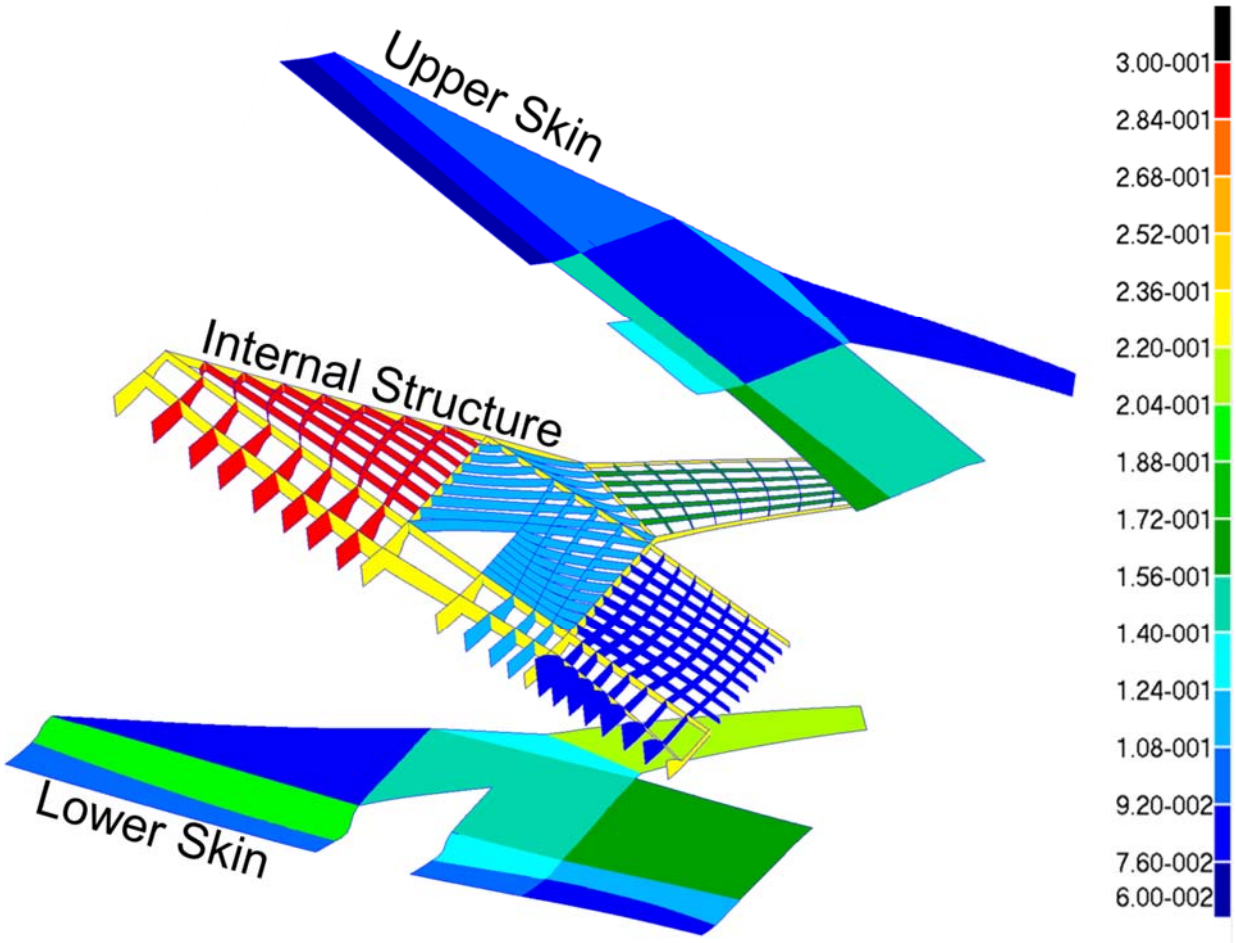

Figure 3.10: Thickness Distribution of the Optimized Structure (in).

The static aeroelastic analysis is performed for every load case listed in Table 3.4. The most severe maneuver from the stress point of view is the 2.5 G pull-up maneuver at Mach 0.836 and 20,000 ft altitude. The von Mises stress distribution in the re-design region of wing structure is plotted in Figure 3.11.

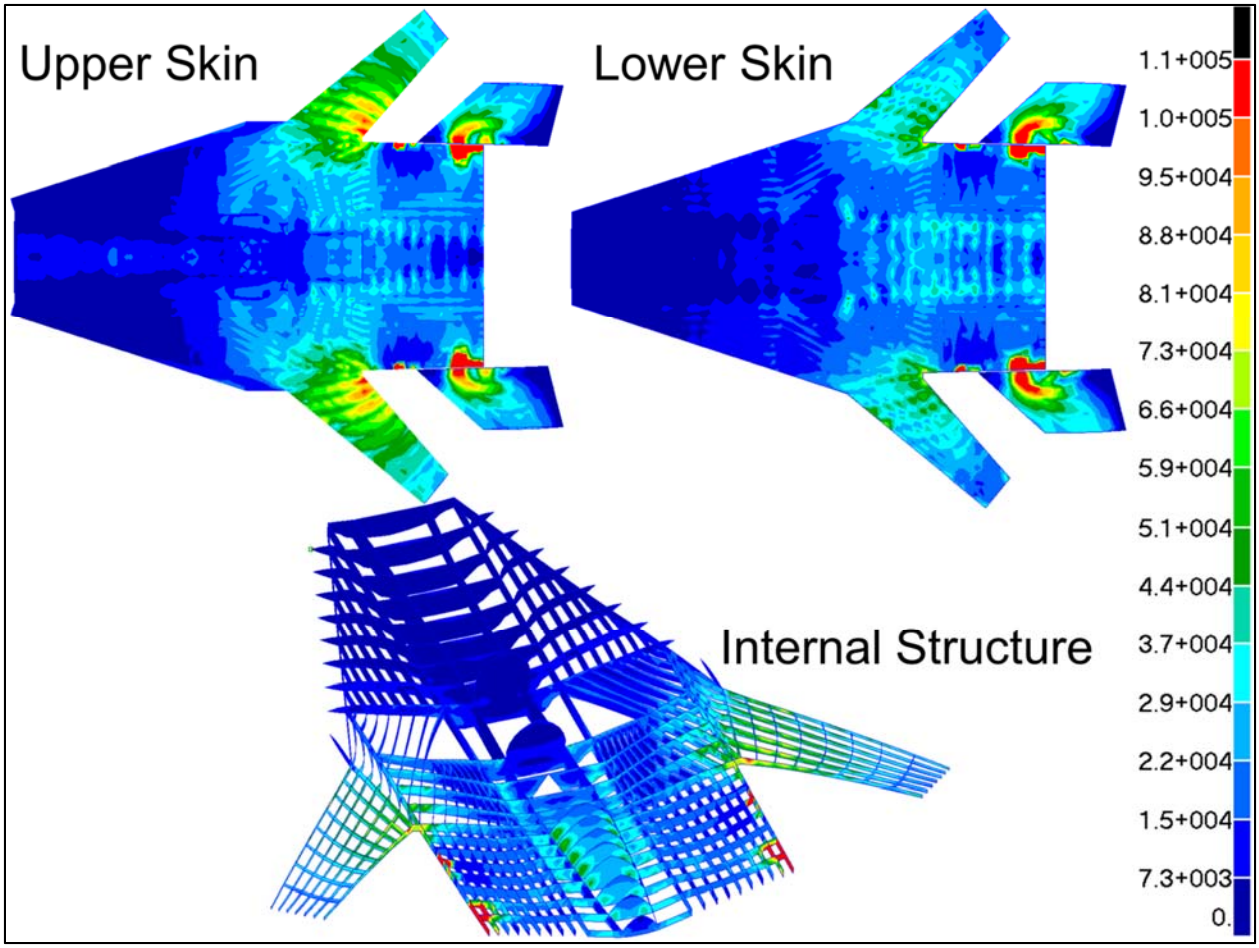

Figure 3.11: von Mises Stress Distribution Associated to the 2.5 g Pull-Up Maneuver

High stress concentration can be observed in the tail connection with the rear section of the wing and at the attachment of the outer wing with the center wing section. The stress concentration in the former location is expected since all the aerodynamic load acting on the large tail surfaces are transmitted to the rest of the structure by only three structural components modeled as rigid bar elements. The stress concentration in the latter location is explainable by the fact that the load acting on the outer wing produces a high load in that particular region of the structure. Moreover, the load coming from the control surfaces are transmitted to the outer wing trailing edge spar through rigid bar elements.

The high stress regions amount to only about 2% of the total wing surface therefore can be considered local effects caused by the use of the rigid bar elements to connect the various parts of the structure. A more accurate modeling of the structure and a localized optimization should solve the issue effectively. The forward section of the wing is practically unstressed for this flight maneuver.

Figure 3.12 shows the von Mises stress distribution for the remaining maneuvers. The most critical maneuver, after the 2.5 g pull-up at Mach 0.836, is the roll at Mach 0.836 at a roll rate of 25 degrees per second. This kind of maneuver generates an asymmetric aerodynamic pressure distribution on the aircraft. The portions of the wing characterized by high stress are the tail-wing connection and the outer wing-center wing attachment, as observed in the previous case. The 1.2 g pull-up maneuver and the 1.5 g pitch-up maneuver at Mach number equal to 1.6 have similar stress distribution with higher stresses localized in the tail-wing connection region. Finally the push over maneuver at Mach number equal to 0.836 and load factor equal to -0.5 is characterized by a very low stress level throughout the whole structure. In conclusion the strength design is driven by the pull-up maneuver at 2.5 g and by the roll maneuver at Mach number equal to 0.836. The most critical regions of the structure, from the stress point of view, are the tail-wing connection region, tail surfaces, the rear wing and the outer wing.

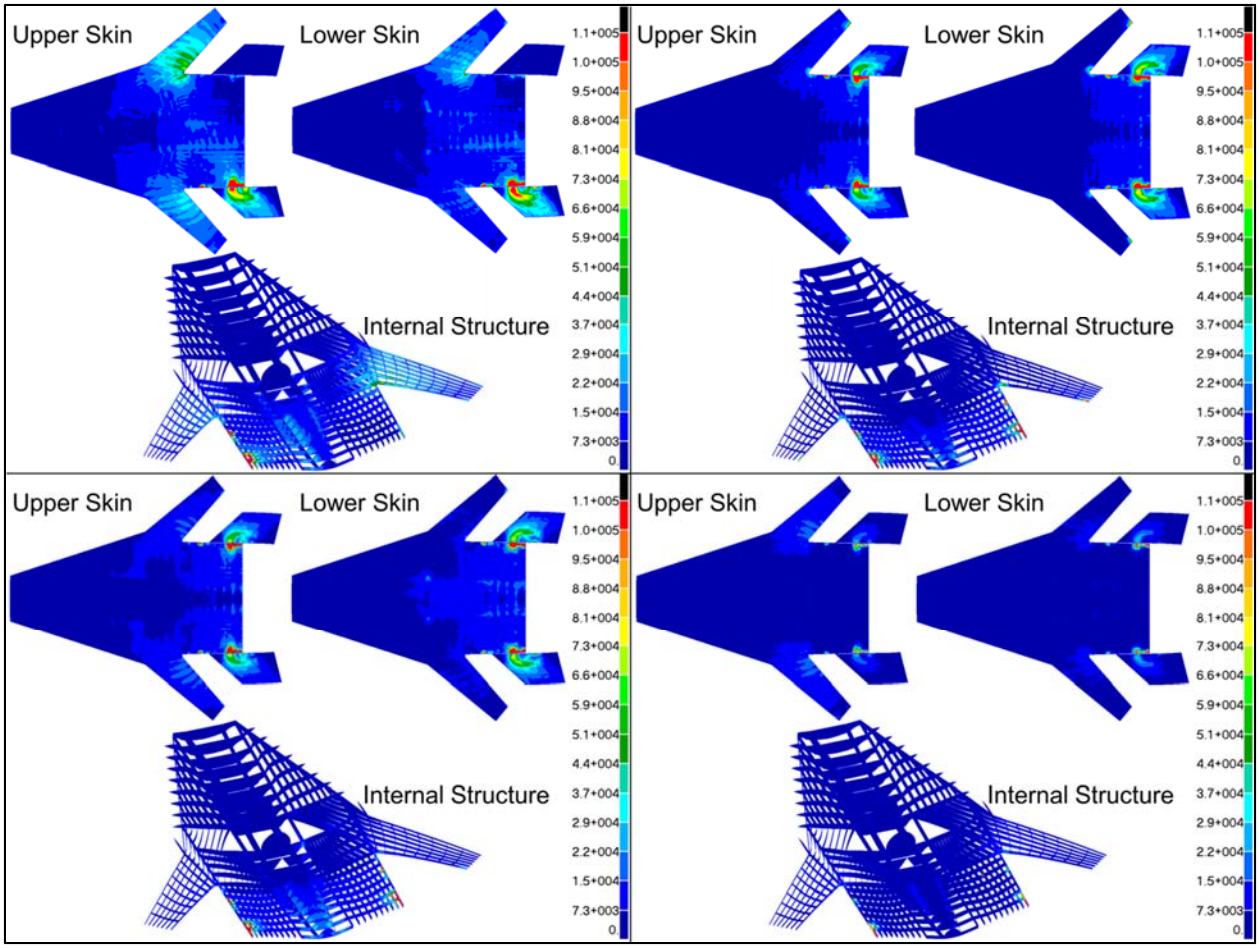

Figure 3.12: von Mises Stress of the Aircraft Structure

Clockwise from pitch-the Top Left Corner: 25 deg/sec Roll at Mach = 0.836, 1.2 g Pull-Up at Mach = 1.6, 1.5 g Pitch-Up at Mach = 1.6, -0.5 g Push Over at Mach = 0.836

The flutter analysis is performed using the PKNL method available in MSC.NASTRAN. The results show that flutter does not occur for the flight conditions studied. In particular, the flutter modes damping is always negative for the range of dynamic pressure considered. Figure 3.13 shows the structural damping as function of the dynamic pressure for the subsonic and supersonic regimes, respectively. The damping value is always negative therefore flutter does not occur.

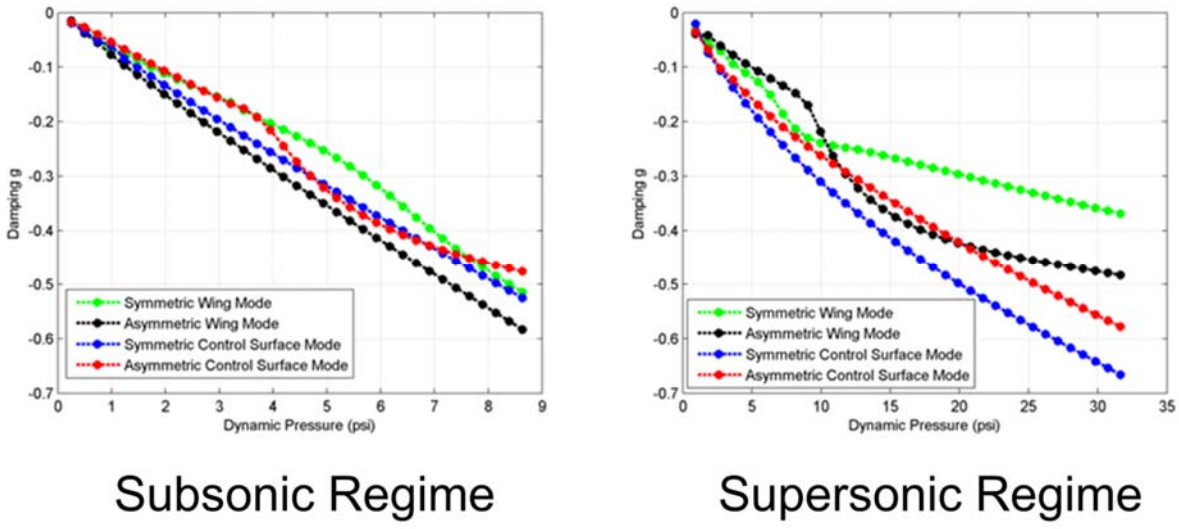

Figure 3.13: Flutter Analysis Results

The baseline and the *SpaRibs*-optimized structure performance are compared in Table 3.5. The use of the *SpaRibs* allows for a mass reduction of the structure 22.6%. Furthermore both the subsonic and supersonic flutter constraints are met.

Table 3.5: Optimized Structure Performance Compared.

	Baseline	**Optimized with *SpaRibs***
Weight (lb)	16,050	12,430 (22.6% Reduction)
Stress Constraints	Satisfied	Satisfied
Subsonic Flutter	Not Satisfied	Satisfied
Supersonic Flutter	Satisfied	Satisfied

3.2 Optimization of NASA Common Research Model

3.2.1 NASA Common Research Model (CRM) Wing Description

The transport aircraft wing configuration NASA Common Research Model (CRM) is studied in this research. The CRM wing is a cantilever wing with a full wingspan of 192.8 ft, aspect-ratio of nine, a taper-ratio of 0.275 [86]. An example of CRM wing layout is shown in Figure 3.14. The wing can be divided into the inner wing and the outer wing sections at the junction located at 37% semi-span. An aerodynamic model of the CRM wing is created using MSC.PATRAN for the aerodynamic load calculation. Figure 3.15 shows the aerodynamic model of CRM wing that consists of three aerodynamic lifting surfaces and 500 aerodynamic boxes. The spline nodes shown in Figure 3.16 are selected at the intersections of top wing skin and *SpaRibs*. A minimum distance requirement of 20 inch is applied on the adjacent spline nodes to avoid selecting too many spline nodes.

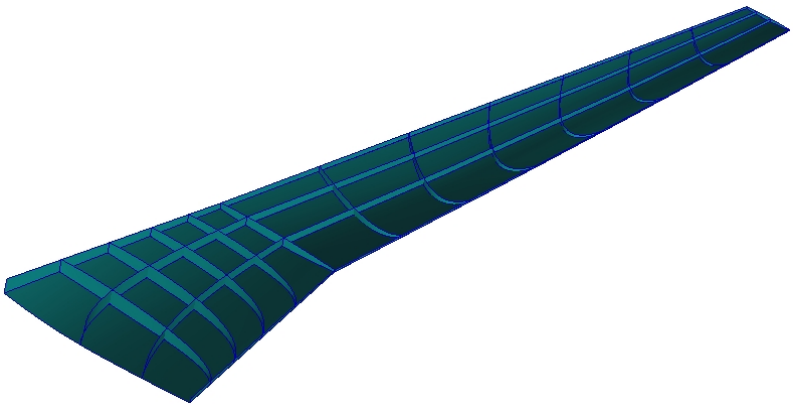

Figure 3.14: Example of NASA Common Research Model

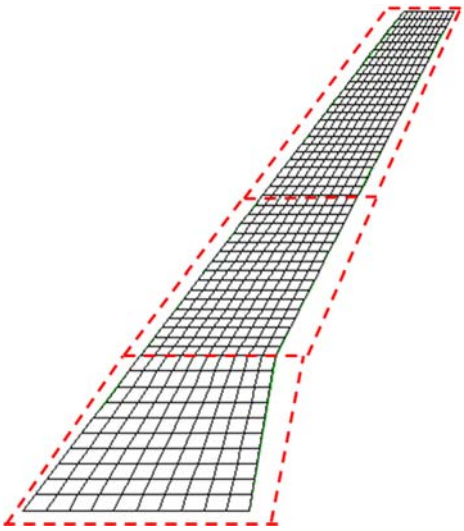

Figure 3.15: Aerodynamic Elements of NASA CRM Wing

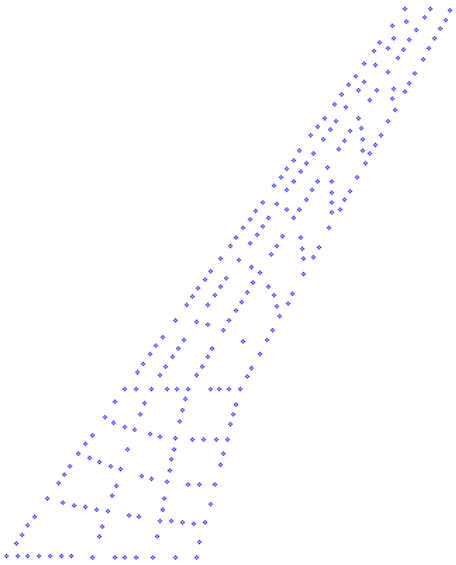

Figure 3.16: Example of Spline Nodes in NASA CRM Wing

3.2.2 Design Variables in Optimization of Subsonic CRM Wing

In the global/local optimization, the topology of the stiffening members and the thicknesses of the panels are optimized, and the outer model line (OML) is not changed in this research. Curvilinear *SpaRibs* are defined in each wing section and the C^0 continuity is enforced on the

junction of the each two adjacent sections. The CRM wing internal structure is generated using 24 design variables with the *linked shape method* [80]. The details of those shape design variables of the spars or ribs in different wing sections are given in Table 3.6 and Table 3.7. The CRM wing is modeled using aluminum alloy 2024-T3 and its material properties are given in Table 3.8.

Table 3.6: Shape Design Variables

SpaRibs	**Design Variables**
Front and Rear Spar	DV1 ~ DV2
Spars in Inner Wing	DV3 ~ DV8
Ribs in Inner Wing	DV9 ~ DV14
Spars in Outer Wing	DV15 ~ DV18
Ribs in Outer Wing	DV19 ~ DV24

Table 3.7: Boundary of Shape Design Variables of Spars and Ribs

Parameter	Description	Lower Bound	Upper Bound
P_1	Number of *SpaRibs*	2	20
P_2	η_1	0.1	0.9
P_3	η_2	0.1	0.9
P_4	$\xi_{11}/\ \xi_{12}$	0.25	4
P_5	$\xi_{21}/\ \xi_{22}$	0.25	4
P_6	$\xi_{31}/\ \xi_{32}$	0.25	4

Table 3.8: Aluminum Alloy 2024-T3 Mechanical Properties

Density (lb/in^3)	0.1
Modulus of Elasticity(ksi)	10,600
Possion's Ratio	0.33
Yield Stress (ksi)	40

Thicknesses of wing skins and *SpaRibs* are specified by non-uniform thickness fields. In this study, non-uniform fields are defined using linear or nonlinear function of the Y-coordinate. Two design variable values are needed to create a linear function. One design variable is the thickness of the skin at the wing root. The other design variable specifies the thickness of panels at the wing tip. Four thickness fields were specified for the four subgroups of wing structure components: upper skin, lower skin, spars and ribs. In some cases, nonlinear thickness fields are more efficient than the linear thickness fields when it comes to the structural weight saving. The motivation of such a nonlinear function comes from that the high stress region of design with linear thickness fields locates around the junction of the outer wing and inner wings, while the skin stresses in the wing tip and wing root region are relatively low. Therefore a straightforward idea is to increase the skin thickness in such high stress region while reducing the skin thickness in the low stress region. In this study, a combination of quadratic and triangular thickness fields has been studied. An example of the nonlinear function is shown in Figure 3.17. In the quadratic function, thickness decreases from the wing root region to the wing tip region faster than it does in linear function. The thickness in the junction region is increased by adding the triangular function and the quadratic function. The size design variables in the CRM wing optimization is presented in Table 3.9.

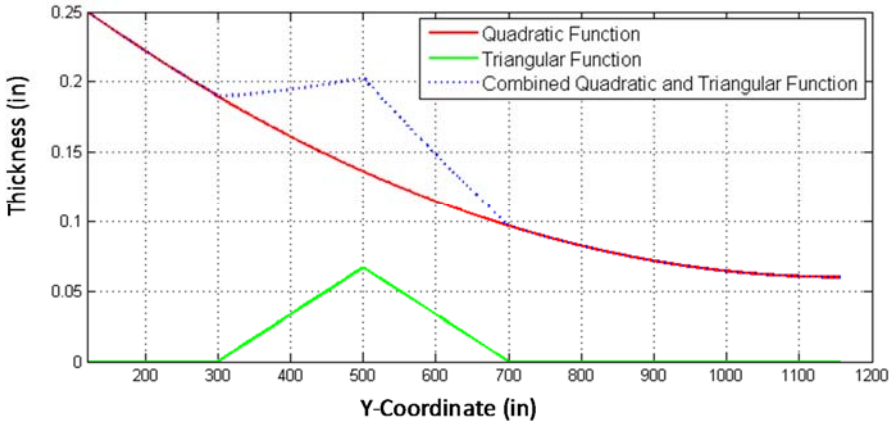

Figure 3.17: Nonlinear Thickness Fields

Table 3.9: Size Design Variables

Wing Components	**Linear Fields**	**Non-linear**
Spars	DV25 ~ DV26	DV25 ~ DV27
Ribs	DV27 ~ DV28	DV28 ~ DV30
Top Wing Skin	DV29 ~ DV30	DV31 ~ DV33
Bottom Wing Skin	DV31 ~ DV32	DV34 ~ DV36

3.2.3 Optimization Procedure of NASA CRM Wing

In this section global optimization is demonstrated for NASA common research model (CRM) considering stress, deformation and flutter constraints. The static aeroelastic analysis is implemented using sequence SOL144 in MSC.NASTRAN. An aerodynamic model of the wing is created to provide aerodynamic loads for static aeroelasic analysis using doublet-lattice method for subsonic problems. The aerodynamic grid nodes do not coincide with structural grids.

A set of splines has been defined for transferring the aerodynamic forces to the structure and transferring displacements from structure to aerodynamic model. Fixed boundary conditions are applied on the CRM wing root. Five flight conditions are defined using angle of attack of -2, 0, 2, 4, 6 degrees respectively, and cruise Mach number of M=0.8 at altitude of 35,000 ft.

The stress constraint is evaluated using Kreisselmeier-Steinhauser (KS) criterion. For this cantilever wing model, structural deformation can be measured using the displacement at the wing tip. Displacement constraint is defined using Eq. 3.4. $(u_z)_{max}$ is maximum vertical displacement at wing tip, b is semi-span of CRM wing.

$$\frac{(u_z)_{\max}}{12\% \cdot b} \leq 1 \tag{3.4}$$

Twist angle constraint is defined using the vertical displacements at the wing tip. As shown in Eq. 3.5, the twist angle at wing tip should not exceed 6 degrees. $(u_z)^+_{max}$ and $(u_z)^-_{max}$ are the maximum vertical displacements in positive and negative direction of z-coordinate, respectively. Here, C_{tip} is the chord length at wing tip.

$$Twist\ Angle\ at\ Wing\ Tip = \left| \frac{(u_z)^+_{max} - (u_z)^-_{max}}{c_{tip}} \right| \frac{180}{\pi} \leq 6 \tag{3.5}$$

Flutter analysis is carried out using PKNL method in solution 145 of MSC NASTRAN. The flutter constraint is defined using the dynamic pressure Q_c at cruise Mach number of M = 0.85 and at altitude of 35,000 ft. A sequence of matched points with a same Mach number of 0.85 but various air densities are included in the flutter analysis. Twenty modes are included in the flutter analysis of the CRM wing. In Eq. 3.6, a safety factor of 1.2 is applied to the flutter constraint.

$$Q_{Flutter} \geq 1.2\ Q_c \tag{3.6}$$

Number of eigenvalues extracted in eigenvalue analysis is a user defined parameter in flutter analysis. For a given structure, some mode shapes result from local vibration but not global level

vibration. In order to obtain a reliable flutter result, enough number of global modes, such as bending and torsional modes, should be included in flutter analysis. Constraints of Natural frequencies and mode shapes are considered in the multidisciplinary optimization. The constraint for first natural frequency is enforced as in Eq. 3.7.

$$f_1 \geq 1.0\ Hz \tag{3.7}$$

In the eigenvalue calculation the eigenvectors are normalized using maximum displacement. In that case the generalized mass of each mode can be used to classify whether a mode is global or local. If the generalized mass of a certain mode is greater than 10% of maximum generalized mass of all the modes included in the eigenvalue analysis, the mode is considered to be a global mode. Based on that criterion, the constraint on number of global modes is defined in Eq. 3.8.

$$Number\ of\ Global\ Modes \geq 5 \tag{3.8}$$

3.2.4 Optimization Results of Common Research Model

The CRM wing configuration is optimized under the above constraints in the global optimization framework using a two-step optimization approach. The topology of *SpaRibs* and thicknesses of panels are optimized in the first step optimization. The size design variables are refined in the second step optimization. The optimization is carried out using linear thickness fields or nonlinear thickness fields. The comparison of the results of the two schemes has been summarized in Table 3.10. The maximum von Mises stress is the active constraint in both of the two cases. The structural weight has been reduced 18.5% using nonlinear thickness fields compared with the results obtain from linear thickness fields approach. Figure 3.18 and Figure 3.19 show the optimal thickness fields and von Mises stress distribution of optimal designs, respectively. In the case using linear thickness fields, thickness decreased from the wing root to

the wing tip, which induced a high stress region at the junction of outer wing and inner wing. In the nonlinear thickness fields design, that high stress region has been divided into two regions, which causes a large area of the wing is close to full stressed state. The reason is that as compared to the linear thickness fields, in the nonlinear thickness fields case, the thickness in the junction region has been increased, and thicknesses in both the wing root and tip region are reduced. The comparison shows that for the stress dominated optimization problem, the nonlinear thickness scheme is much more efficient than linear thickness fields scheme. For the design optimized using nonlinear thickness fields, the stress responses are presented in Table 3.11, and optimal topology of *SpaRibs* is shown in Figure 3.20. Modal analysis is carried out to output the mode shapes of the first 20 flexible modes. Eight of the 20 modes are global models. The global mode shapes of the CRM wing are shown in Figure 3.21.

Table 3.10: Comparison of Optimal Designs using Different Thickness Fields

Optimal Design	Structural Weight	Maximum von Mises Stress in KS Criterion
Thickness with Linear Fields	9182.4 lbs	0.999
Thickness with Nonlinear Fields	7481.1 lbs	0.999

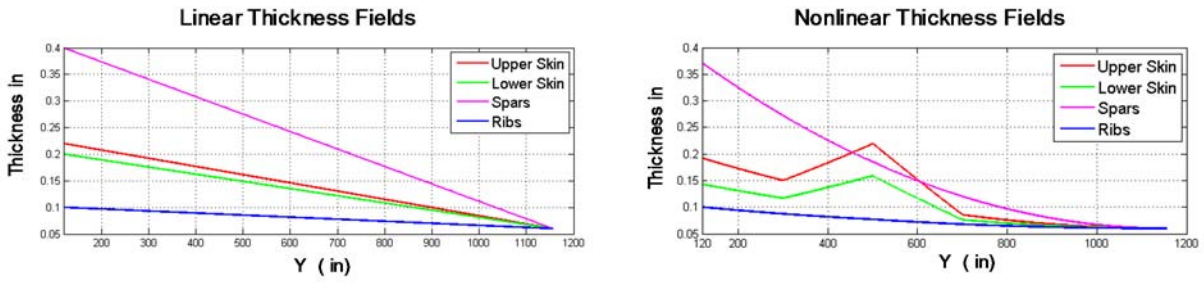

Figure 3.18: Optimized Thickness Fields

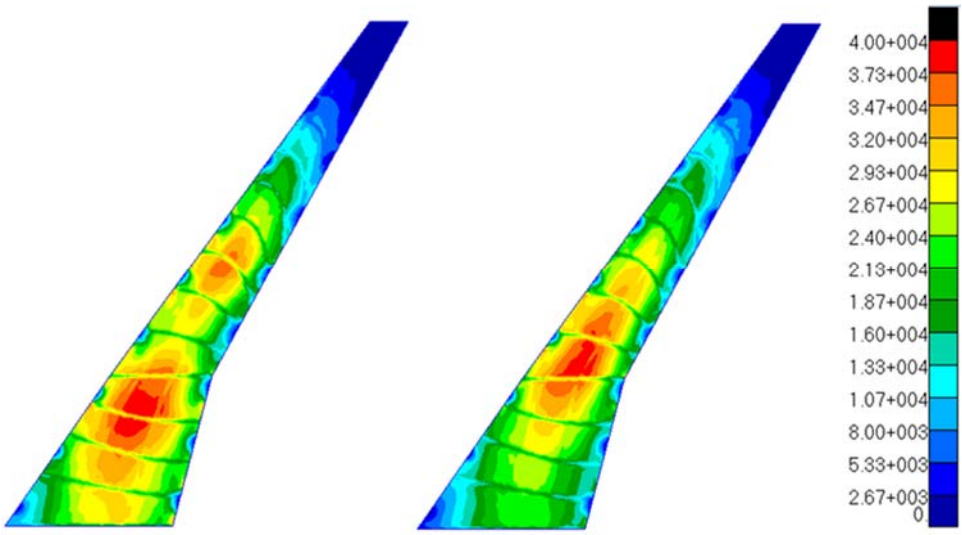

(a) Nonlinear Thickness Fields **(b) Linear Thickness Fields**

Figure 3.19: von Mises Stress Distribution

Table 3.11: Constraints of Global Optimal Design with Nonlinear Thickness Fields

Constraints	Optimal Design	Low Bound	Up Bound
M0.85 -2 Degree KS	0.237	NA	1
M0.85 0 Degree KS	0.039	NA	1
M0.85 2 Degree KS	0.265	NA	1
M0.85 4 Degree KS	0.628	NA	1
M0.85 6 Degree KS	0.999	NA	1
Max Displacement/Semispan	0.106	NA	0.125
Max Twist Angle (Degree)	3.96	NA	6
First Natural Frequancy (Hz)	1.21	1.0	NA
Number of Global Modes	5	5	NA
Flutter Dynamic Pressure (psi)	6.78	2.1	NA

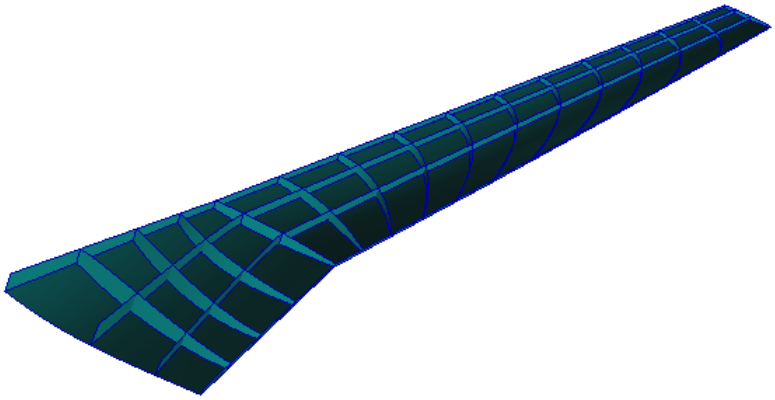

Figure 3.20: Optimal Design Using Nonlinear Thickness Fields

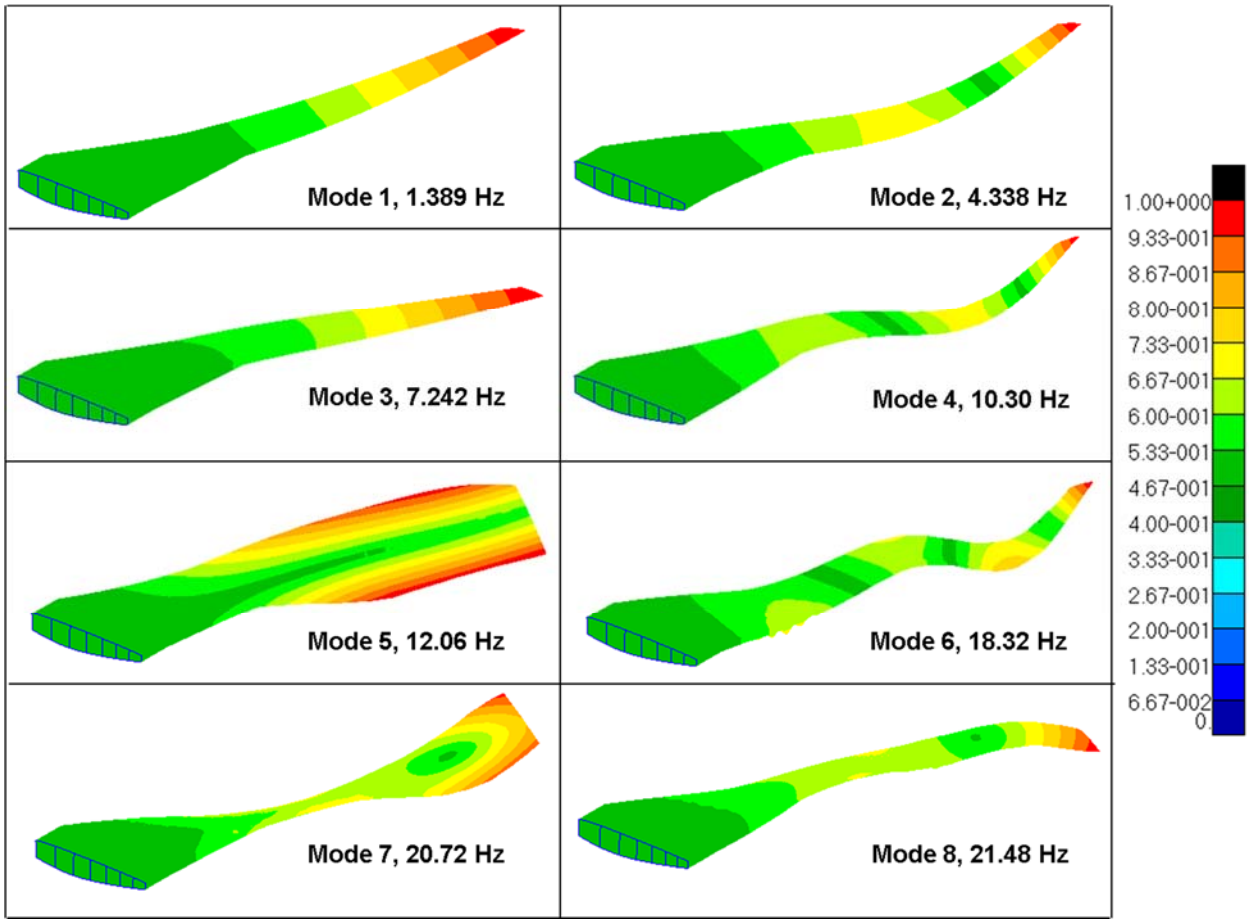

Figure 3.21: Global Modes of Optimal CRM Wing

3.2.5 Pre-stressed Modes and Unstressed Modes in Flutter Analysis

In this research, the effect of pre-stressed mode shapes on the flutter velocity is studied. Flutter analysis of the CRM model is performed in two cases using different mode shapes: the mode shapes of stressed or unstressed wing. The pre-stressed mode shapes are calculated in pre-stressed modal analysis, in which case the applied loads are computed by static aeroelastic analysis using MSC.NASTRAN solution SOL144. Then the pre-stressed modes are imported into flutter analysis which is carried out using NASTRAN solution SOL145. In that analysis, pre-stressed mode shapes are computed using the load case defined by the angle of attack of 6 degrees. The dynamic pressure vs. damping curves of the two cases in Figure 3.22 show that the flutter dynamic pressure of pre-stressed mode case is 7.14 psi which is about 5% higher than flutter dynamic pressure of 6.78 psi in the unstressed mode case, both of the two cases satisfy flutter constraint. Figure 3.23 shows the flutter frequencies computed by the un-stressed and pre-stressed flutter analyses.

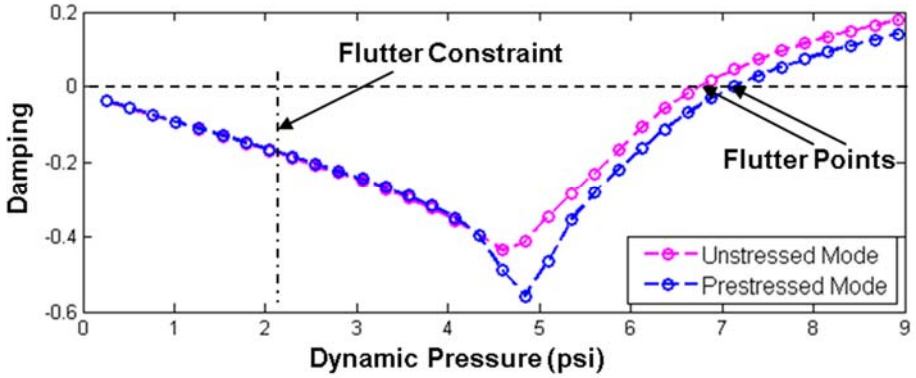

Figure 3.22: Flutter Dynamic Pressure

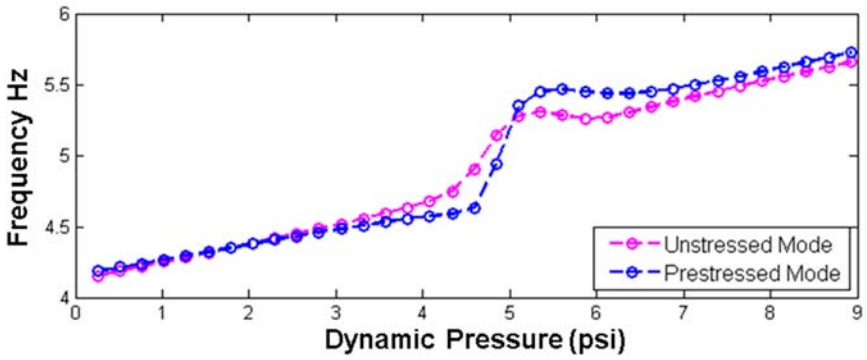

Figure 3.23: Flutter Frequency

3.3 Summary

In this chapter, the aircraft wing optimization framework ***EBF3WingOpt*** has been applied to a concept supersonic wing Boeing High Speed Commercial Transport aircraft (Boeing HSCT) and subsonic wing NASA Common Research Model (NASA CRM). The global wing optimization tool (***EBF3WingOpt***) has proven its efficiency in optimizing the weight of a wing box using *SpaRibs* as compared to using the classic straight spars and ribs. The method has been applied with success for designing the complex wing box configurations. The geometry of *SpaRibs* is parameterized using *Linked Shape Method*. Both topology optimization and size optimization are performed for the Boeing HSCT wing and NASA CRM wing subject to von Mises stress and flutter constraints. In the trim analysis and flight load calculation, multiple flight conditions are considered. The internal structure of Boeing HSCT is optimized subjected to stress and flutter constraints and multiple flight conditions. The baseline N+2 Boeing configuration is at first described and subsequently compared with the design optimized using ***EBF3WingOpt*** framework. The results show that the use of the *SpaRibs* allows for the reduction of the aircraft's

primary structure weight without violating the constraints. The results show a reduction of the weight of the wing/tail load bearing structure of about 20%. The internal structure of NASA CRM wing is optimized using curvilinear spars and ribs while considering stress, displacement and flutter constraints. The thickness distribution of CRM wing is optimized using linear thickness fields and non-linear thickness fields. The comparison shows the advantage of non-linear thickness fields in the wing weight reduction. The pre-stressed flutter analysis is implemented for the optimal CRM design obtained in global wing optimization. The result shows the pre-stressed flutter dynamic pressure is 5% higher than the un-stressed flutter dynamic pressure.

Chapter 4

EBF3PanelOpt: Un-Stiffened Panel Optimization

Plenty of previous researches have shown that the panel buckling is a crucial problem in aircraft structural design. In this chapter, local panel optimization framework ***EBF3PanelOpt*** is developed to minimize the structural weight by optimizing the local panels of wing structure. The un-stiffened panel optimization is implemented and applied on the NASA common research model (CRM) wing. The panel thicknesses are optimized using the results of stress and buckling analyses to minimize the wing weight subject to strength and buckling constraints.

4.1 Local Panel Optimization Procedure of CRM Wing

CRM wing is optimized using un-stiffened panels while considering stress, displacement, flutter and buckling constraints. As shown in Figure 4.1, a CRM design with 3 straight spars and 37 straight ribs, provided to us by NASA, is decomposed into local panels bordered by spars and ribs. Figure 4.2 presents the thickness and stress distributions, and fundamental buckling mode shape of this CRM design, which has been optimized subject to stress and flutter constraints, but without considering buckling constraint. The corresponding buckling eigenvalue of the buckling mode shape shown in Figure 4.2 is only 0.141, that means the CRM design violates the buckling constraint. In the local panel optimization, the topology of CRM wing structure is not optimized. The un-stiffened panel optimization is performed based on this CRM design to make it satisfy buckling constraint.

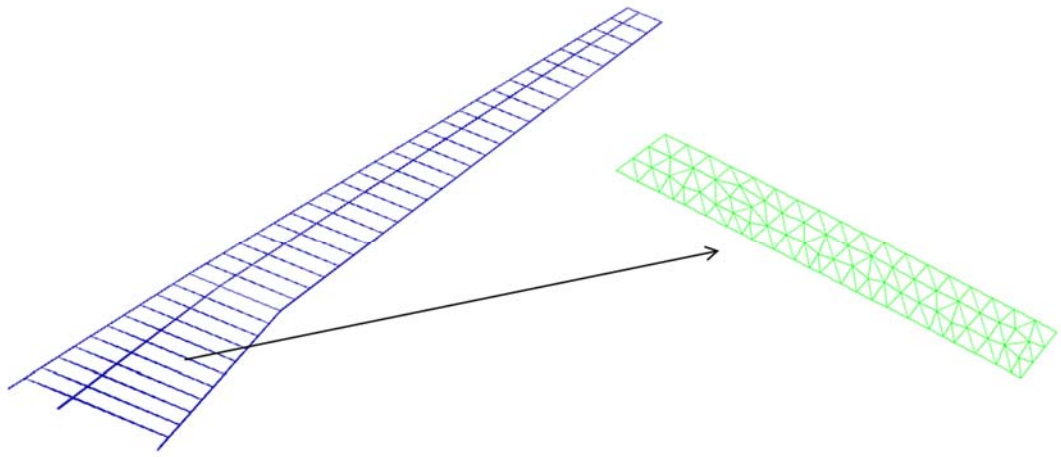

Figure 4.1: CRM Design with 37 Straight Ribs Provided by NASA

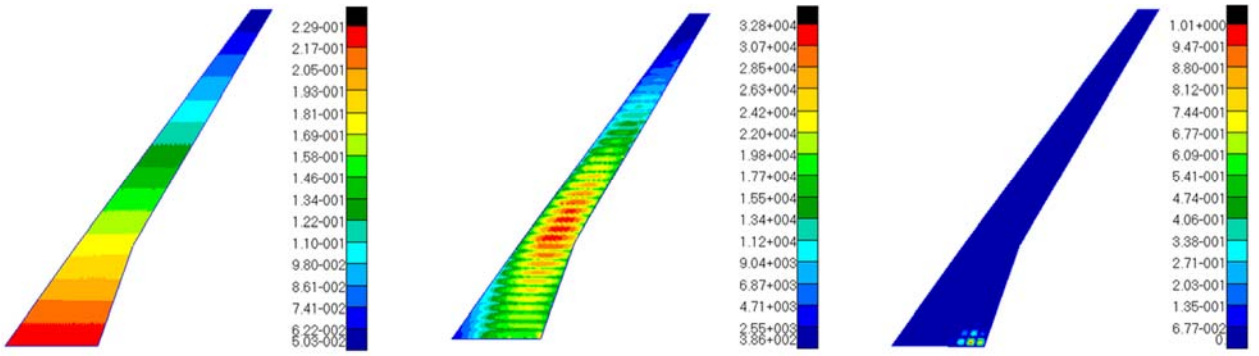

(a) Thickness **(b) von Mises Stress** **(c) Fundamental Buckling Mode Shape (AOA 6°)**

Figure 4.2: Results of Baseline CRM Design with 37 Straight Ribs

Two flight conditions are considered in the optimization: angle of attack equals -2 or 6 degrees. In the local panel optimization, the stress and buckling constraints should be satisfied in both of the two load cases. The aerodynamic forces applied on the wing structure are computed in static aeroelastic analysis using MSC.NASTRAN solution SOL144. The force fields are multiplied by a safety factor of 1.15 and applied on the global wing model for the static and buckling analysis, which generates the displacement fields of the wing model. The buckling constraint is defined in Eq. 4.1:

$$\lambda_p > 1.0 \tag{4.1}$$

where λ_p is fundamental buckling eigenvalue. If the λ_p is greater than 1, it means the critical buckling load is greater than the applied load.

The process of un-stiffened panel optimization is illustrated in Figure 4.3. In the local panel optimization, the buckling analyses are carried out for the global wing and local panels. Each local panel is optimized by a uniform thickness to instead of the thickness fields that used in the baseline CRM wing model. The thicknesses of the local panels are optimized to increase the buckling eigenvalue to be greater than 1. Then the global model is updated using the optimized

panel thicknesses in each optimization cycle. The convergence criterion, as shown in Eq. 4.2, is defined using the number of panels that violate the stress or buckling constraints, and the relative change of total wing weight in the i^{th} optimization cycle.

Number of Panels Violate Constraint < 5

$$\frac{|W_i - W_{i-1}|}{W_i} < 1\% \tag{4.2}$$

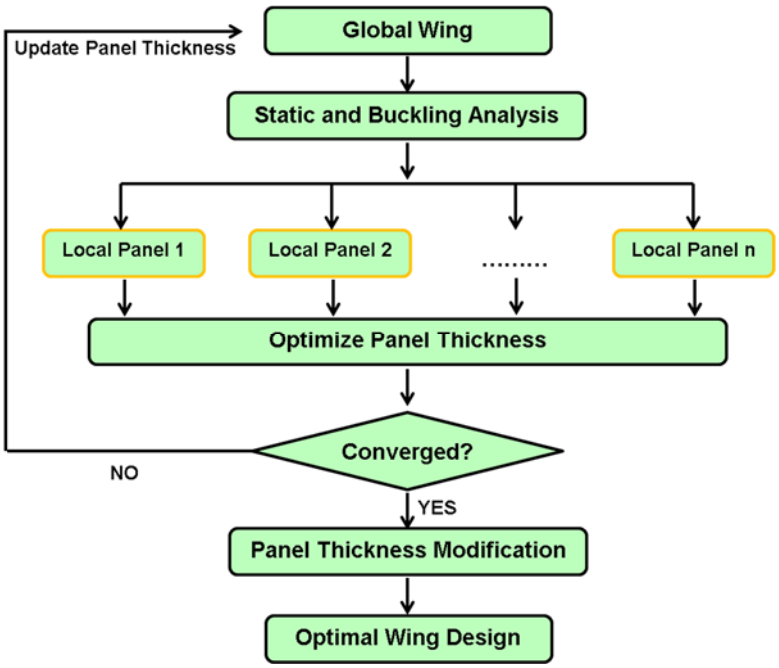

Figure 4.3: Local Panel Optimization Procedure

In the local panel optimization, the boundary conditions of local panels are defined using the translational displacements of the grid points on the panel edges, which are not exactly the same as the actual boundary constraints applied on the local panels in the global wing model. Therefore, even if all the local panels satisfy the local buckling constraints, the buckling eigenvalue of the global wing usually does not satisfy the global buckling constraint. A panel

thickness modification process is performed based on the wing design which satisfies the convergence criterion of the iterative local panel optimization. The detailed process of panel thickness modification is described in Figure 4.4. Buckling eigenvectors of the first m buckling modes of the global wing are computed and normalized to the maximum eigenvector using MSC.NASTRAN. The grid points with the maximum buckling eigenvectors (v_{max} = 1.0) locate in the buckled panels. As shown in Figure 4.4, the maximum buckling eigenvector of the 1st buckling mode is found in the local panel i_1. If the fundamental buckling eigenvalue λ_p of the global wing is less than 1, the thicknesses of the buckled panels should be optimized to satisfy the buckling constraints. The optimal wing design which satisfies the global buckling constraints can be obtained through the iterative panel thickness modification process.

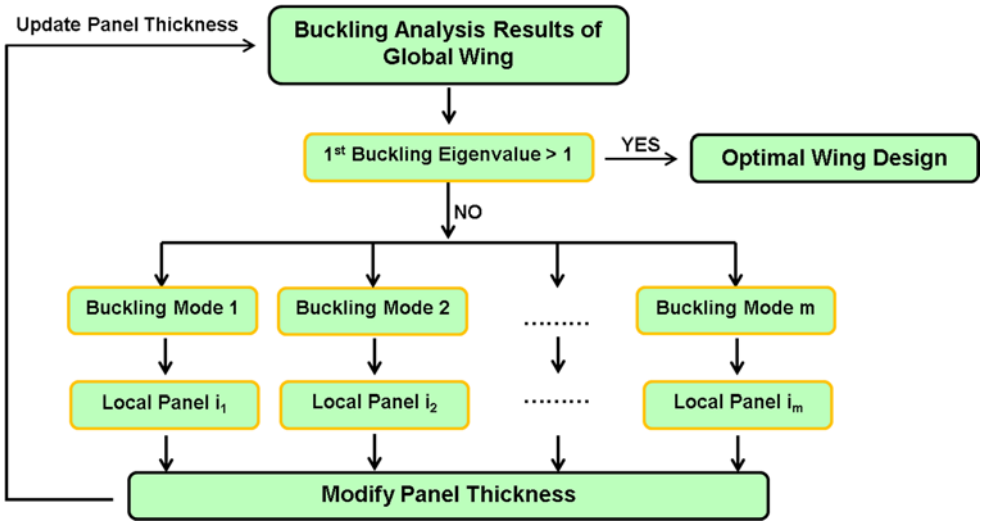

Figure 4.4: Modification of Local Panel Thickness

4.2 Buckling Analysis of Local Panel

In the buckling analysis of panel, boundary conditions are usually defined using the forces or displacements that applied on the panel edges. The local panels in the CRM wing are connected to the spars or ribs at the panel edges. If the thickness of a certain panel is changed, the forces applied on that panel edges may change dramatically. However, because the support of spars and ribs, the displacements at the panel edges only change a little bit. Therefore displacements are selected as boundary conditions and applied on the panel edges in the local panel optimization.

The displacement data of the grid points on panel edges are extracted from the displacement fields of the global wing. The displacement vector of a grid point consists of six components: three translational displacements and three rotational displacements. Two boundary conditions have been considered: only apply translational displacements on panel edges (termed Case 1), or apply both translational and rotational displacements (termed Case 2). The Case 1 is equivalent to assuming that the panel edges are constrained by simple supports. The Case 2 means the panel edges are clamped. The static and buckling analyses are performed for the panel with the two types of boundary conditions. The buckling analysis is also carried out for the global CRM wing. Local buckling modes can be found in several local panels from the buckling results of the global wing. A local buckling mode shape is extracted from the global wing model and shown in Figure 4.6 (termed Case 3), in comparison to the fundamental buckling mode shapes of the same panel computed in Case 1 and Case 2. The corresponding buckling eigenvalues are compared in Table 4.1. The buckling eigenvalue of case 1 is closer to the buckling result of the global wing. Therefore, the boundary conditions in buckling analysis of local panels should be defined using the translational displacements at the panel edges.

Table 4.1: Fundamental Buckling Eigenvalues of Local Panel

	Case 1	**Case 2**	**Case 3**
1st Buckling Eigenvalue	1.01	1.69	1.08

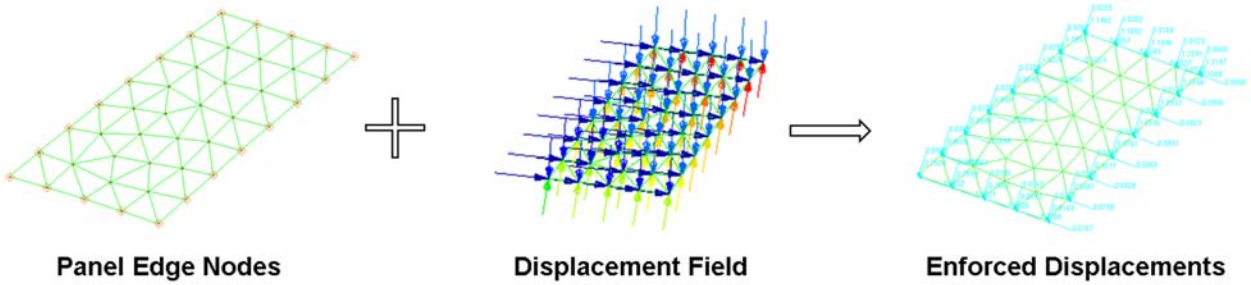

Figure 4.5: Boundary Conditions in Local Panel Analysis

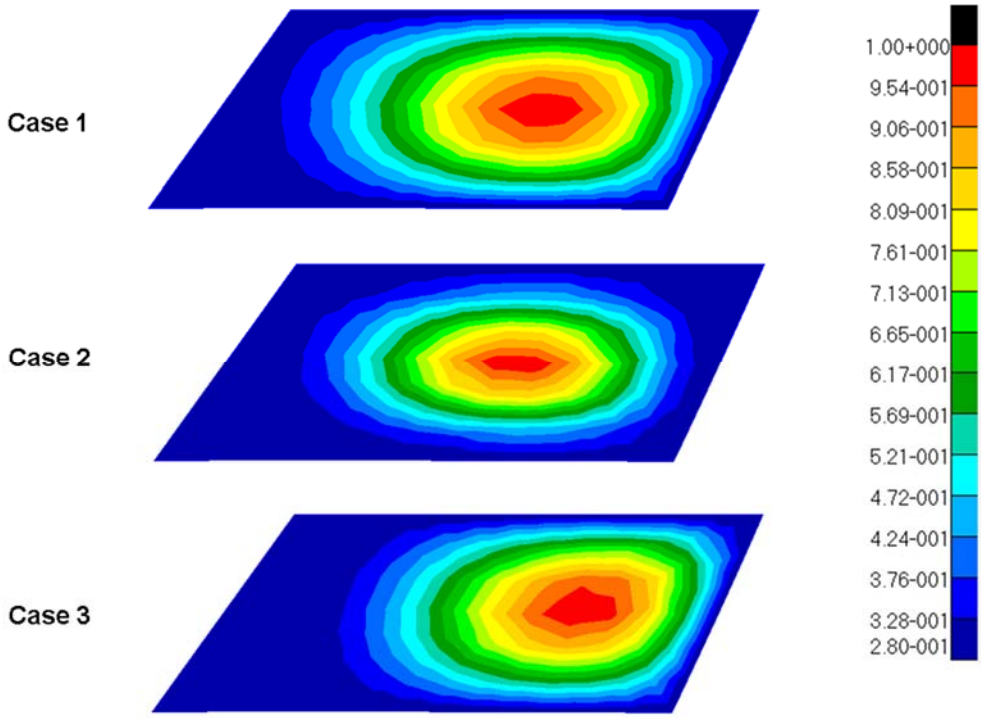

Figure 4.6: 1st Buckling Mode Shape of Local Panel with Various Boundary Conditions

4.3 Panel Thickness Optimization

For the thin rectangular flat plate with compressive loads applied on two opposite edges, the critical buckling stress can be computed using the analytic solution given by the following formula [47, 53].

$$\sigma_{CR} = \frac{k\pi^2 E}{12(1-v^2)}\left(\frac{t_{skin}}{b_{skin}}\right)^2 \tag{4.3}$$

where t_{skin} is the plate thickness, and b_{skin} is the length of the panel edges with compressive loads. *k* is a constant depends upon the aspect ratio of the panel being investigated. Thickness of each local panel is optimized using the first buckling eigenvalue and maximum von Mises stress in full stress optimization scheme as shown in Eq. 4.4. t_{opt1} is the optimized thickness of local panel considering maximum von Mises stress $(\sigma_{vm})_{max}$ in that panel. t_{opt2} is the optimized thickness using first buckling eigenvalue λ_p of that panel. T_{opt} is the optimized thickness of local panel.

$$t_{opt1} = t_0 (\sigma_{vm})_{max} / \sigma_y$$

$$t_{opt2} = t_0 (1/\lambda_p)^{1/2}$$

$$t_{opt} = max(t_{opt1}, t_{opt2}) \tag{4.4}$$

The local panel optimization is an iterative process. In each optimization cycle, the local panel thicknesses are optimized. Then the global finite element model needs to be updated using the new panel thicknesses. Displacement fields of global model are computed by the aerodynamic and static analyses. The thicknesses and boundary conditions of local panels are changed in each optimization cycle, which causes oscillation of panel thicknesses. In order to suppress the oscillation and obtain a fast converged optimal design, move limits are defined in the panel

thickness optimization process. A relative move limit is defined to restrain the change of panel thickness in a single iteration, as shown in the following formula

$$\left|t_i - t_{i-1}\right| \le 20\% t_{i-1} \tag{4.5}$$

where t_i is the initial panel thickness in ith iteration and the optimized thickness in the (i-1)th iteration. Such a move limit has been applied in the local panel optimization. As shown in Figure 4.7, the oscillation in the panel thickness indicates under-relaxation should be applied on the move limit. The move limit 2 is less than a half of the thickness change in the last iteration, as shown in Eq. 4.6.

$$\left|t_i - t_{i-1}\right| \le \min\left(20\% t_{i-1}, \frac{\left|t_{i-1} - t_{i-2}\right|}{2}\right) \tag{4.6}$$

As shown in the Figure 4.7.b, the thickness oscillation is suppressed using the modified move limits 2. A proper under-relaxation factor should be chosen for local panels, otherwise the calculated thickness may converge to some value that does not satisfy the stress or buckling constraints. In order to solve this problem, the under-relaxation factor should be increased if the calculated thickness change is relatively small. The move limit 3 is given in Eq. 4.7, where the under-relaxation factor k is determined by the calculated thickness change; t_{opt} is the calculated thickness using Eq. (4.4). The panel thickness and corresponding buckling eigenvalues obtained using move limit 2 or move limit 3 are compared in Figure 4.8. Compared to the results of move limit 2, the optimization using move limit 3 converges much faster and satisfies the buckling constraint. Therefore, move limit 3 is applied in the local panel optimization in this research.

$$\left|t_i - t_{i-1}\right| \le \max\left(\left|t_{opt} - t_{i-1}\right| k, \min\left(20\% t_{i-1}, \frac{\left|t_{i-1} - t_{i-2}\right|}{2}\right)\right) \tag{4.7}$$

$$\text{if } \frac{\left|t_{opt}-t_{i-1}\right|}{t_{i-1}} \geq 20\%, \quad \text{k} = 0.5; \quad \text{else} \quad k = 1 - \frac{2.5\left|t_{opt}-t_{i-1}\right|}{t_{i-1}}$$

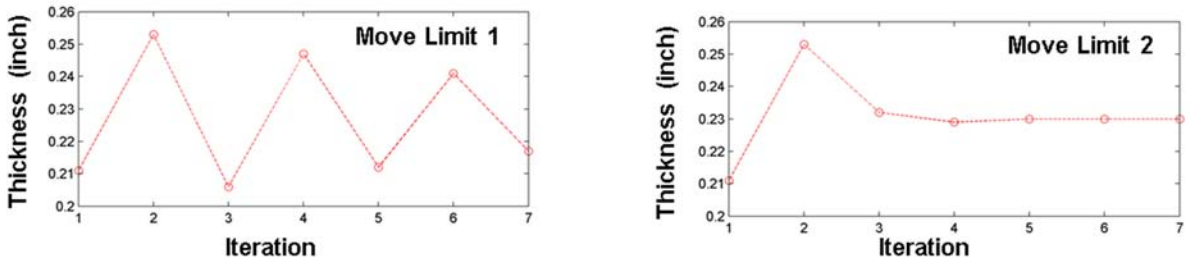

(a) Panel Thickness with Move Limit 1 **(b) Panel Thickness with Move Limit 2**

Figure 4.7: Comparison of Move Limit 1 and 2 of Panel Thickness

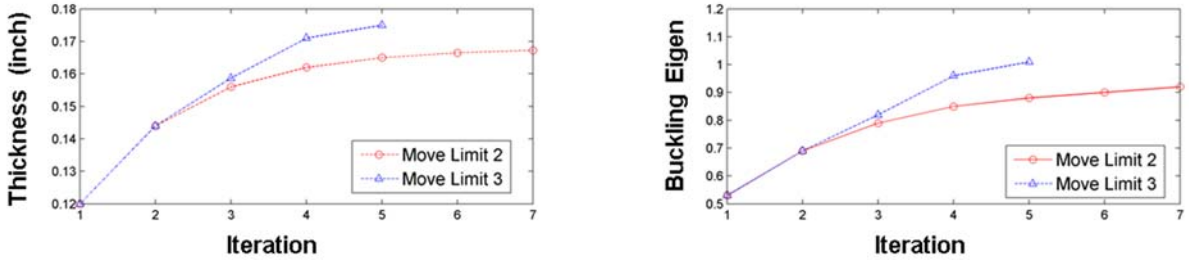

(a) Panel Thickness History **(b) Fundamental Buckling Eigenvalue History**

Figure 4.8: Comparison of Move Limit 2 and 3 of Panel Thickness

4.4 Results of Un-Stiffened Panel Optimization

In the local panel optimization, stress and buckling constraints are applied on all the local panels. The static, buckling and flutter analyses are carried out for the optimal CRM wing so as to check the multidisciplinary constraints for the global wing. Figure 4.9 is a trace plot for the convergence history of the un-stiffened panel optimization. The global wing weight, 1st buckling eigenvalue of global wing, aerodynamic lift force, and the number of panels that violate the buckling constraint are traced in all the optimization iterations. The results of un-stiffened panel optimization are summarized in Table 4.2. It shows the optimal CRM design, which is obtained in the seventh iteration, satisfies the buckling constraints. However, the wing weight increases 66.1% compared to the baseline CRM design.

Table 4.2: Results of Un-Stiffened Panel Optimization

	Baseline Design	**Local Panel Optimized**
Structural Weight of CRM Design (lbs)	11,599	19,269
1st Buckling Eigenvalue at AOA -2°	0.467	1.0009
1st Buckling Eigenvalue at AOA 6°	0.141	1.0002

Buckling eigenvalue is the dominant constraint as compared to the stress constraint for most local panels. Figure 4.10 presents the fundamental buckling eigenvalues of the local panels in the optimal CRM wing. Most of the buckling eigenvalues have been optimized to 1. Much greater buckling eigenvalues are observed in some local panels, the reason is that the thicknesses of those panels have approached 0.05 inch, which is the lower bound of panel thickness.

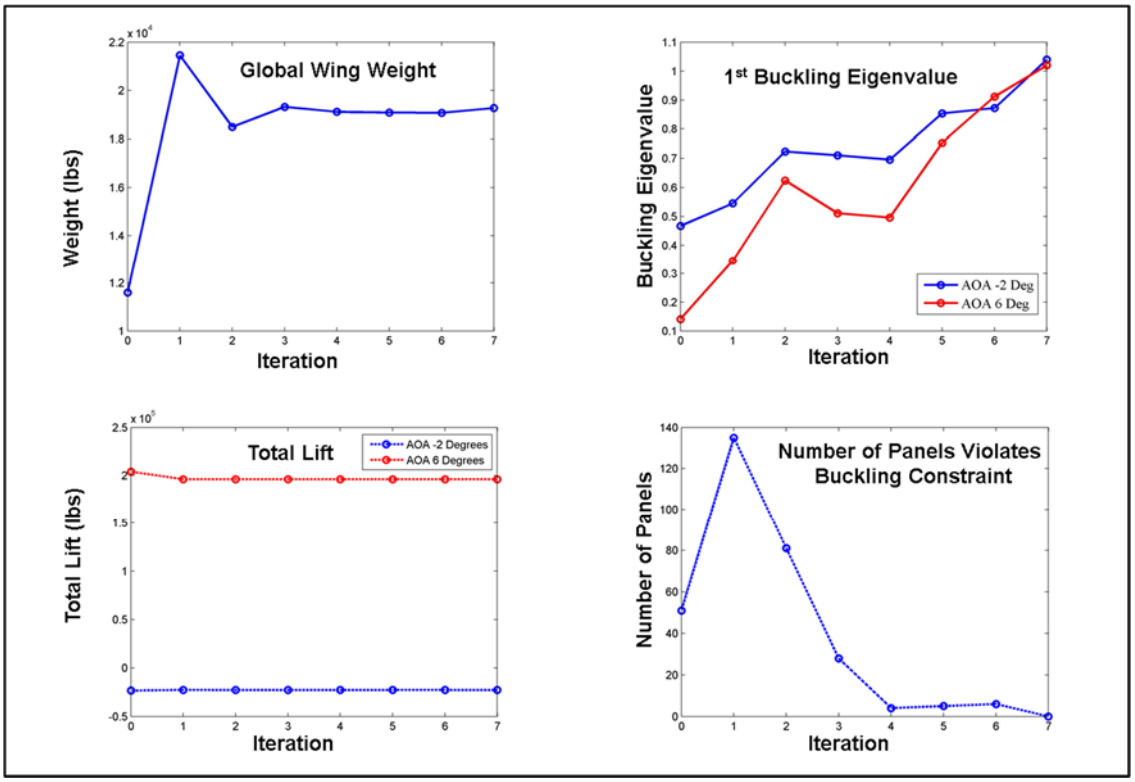

Figure 4.9: Convergence History of Un-Stiffened Panel Optimization of NASA CRM Wing

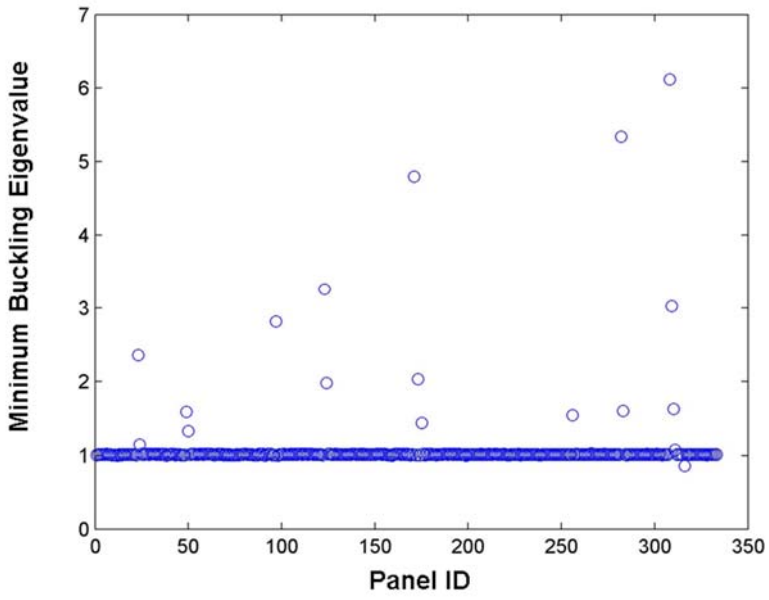

Figure 4.10: Fundamental Buckling Eigenvalues of Optimal Local Panels

The results in the Figure 4.9 show that the convergence criterion is satisfied in the sixth optimization iteration. However, the fundamental buckling eigenvalues of the global wing in the two load cases are around 0.9, which does not satisfy the buckling constraint. The panel thickness modification process, which is described in Figure 4.4, is performed for the CRM design obtained in the sixth iteration. The buckling eigenvectors of the first ten modes are computed in the buckling analysis of the global CRM wing. The thicknesses of the buckled local panels are modified using the formula shown in Eq. 4.4. An optimal wing design is obtained and two selected buckling mode shapes of the un-stiffened panel optimized design are presented in Figure 4.11. The corresponding buckling eigenvalues are 1.0066 and 1.0025 respectively. In the ideal wing design which is dominated by the buckling constraint, most local panels should buckle together, which also means most panels buckle in the same buckling mode. The buckling eigenvalues of the first ten buckling modes of the optimal CRM wing are presented in Table 4.3. In different global buckling mode shapes, the local buckling is observed in different regions. The result shows that buckling eigenvalues of the first ten modes are very close to 1. It means the un-stiffened CRM wing has been well optimized.

The distribution of optimal local panel thicknesses is shown in Figure 4.12. In the optimal design of CRM wing, the thicknesses of local panels decrease from wing root to wing tip. The results of von Mises stress distribution and displacement of the CRM wing are shown in Figure 4.13 and Figure 4.14, respectively. The maximum stress is observed in the region near the junction between the outer wing and the inner wing. The maximum von Mises stress is much higher than the yield stress of the material Aluminum alloy *2024-T3*. The displacement distribution shows that the unstiffened panel optimal CRM design can satisfy the max displacement constraints defined in the Chapter 3.

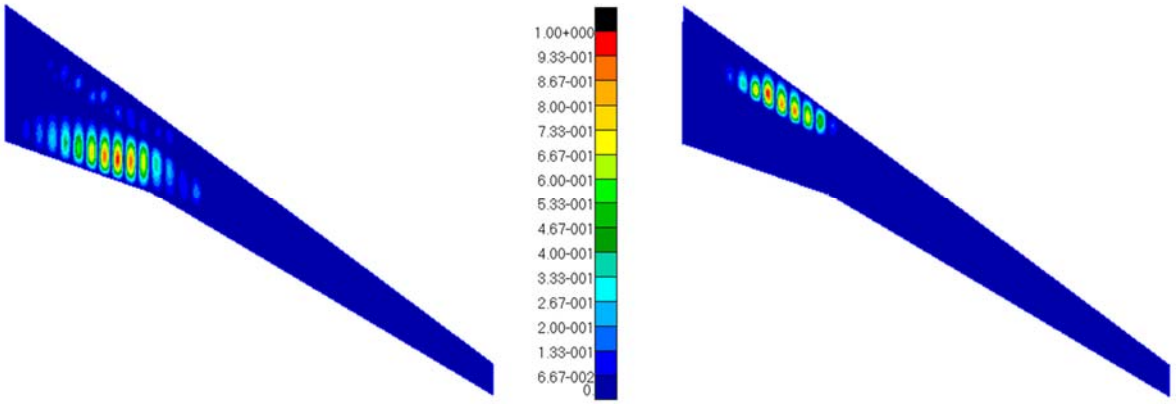

(a) Angle of Attack -2 Degrees, Lower Skin

Buckling Eigenvalue 1.0066

(b) Angle of Attack 6 Degrees, Upper Skin

Buckling Eigenvalue 1.0025

Figure 4.11: Buckling Mode Shapes of Un-Stiffened Panel Optimization Design

Table 4.3: Buckling Eigenvalues of the First Ten Modes

Mode	**AOA -2º**	**AOA 6º**
1	1.0009	1.0002
2	1.0016	1.0025
3	1.0055	1.0058
4	1.0066	1.0093
5	1.0083	1.0164
6	1.0093	1.0201
7	1.0098	1.0211
8	1.0123	1.0263
9	1.0199	1.0322
10	1.0289	1.0322

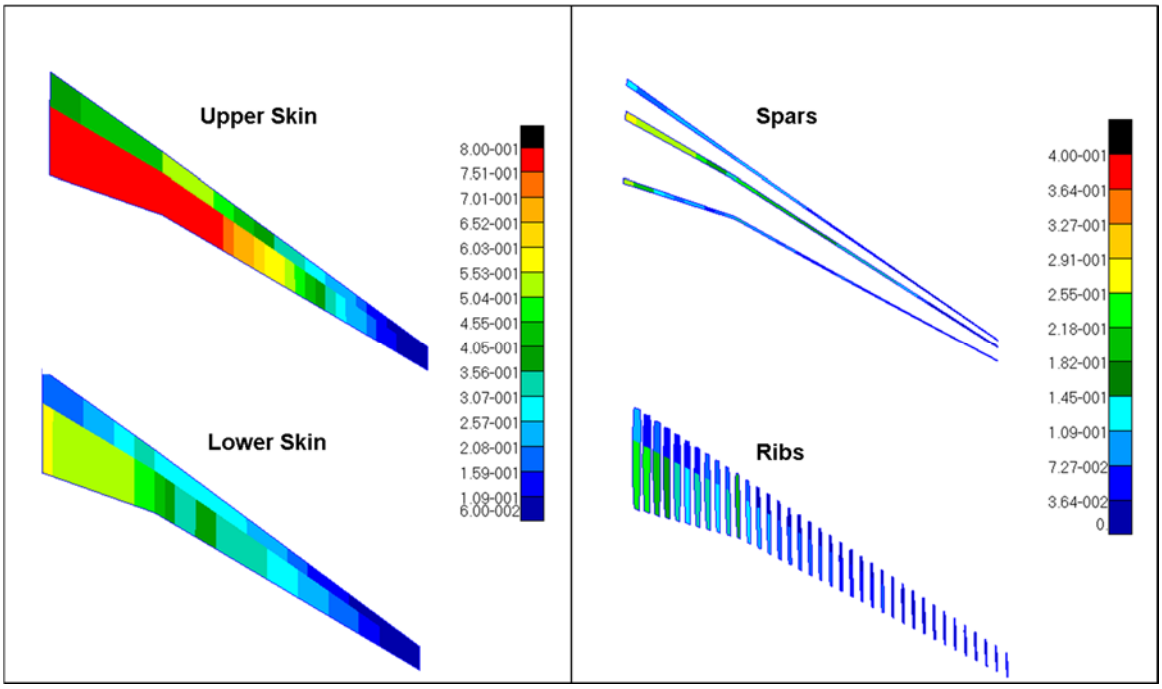

Figure 4.12: Optimal Thicknesses of Wing Panels

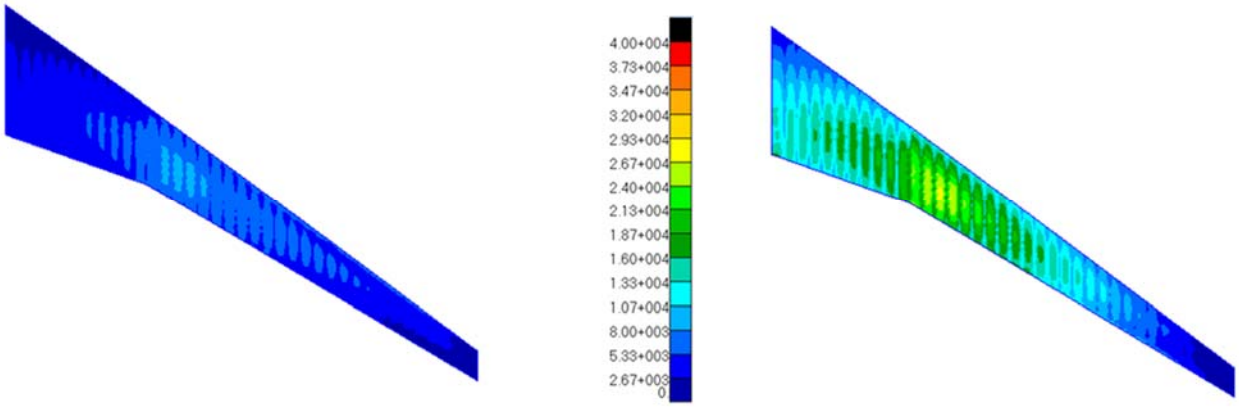

(a) Angle of Attack -2 Degrees, Lower Skin **(b) Angle of Attack 6 Degrees, Upper Skin**

Figure 4.13: von Mises Stress of Un-Stiffened Panel Optimization Design

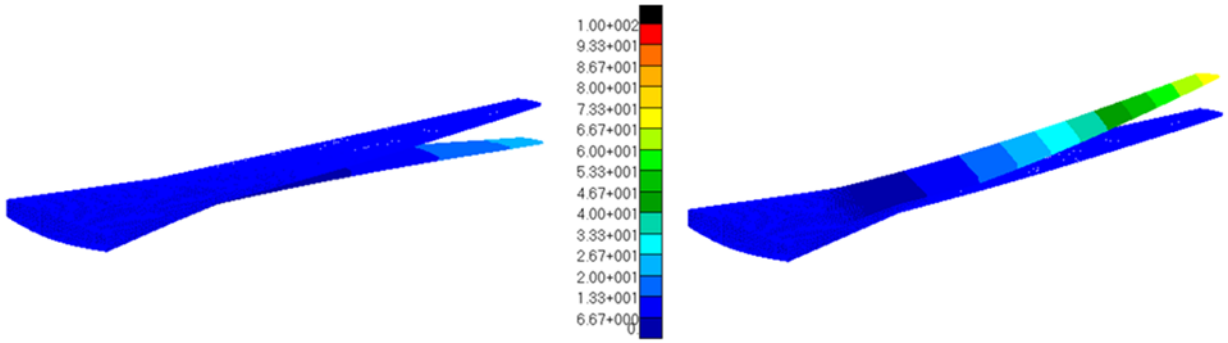

(a) Angle of Attack -2 Degrees **(b) Angle of Attack 6 Degrees**

Figure 4.14: Displacement in *Z* Direction of Un-Stiffened Panel Optimization Design

4.5 Summary

The local panel optimization framework ***EBF3PanelOpt*** has been developed and applied to the NASA CRM wing with un-stiffened panels. The thicknesses of un-stiffened local panels are optimized subject to the stress and buckling constraints. The boundary condition of panel buckling analysis is defined using the displacements of the grid points on the panel edges. An iterative panel optimization framework is developed while considering the interaction between the global wing model and the local panel model. The local panel optimization procedure has been applied to the baseline CRM design with 3 spars and 37 ribs provided by NASA, which does not satisfy the buckling constraint. The CRM has been optimized considering strength, buckling, and displacement constraints by optimizing the panel thickness. The results show that the buckling eigenvalue is the critical constraint for most of local panels. The un-stiffened panel optimization procedure shows its efficiency in minimizing wing weight with stress and buckling constraints.

Chapter 5

EBF3PanelOpt: Stiffened Panel Optimization

Optimization of stiffened panel with straight or curvilinear stiffeners has been implemented in the ***EBF3PanelOpt*** framework. Stiffeners are added on the panels to increase the rigidity and improve the buckling performance of local panels. The stiffened panel optimization is integrated in the ***EBF3PanelOpt*** framework, and has been applied to the optimization of NASA CRM wing considering stress and buckling constraints. The integration of global wing optimization and local panel optimization is discussed in this chapter. An approximate method has been developed for the stiffened panel optimization, in order to optimize both the global wing and local panel design variables at an acceptable computational cost. An efficient method for optimizing the curvilinear stiffeners is also presented in this Chapter.

5.1 Description of Stiffened Panel

The results of un-stiffened panel optimization show that buckling constraints are critical constraints for most of local panels. Therefore, there is potential to reduce the panel thickness as improving the buckling performance of panels using stiffeners. In the stiffened panel optimization, the local panels are extracted from the finite element model of the global wing structure. As shown in Figure 5.1, the blade stiffeners, which are modeled using shell elements, are added on the panels along the spanwise direction to resist the in-plane compression in the CRM wing skins. The geometry parameterization of stiffeners has been discussed in Chapter 2. The geometry of each stiffener is defined by 4 shape design variables that define the location and curvature, and 2 size design variables that define the height and thickness of the stiffener. The stiffened panel is meshed using a fine grid instead of the coarse grid used in the global model. The finite element model of panel and stiffeners is created using shell elements.

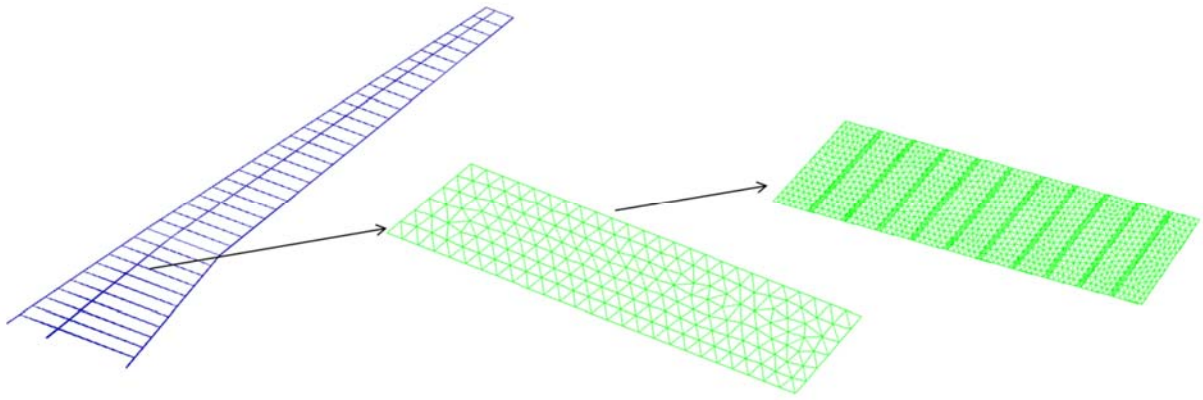

Figure 5.1: CRM Wing with Stiffened Panels

5.2 Interconnection between Global Wing and Stiffened Panel

In the stiffened panel optimization, the panel geometry is changed by adding the stiffeners on the panels, and panel thickness is also optimized. Then the global wing model needs to be updated using those optimized shape and size parameters of stiffened panels. The geometry of global model is rebuilt in two steps using finite element models of local panels: firstly, create panel surfaces using the local panel FE models; then create stiffener surfaces on the local panel using the optimal design variables obtained from stiffened panel optimization.

In the local panel analysis, the boundary conditions of local panels are defined using the displacements on the panel edges. Since the grid nodes of the stiffened panel model do not match the grids in the global model, the displacements on the panel edges need to be calculated by interpolation. Figure 5.2 illustrates the translational displacements that are applied on the panel edges as boundary conditions for the static and buckling analyses. The translational displacements are computed by interpolating the displacements of the coarse grid extracted from the global wing model onto the finer grid in the stiffened panel model.

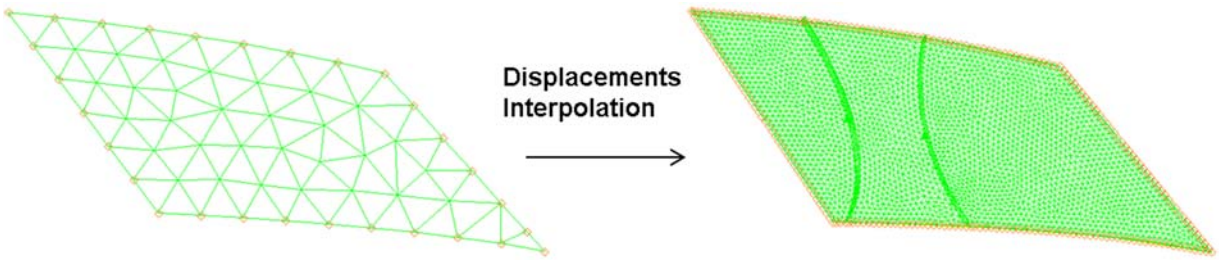

Figure 5.2: Boundary Condition of Stiffened Panel

The boundary condition of local panel analysis is defined using the translational displacements. The interpolation of the x, y, and z component of displacements are computed separately. Displacements at the panel edges are extracted from the global model results. Since the panel edges are not changed in the local panel optimization, the displacements at the four vertices of local panels are defined using the displacements at the same grid points in the global wing model. The second order Lagrange interpolation polynomial is used for the interpolation of displacements on the stiffened panel edges. The grid nodes on the panel edges are defined as set A. For each grid point on the stiffened panel edges, three nearest grid points are selected from the grids set A. As shown in Figure 5.3, the horizontal axis presents the distance from the new grid point, and vertical axis presents the displacement. The new grid node is shown in blue point. The static analysis is performed for the local panel with the boundary conditions defined using the interpolation method. The displacement and stress distribution computed in the local panel analysis have been compared with the results of the same panel obtained by global wing analysis, as shown in Figure 5.4. The comparison shows that the displacement and stress distribution of the reconstructed local panel are almost as same as the results extracted from the global wing model.

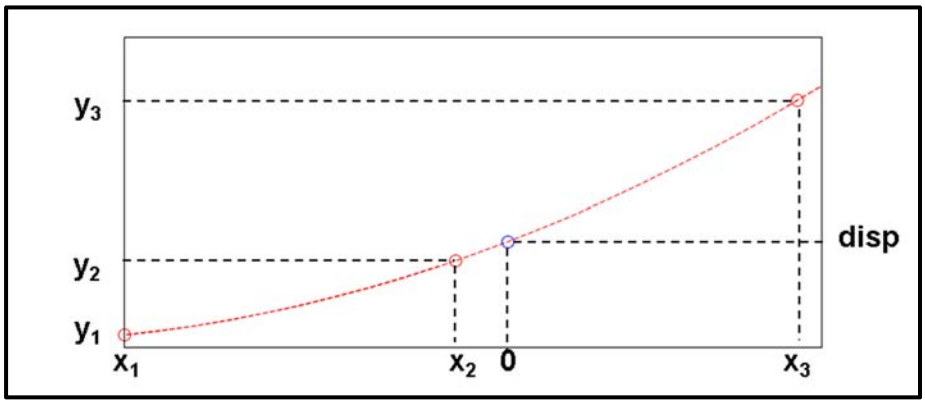

Figure 5.3: Interpolation of Displacements

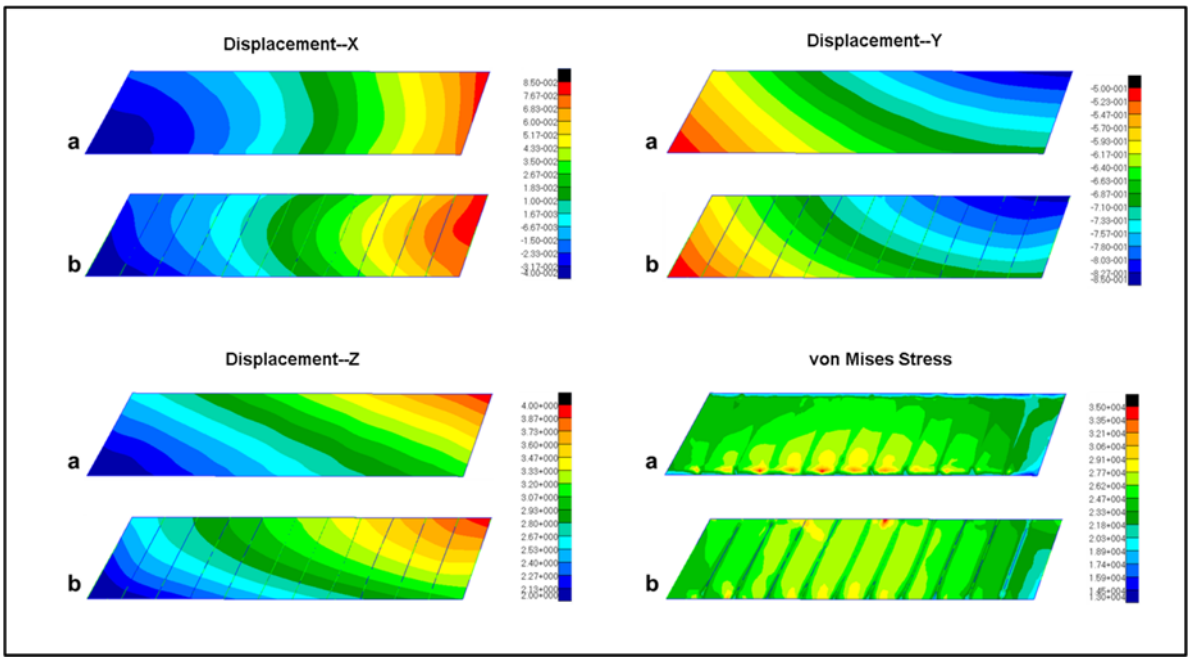

(a) Interpolation Results **(b) Results of Global Wing Analysis**

Figure 5.4: Comparison of Stress Distribution

5.3 Panel Thickness Optimization of Stiffened Panel

In the stiffened panel optimization, each local panel has a uniform thickness, which is optimized considering buckling and stress constraints. Several different types of stiffeners, such as blade, T shape and L shape stiffener, have been implemented in the ***EBF3PanelOpt***. In the case that the buckling eigenvalue is the critical constraint, the objective of stiffened panel optimization is to find the minimum plate thickness that leads the buckling eigenvalue to be greater than 1. As we have discussed in Chapter 1, the analytic solution of critical buckling stress of stiffened panel with a thin plate is shown in following formula.

$$\sigma_{\mathrm{CR}} = \mathrm{p}\left(\frac{t_{skin}}{b_{skin}}\right)^2 \tag{5.1}$$

where t_{skin} is the thickness of panel skin, and b_{skin} is the spacing between two adjacent stiffeners, p is a constant related to the panel dimension and material properties. This formula is only valid in the thin plate condition, which means that the plate is very thin relative to the size of the stiffeners. In that case, the buckling mode is constrained in the small region between the two adjacent stiffeners, as shown in case (a) of Figure 5.5. If the plate is very thin, the formulas in Eq. 4.8 can be used in the panel thickness optimization.

The effect of plate thickness on the buckling behavior of stiffened panels has been studied. The fundamental buckling mode shapes and eigenvalues of the stiffened panel with different panel thicknesses are shown in Figure 5.5 and Figure 5.6. The panel geometry and boundary conditions are the same in the buckling analyses, in other words the only difference is the plate thickness. As shown in Figure 5.5, the plate thickness increases from 0.15 inch to 1.0 inch, meanwhile the wavelength of the 1st buckling mode shape also increases from the spacing between two

stiffeners to the width of the panel. However, all the 1st buckling eigenvalues are close to 1. The reason is that the panel does not satisfy the thin plate condition, so the the 1st buckling mode shape exceeds the space between two adjacent stiffeners.

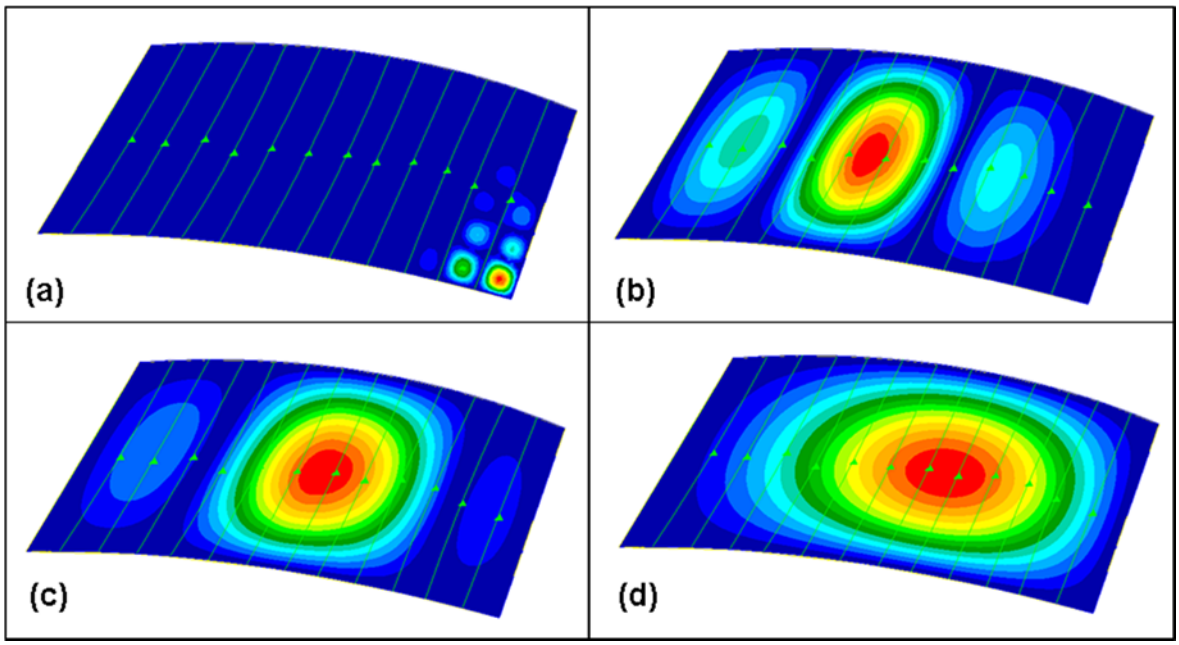

(a) plate thickness 0.15 in, 1st buckling eigenvalue 0.967 **(b) plate thickness 0.25 in, 1st buckling eigenvalue 0.991**

(c) plate thickness 0.50 in, 1st buckling eigenvalue 0.892 **(d) plate thickness 1.0 in, 1st buckling eigenvalue 0.973**

Figure 5.5: Fundamental Buckling Mode Shapes of Stiffened Panel

Figure 5.6 shows the fundamental buckling eigenvalues of three stiffened panels with plate thickness from 0.05 inch to 1.0 inch. In Figure 5.6 (a) and (c), only one crossing point is observed between the buckling eigenvalue curve and the horizontal line that presents buckling eigenvalue equals one. In Figure 5.6 (b), there are three points on the buckling eigenvalue curve where buckling eigenvalues equal 1. The corresponding plate thickness at the first crossing point is around 0.15 inch, which is the optimal plate thickness for that stiffened panel optimization. For all of the three panels shown in Figure 5.6, if the plate thickness is less than 0.2 inch, the

fundamental buckling eigenvalue is approximately proportional to the square of plate thickness. That means the thin plate condition is valid in that thin plate region, and the buckling mode shape is localized in the small pocket between stiffeners. In Figure 5.6 (c), the buckling eigenvalues in the thin plate region are much smaller than one. Therefore, in order to optimize that stiffened panel, the stiffener size, such as stiffener height and thickness, should be increased so as to constrain the buckling in the local pockets between adjacent stiffeners. In the stiffened panel optimization procedure, a small value is selected as the initial trial plate thickness, then the buckling analysis is carried out and the panel thickness optimization method discussed in Chapter 4 is used to search for the optimal panel thickness subject to stress and buckling constraints.

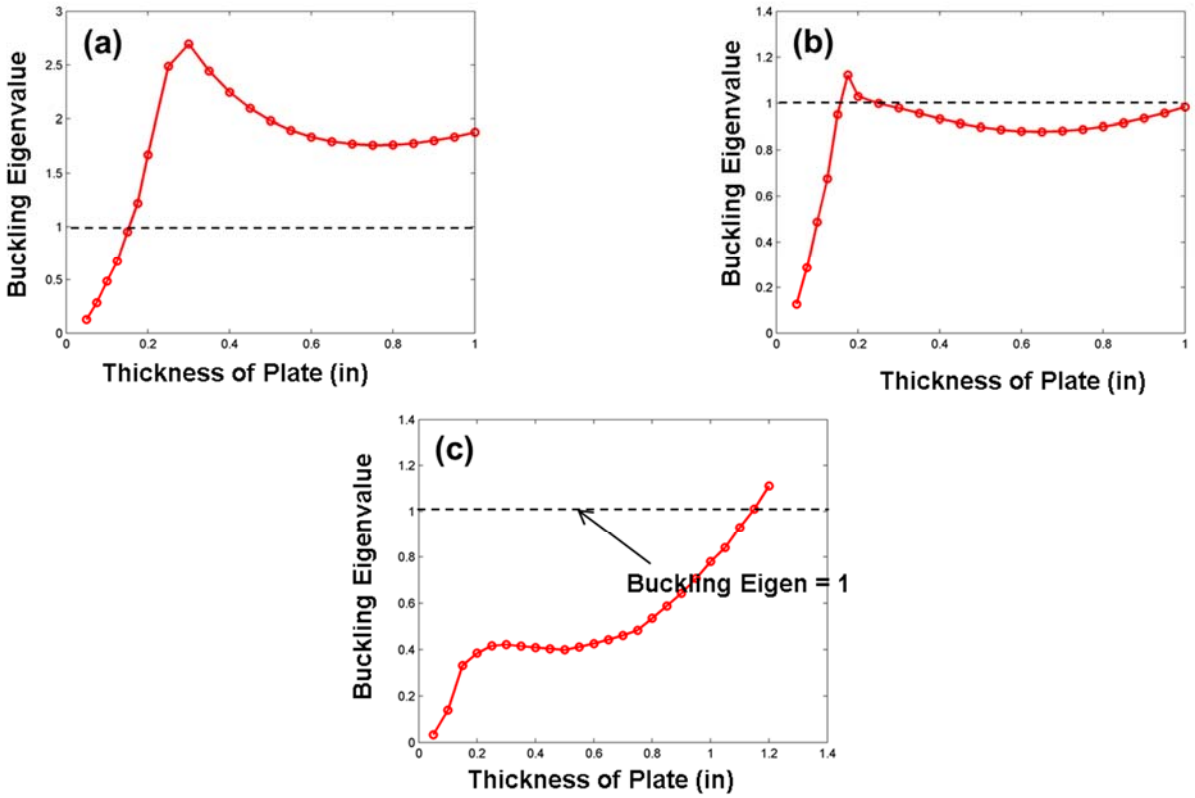

Figure 5.6: Fundamental Buckling Eigenvalues of Stiffened Panel

Figure 5.7 illustrates the searching process of the optimal thickness of stiffened panel. Firstly, a small value is selected as the trial panel thickness to satisfy the thin plate requirement. For instance, 0.1 inch is selected as the initial panel thickness in this optimization process. Then the fundamental buckling eigenvalue is carried out for the stiffened panel with the corresponding boundary conditions. If the 1st buckling eigenvalue satisfies the constraint, the searching process is stopped and output the optimal panel thickness. If the buckling eigenvalue does not satisfy that criterion, the panel thickness is optimized and the new buckling eigenvalue is computed again. A move limit is applied to the panel thickness as the discussion about panel thickness optimization in Chapter 4. That stiffened panel thickness optimization process has been implemented and integrated into ***EBF3PanelOpt***.

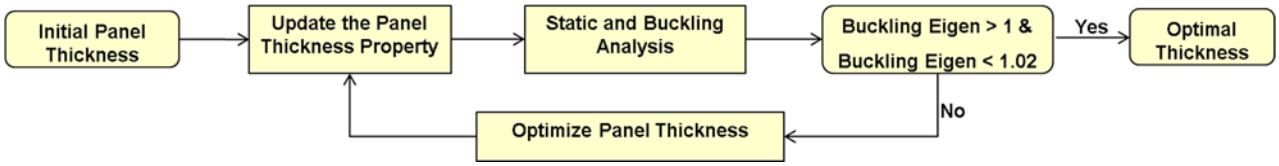

Figure 5.7: Process of Stiffened Panel Thickness Optimization

5.4 Effect of Stiffener Size in the Stiffened Panel Optimization

We know that the stiffeners can improve the buckling performance of stiffened panel by restraining the local buckling mode in the small pockets between adjacent stiffeners. As shown in Figure 5.8 (a), the panel is stiffened by evenly distributed stiffeners with a height of 3 inch and a thickness of 0.3 inch. The panel thickness is optimized to be 0.24 inch. The corresponding fundamental buckling eigenvalue of the stiffened panel is 1.01, which is calculated with a boundary condition applied to the panel edges. Then reducing the stiffener height to 2 inch, we

performed the buckling analysis for the same panel. The fundamental buckling eigenvalue becomes 0.67 and the buckling mode shape is presented in Figure 5.8 (b). The comparison shows that the stiffener size has significant effect on the buckling performance of the stiffened panel. In the stiffened panel optimization, proper stiffener height and thickness need to be found at an acceptable computational cost.

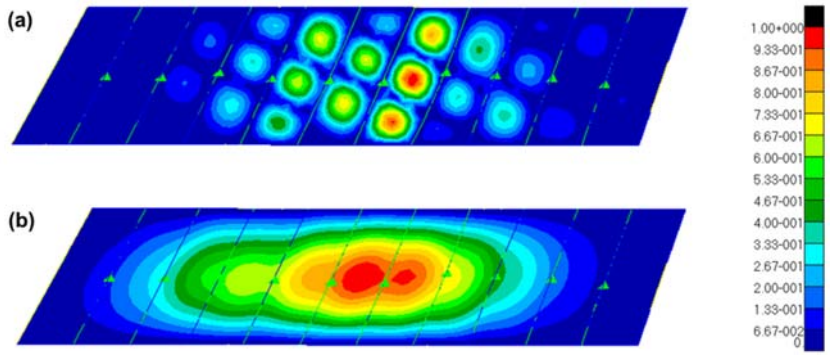

Figure 5.8: Buckling Mode Shapes of Stiffened Panels with Different Stiffener Height

5.5 Number of Stiffeners

The number of stiffeners on the stiffened panel is an important factor for the buckling behavior of the panel. As has been discussed in Chapter 1, for a thin plate, the critical buckling stress is related to the ratio of plate thickness and the spacing between two adjacent stiffeners. That means the buckling performance of stiffened panel can be improved by adding more stiffeners. However, the total weight of stiffened panel may increase because of the increased weight of stiffeners.

A study of a stiffened panel is performed to find the best number of stiffeners to minimize the panel weight subject to stress and buckling constraints. As shown in Figure 5.9, the parallel

stiffeners are placed on the panel evenly along the spanwise direction. The number of stiffeners is changed from 4 to 20. The panel thickness is optimized to make the fundamental buckling eigenvalue approach 1. All the analyses are carried out with a same boundary condition and panel geometry. The optimal stiffened panel weights, which include the weight of plate and stiffeners, and corresponding fundamental buckling eigenvalues are presented in Table 5.1 and Figure 5.10. The optimal panel weight decreases dramatically in the region in which the number of stiffeners is less than 10. Then the panel weight curve becomes relatively smooth with the increment in the number of stiffeners. The minimum optimal panel weight is observed in the panel with 18 stiffeners.

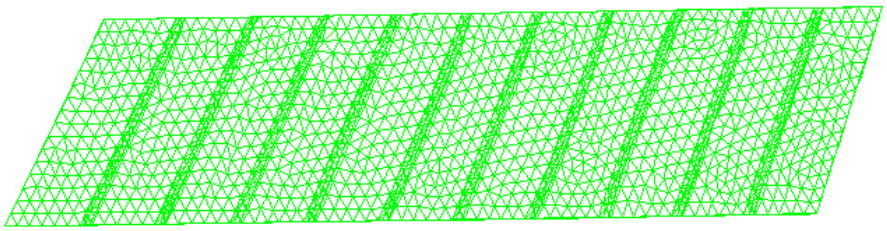

Figure 5.9: Stiffened Panel with 10 Stiffeners

Table 5.1: Effect of Number of Stiffeners in the Stiffened Panel Optimization

Number of Stiffeners	4	8	12	16	18	20
Avg. Stiffener Spacing (inch)	29.3	14.6	9.8	7.3	6.5	5.9
1st Buckling Eigenvalue	1.005	1.007	1.002	1.005	1.003	1.004
Stiffened Panel Weight (lbs)	196.4	117.0	93.7	84.9	83.1	84.2

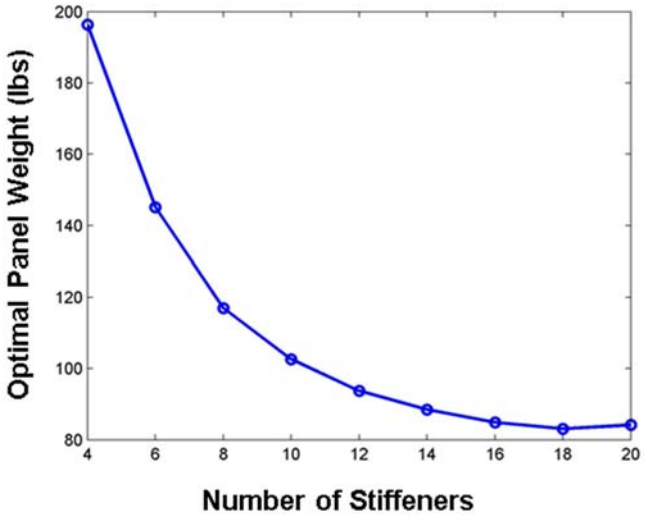

Figure 5.10: Number of Stiffeners in the Stiffened Panels

In the aircraft structure design, the spacing between stiffeners is constrained by the panel size and the manufacturing cost. In this research, all the stiffeners are placed on the wing skin panels. A different number of stiffeners are added on the panels with different size. More stiffeners are added onto the larger size panels which are close to the wing root. Considering there are hundreds of local panel in the CRM wing, finding the optimal stiffeners number of each local panel using the above optimization process becomes computationally unacceptable. Furthermore, reducing the stiffener spacing also means increasing the manufacturing cost. Therefore, the number of stiffeners in stiffened panel is determined using the following requirement: the average distance between adjacent stiffeners is about 12 inch.

5.6 Stiffened Panel Optimization Procedure

The global-local stiffened panel optimization has been performed for the CRM wing with 37 straight ribs, the wing has been presented in the un-stiffened panel optimization of Chapter 4. Similar as the un-stiffened panel optimization, the stiffened panel optimization process consists of global wing analysis, which calculates the aerodynamic loads and displacements of the global CRM wing model, and the stiffened panel analysis, that carries out the static and buckling analyses for each stiffened panel. The finite element model of stiffened CRM wing is constructed using shell elements to present the wing panels and stiffeners. Blade stiffeners are added on the wing skin panels to increase the axial stiffness and improve the buckling performance. In the global wing analysis, the grid points at the wing root are fixed. Then as similar as the unstiffened panel optimization, a global static and buckling analysis is carried out to check the stress and buckling constraints, and generate the global displacement fields for the next iteration of the stiffened panel optimization. In this research, the stiffened panel thickness is optimized to minimize the stiffened panel weight using the similar approach of panel thickness optimization that was discussed in Chapter 4. In each optimization cycle, the global CRM model is updated using the optimal design variables obtained in local panel optimization. The boundary conditions of stiffened panels are also updated in each optimization cycle. A minimum thickness requirement of 0.05 inch is applied to all the local panels. As shown in Eq. 5.2, the convergence criterion is defined using the number of panels that violate the stress or buckling constraint, and the relative change of total wing weight in the optimization cycle.

Number of Panels Violate Constraint < 3

$$\frac{|w_i - w_{i-1}|}{w_i} < 0.2\% \tag{5.2}$$

The thickness and height of the stiffeners in each panel are uniform. In order to find the proper stiffener size without increasing too much computational time, only six stiffener height and thickness combinations are considered in the stiffened panel optimization: (2, 0.1), (2, 0.2), (3, 0.2), (3, 0.3), (4, 0.3), (4, 0.4); the first and second values are the stiffener height and thickness in inch, respectively. The proper stiffener size can be selected by the process illustrated in Figure 5.11. The initial stiffener height is given by the initial panel thickness. Then the panel thickness optimization is carried out as the iterative optimization process discussed in Figure 5.7. If the final fundamental buckling eigenvalue does not satisfy the buckling constraint, a higher or thicker stiffener size combination will be selected to substitute for the previous values.

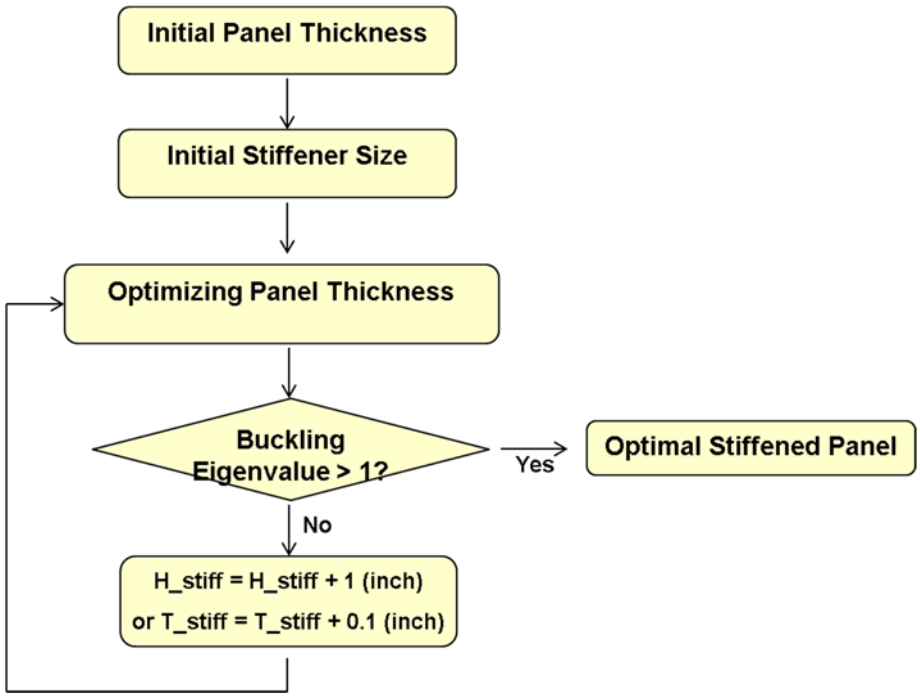

Figure 5.11: Optimization Process of Stiffener Size

Parallel computing using multiple processors can be implemented in the local panel optimization to reduce the computational time. Since the CRM wing has been decomposed into hundreds of local panels, the design variables of each stiffened panel are not related to the design variables of the other panels. The parallel computing procedure is developed using MATLAB and Python programming to incorporate the MSC.PATRAN and MSC.NASTRAN.

5.7 Results of Stiffened Panel Optimization of CRM Wing

The stiffened panel optimization is applied to the NASA CRM wing with 3 spars and 37 ribs. A comparison of the optimal structural weight of the un-stiffened and stiffened CRM design has been shown in Table 5.2. The CRM wing is optimized subject to strength and buckling constraints in both of the two optimization procedures. Compared to the un-stiffened panel optimization result, the stiffened panel optimization reduces the structural weight of the CRM design by 39.8 %. The computational cost of local panel optimization is very high. Although parallel computing has been implemented in the optimization process using eight processors, the CPU time of stiffened panel optimization is still more than 5 hours. Figure 5.12 shows the comparison of the optimal panel thickness in the CRM wing skins. Figure 5.13 shows the optimal panel thickness in the spars and ribs in the stiffened CRM wing. The thickness results show a trend that the panel thicknesses decrease from the wing root to the wing tip. The convergence history of the stiffened panel optimization, which is presented in Figure 5.14, shows that the wing weight has been reduced dramatically in the first iteration that causes a large number of panels to violate the buckling constraint. The wing weight changes slowly in the following iterations. The convergence criterion is finally satisfied in the fourth iteration. Figure

5.15 shows that only one panel violates the buckling constraint in the design obtained in the fourth iteration. The minimum thickness constraint is active in about 20 panels, which makes the corresponding buckling eigenvalues to be greater than 1. The von Mises stress and displacement distribution are shown in Figure 5.16 and Figure 5.17 respectively. The buckling analysis is performed for the optimal CRM wing and the fundamental buckling mode shapes are presented in Figure 5.18.

Table 5.2: Results of Local Panel Optimization

	Un-Stiffened Design	**Stiffened Design**
Optimal Weight (lbs)	19,269	11,593 (39.8% saving)
CPU Time (min)	140	340

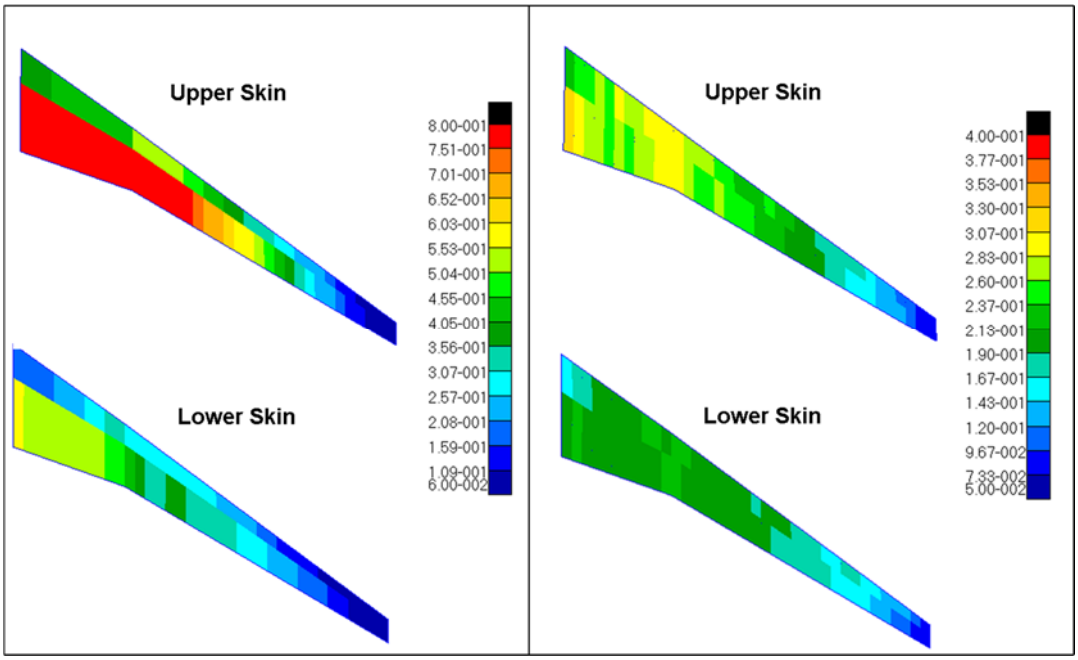

(a) Thickness Distribution in Un-Stiffened CRM Wing Skins **(b) Thickness Distribution in Stiffened CRM Wing Skins**

Figure 5.12: Thickness Distribution of Un-Stiffened and Stiffened NASA CRM Wing

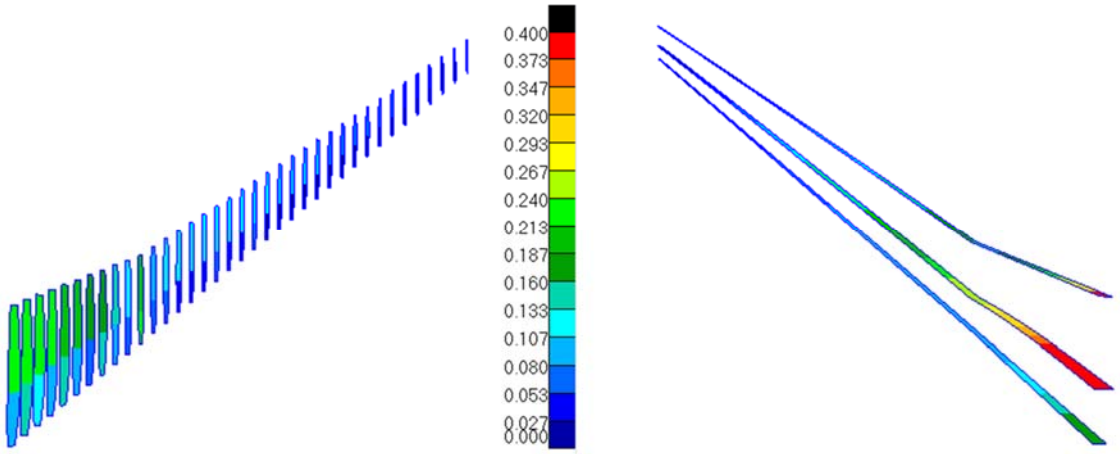

Figure 5.13: Optimal Thickness of Spars and Ribs of Stiffened NASA CRM Wing

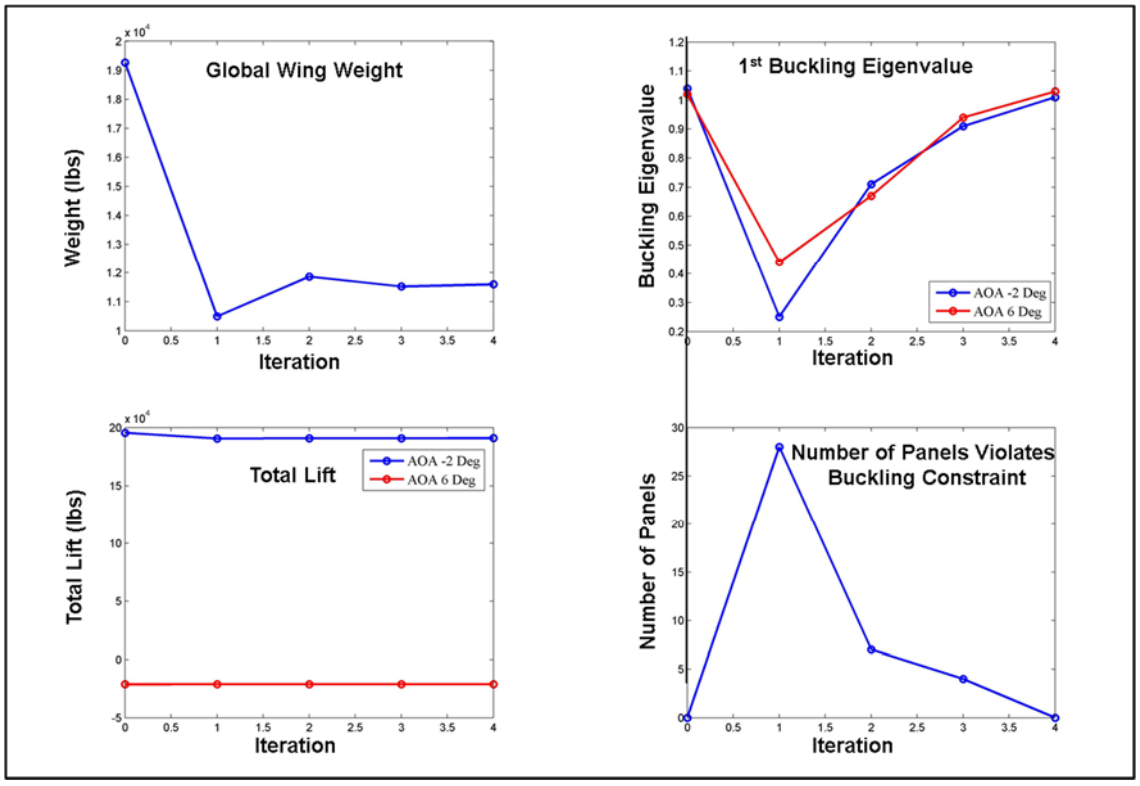

Figure 5.14: Convergence History of Stiffened Panel Optimization of NASA CRM Wing

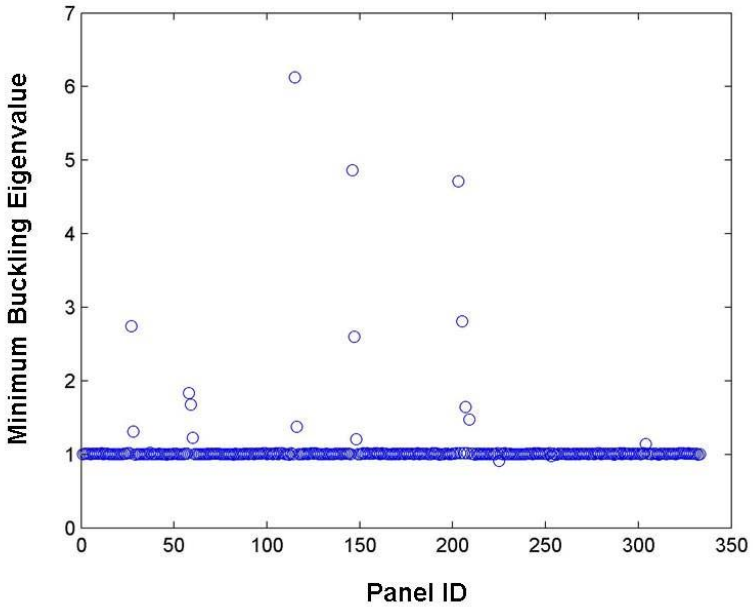

Figure 5.15: Fundamental Buckling Eigenvalues of Optimal Local Panels

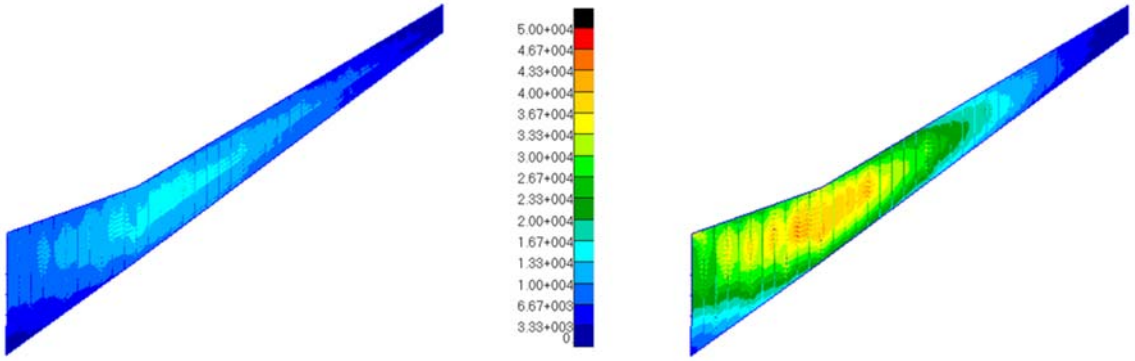

(a) Angle of Attack -2 Degrees, Lower Skin **(b) Angle of Attack 6 Degrees, Upper Skin**

Figure 5.16: von Mises Stress of Stiffened Panel Optimization Design

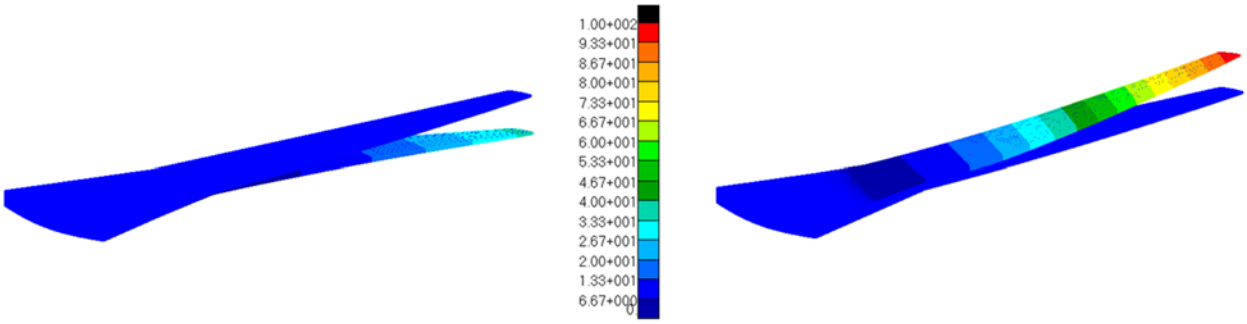

(a) Angle of Attack -2 Degrees **(b) Angle of Attack 6 Degrees**

Figure 5.17: Displacement in Z Direction of Stiffened Panel Optimization Design

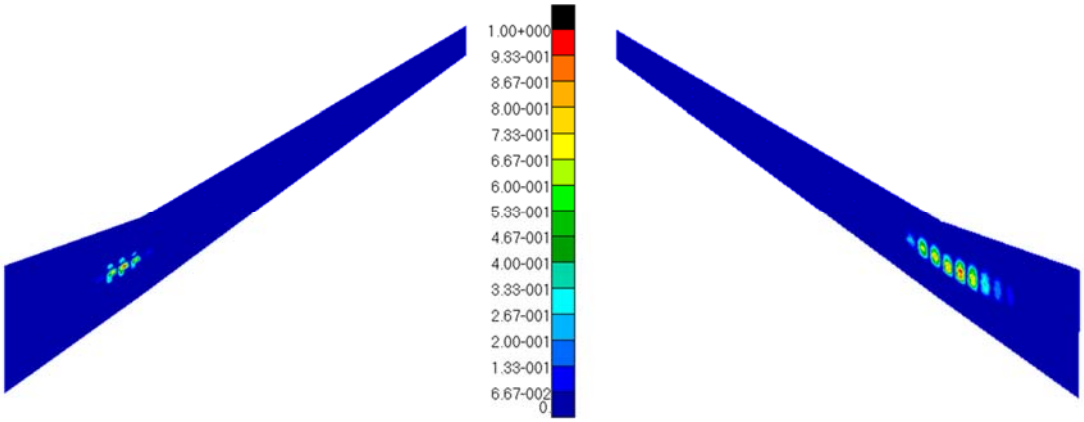

(a) Angle of Attack -2 Degrees, Lower Skin

1st Buckling Eigenvalue 1.038

(b) Angle of Attack 6 Degrees, Upper Skin

1st Buckling Eigenvalue 1.001

Figure 5.18: Fundamental Buckling Mode Shapes of CRM Design with 37 Ribs

5.8 Integration of Global Wing and Local Panel Optimization

5.8.1 Global-Local Optimization Framework

In the local panel optimization, the local panels are optimized by the ***EBF3PanelOpt*** and the global wing model is updated using these optimal parameters of the local panels. However, the global wing topology, such as the number and shape of spars and ribs, is not optimized by the ***EBF3PanelOpt***. In order to search the best combination of global wing design variables and local panel design variables, both global wing optimization and local panel optimization should be incorporated into an integrated optimization framework. The objective of the optimization is to minimize the wing weight subject to stress, buckling and flutter constraints. The design variables in the global-local optimization framework can be decomposed into topology variables of global wing and local panel design variables. The global wing topology variables include the design variables which determine the number of spars and ribs (termed numerical variables), and the design variable which define the shape of spars and ribs (termed shape variables). The local panel variables are optimized in local panel optimization with a set of fixed global wing design variables. As illustrated in Figure 5.19, the optimal weight of stiffened wing can be computed using a set of global variables which define the geometry of spars and ribs. The geometry of global wing with curvilinear spars and ribs is created using a set of numerical variables and topology design variables in the ***EBF3WingOpt***. Then in the stiffened panel optimization, the optimal weight of the wing structure is computed by optimizing the local panel design variables, such as the panel thickness, height and thickness of stiffeners, and curvature of stiffeners.

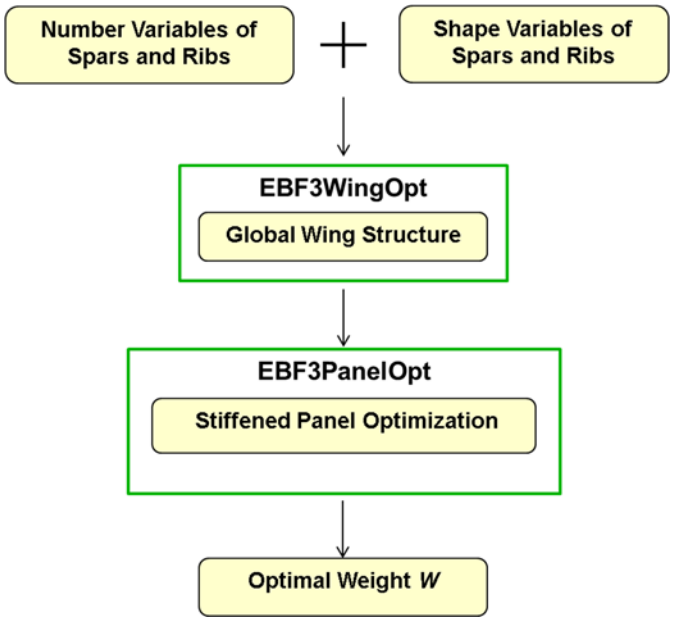

Figure 5.19: Optimal Weight Calculation of Stiffened CRM Wing

In this research, the integration of global wing optimization and local panel optimization is implemented using a two-step optimization approach, which is presented in Figure 5.20. In the first step optimization, the number of the spars and ribs are optimized, and a set of global shape variables of the spars and ribs are fixed. In this optimization stage, the ribs are distributed evenly in each wing box. The local panel variables of the aircraft wing are optimized in the stiffened panel optimization so as to minimize the structural weight. The optimal wing weight is sent to the optimizer. Then the number of spars and ribs are optimized using particle swarm optimization (PSO) to find the aircraft wing design with minimum weight. A convergence criterion is defined for the iterative global-local optimization as the relative change of optimal wing weight is less than 1% in two consecutive iterations.

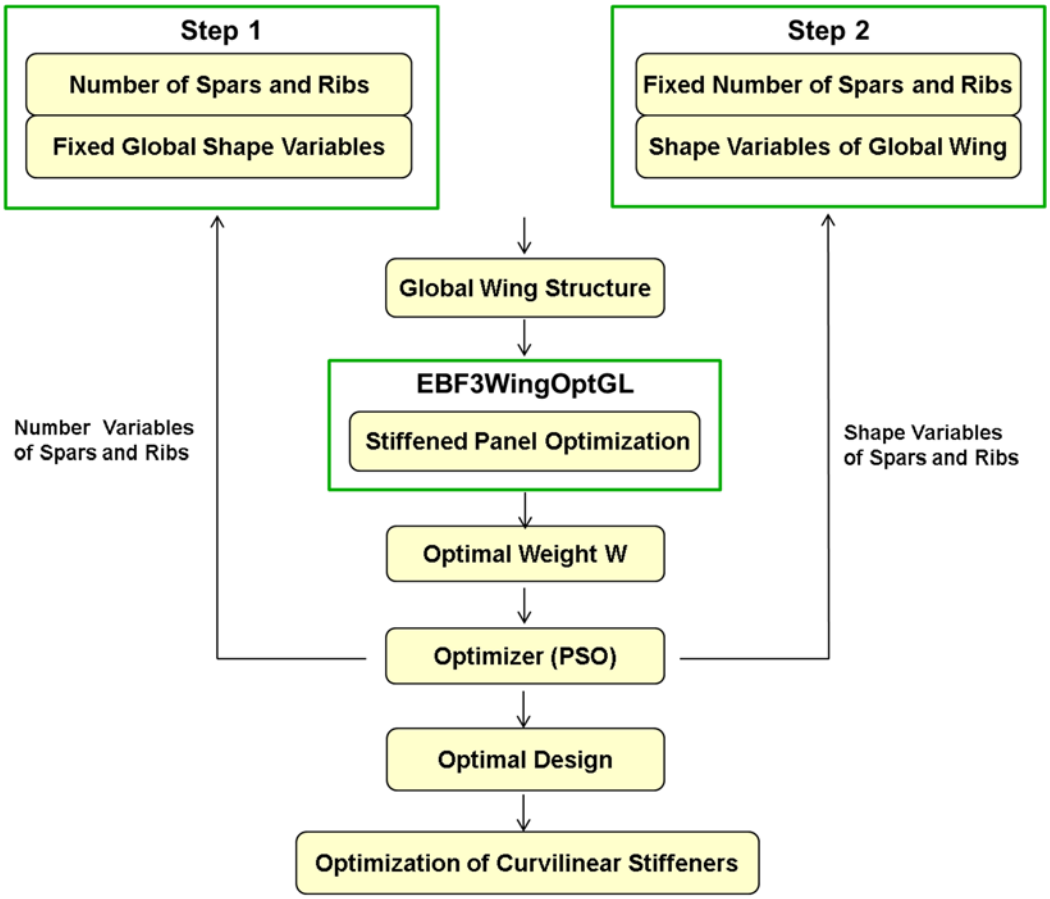

Figure 5.20: Integrated Global-Local Optimization Framework

In the second optimization step, the shape variables of spars and ribs are optimized with the fixed numerical variables of spars and ribs, which are obtained in the first step optimization. The shape variables of spars and ribs are subjected to the constraints in Table 3.7. Similar to that in the first step, the wing structure with curvilinear spars and ribs, which is constructed using the ***EBF3WingOpt*** module, is optimized using ***EBF3PanelOpt*** to output the optimal weight of that wing design to the optimizer. Compare to the numerical variables of global wing, the wing shape variables have a much more complex design space, which means the computational cost of shape optimization of spars and ribs is much higher. The parallel computing has been implemented for

the local panel optimization using MATLAB to reduce the CPU time. An optimal wing design with straight stiffeners can be obtained through the first and second step optimization. Then the stiffened panels are optimized using curvilinear stiffeners to improve the buckling performance and minimizing the structural weight.

5.8.2 Approximate Stiffened Panel Optimization

The integration between global wing optimization and local panel optimization is computationally expensive. A more efficient panel optimization approach needs to be developed to reduce the computational cost. In the global-local optimization, the objective of stiffened panel optimization is to find the optimal weight of the CRM design with fixed wing internal topology. We are concerned about the optimal wing weight rather than the details of the stiffened CRM wing, an approximate method can be used to find the approximate optimal wing weight with a much less computational cost, compared to the stiffened panel optimization discussed earlier in this chapter. In the previous thickness distribution results obtained by local panel optimization, the panel thickness decreases from the wing root to the wing tip. This trend means that the thickness of a certain panel can be guessed using the thicknesses of its nearby panels. In other words, we do not need to run the static and buckling analyses for all the hundreds of local panels in the CRM wing to optimize the thicknesses of the local panels. In this case, the computational cost of stiffened panel optimization can be reduced dramatically. In this research, an approximate method is developed so as to find the approximate stiffened panel design variables in a more efficient way. In each optimization cycle of the local panel optimization, only 20% ~ 25% selected panels are optimized by the stiffened panel analysis. The approximate

thicknesses of other panels can be obtained using a third order polynomial curve that fits to those optimized panel thicknesses.

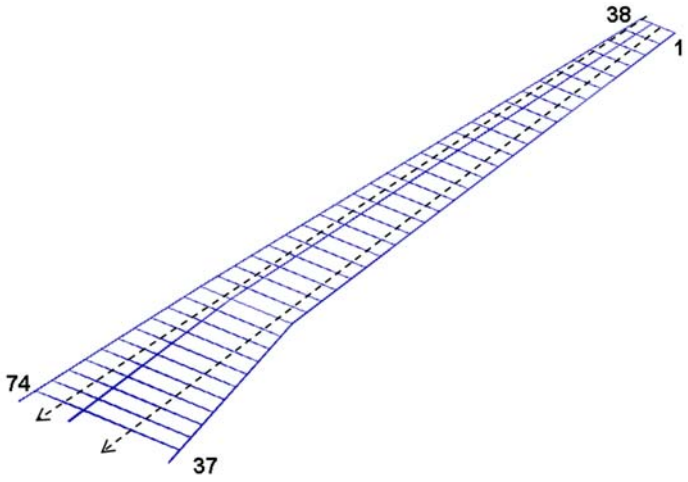

Figure 5.21: Upper Skin Panels

The approximate optimization approach has been applied to optimize the thickness of the upper skin panels in the CRM wing with 3 spars and 37 ribs. As shown in Figure 5.21, the upper skin panels are divided into two groups: panels No. 1 to 37 in 'Group 1' are close to the trailing edge, and panels No. 38 to 74 in 'Group 2' are close to the leading edge. Five evenly distributed panels are selected in each panel group and optimized by stiffened panel analysis. Then a third order polynomial curve is created by fitting to the five panel thicknesses in each group. The thicknesses of other panels are computed using the third order polynomial. The comparison of the actually optimized panel thickness and approximately optimized thickness calculated by the polynomial curve fitting are shown in Figure 5.22. Compared to the results of stiffened panel optimization, the errors of total weight of the two panel groups obtained using the approximate approach are 1.2% and -2.3% respectively.

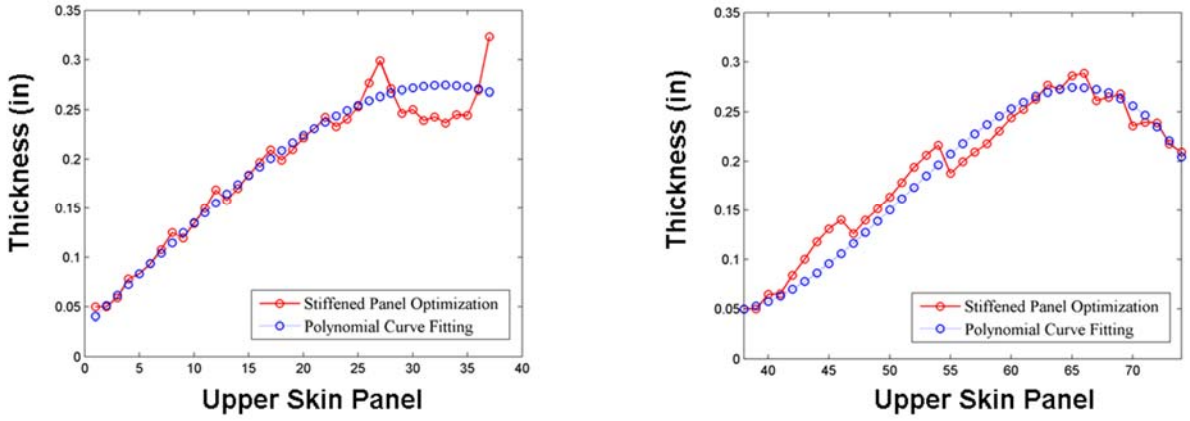

(a) Upper Skin Group 1, Error of Weight 1.2% **(b) Upper Skin Group 2, Error of Weight -2.3%**

Figure 5.22: Comparison of Optimal Thickness of Upper Skin Panels

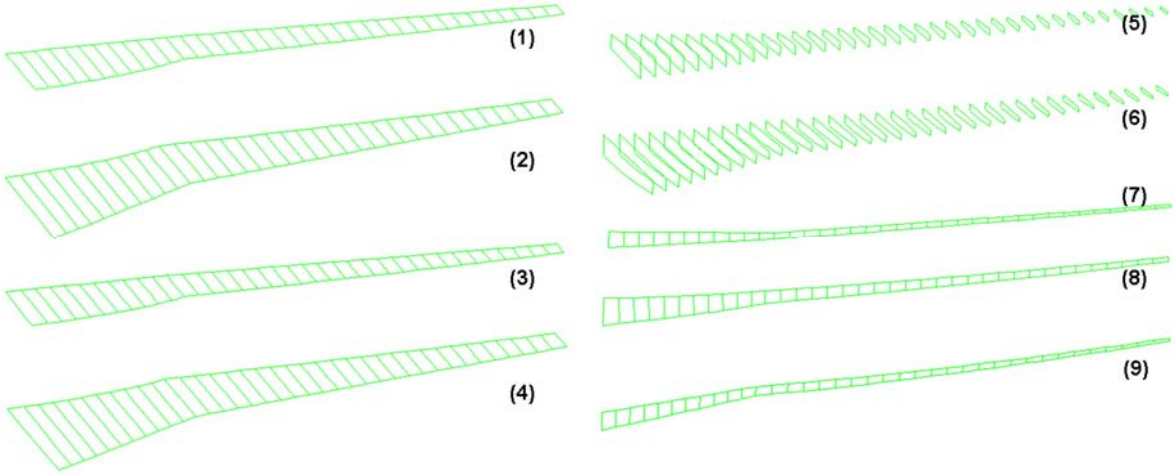

Figure 5.23: Decomposition of CRM Wing Panels

In the approximate stiffened panel optimization approach, the panels of the CRM wing with 3 spars are decomposed into 9 groups as shown in Figure 5.23. The panels in each group locate along the spanwise direction. The approximate panel optimization and the previous stiffened panel optimization are carried out for each group of panels. The error of the approximate optimal weight has been calculated and shown in Table 5.3. All the optimal weight errors of the panel

groups are less than 3%. Table 5.4 shows the computation time of the approximate optimization is only 135 minutes compared to 340 minutes using the stiffened panel optimization. Parallel computing are performed using eight processors in the two optimization cases. The error of approximate optimal weight of the CRM wing is about 0.7%.

Table 5.3: Error of Approximate Stiffened Panel Optimization of Panel Groups

Panel Group	**1**	**2**	**3**	**4**	**5**	**6**	**7**	**8**	**9**
Approx. Optimal Weight(lb)	1585	2587	1181	1856	727	1922	305	942	408
Optimal Weight (lb)	1622	2556	1205	1885	738	1917	310	945	416
Relative Error(%)	-2.3	1.2	-2.0	-1.5	-1.5	0.3	-1.6	-0.3	-0.2

Table 5.4: Comparison of Computation Time

	Stiffened Panel Optimization	Approximate Panel Optimization
Optimal Weight(lb)	11,593	11,514
CPU Time(min)	340	135

The approximate stiffened panel optimization has been applied to several CRM wing designs to evaluate the errors of wing weight. Based on the results, the distribution of the weight errors of panel groups can be considered as a random distribution between -3% and 3%. Since there are 9 groups in a CRM wing with 3 spars, the error of the total weight of CRM can be estimated using Eq. (5.3).

$$error = \left(\sum_{i=1}^{9} \boldsymbol{\delta_i m_i}\right) / \left(\sum_{i=1}^{9} \boldsymbol{m_i}\right) \tag{5.3}$$

where $-\mathbf{3}\% < \boldsymbol{\delta_i} < \mathbf{3}\%$, $\boldsymbol{m_i}$ is the weight of the ith group of panels. The cumulative probability distribution of the wing weight error of approximate panel optimization is calculated using the

Equation 5.8. As presented in Figure 5.24, the error of the optimal weight of the CRM wing is less than 1.04% with 90% confidence. This error of optimal wing weight is acceptable in the global-local stiffened panel optimization.

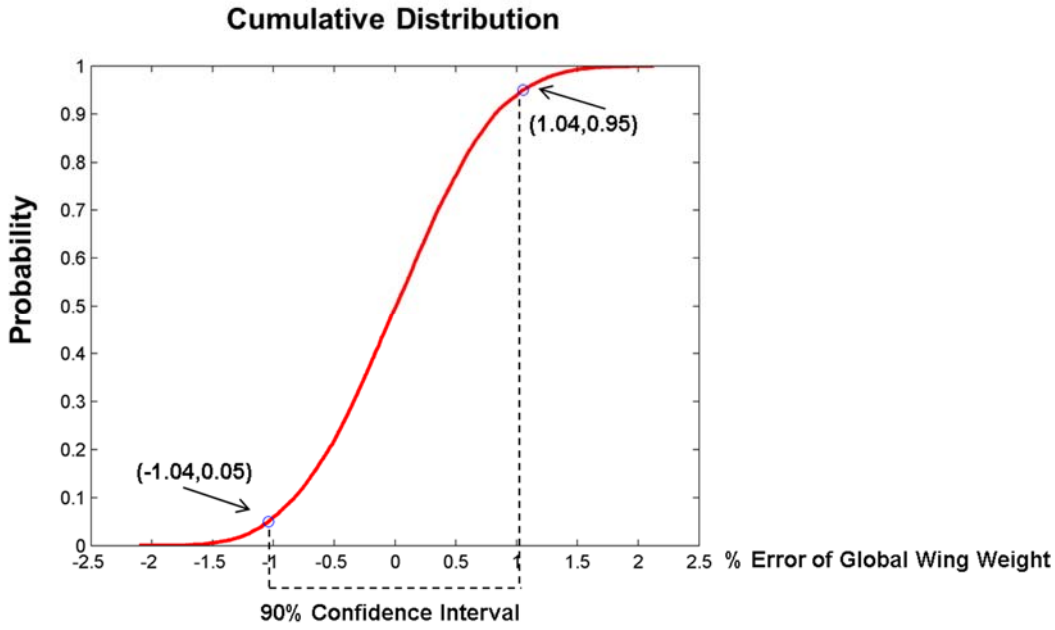

Figure 5.24: Cumulative Probability Distribution of Weight Error

5.8.3 Initial Panel Thickness

Initial panel thicknesses should be defined in the local panel optimization. The computational cost of the iterative optimization procedure can be saved by choosing proper panel thicknesses. In the approximate panel optimization of stiffened CRM wing, initial panel thicknesses are computed using the interpolation of panel thicknesses. The panel thickness interpolation is illustrated in Figure 5.25. The CRM wing with 3 spars and 37 ribs has been optimized in stiffened panel optimization and the optimal panel thicknesses are known. A new CRM design with 20 ribs is created using given global wing design variables. The coordinates of the panel

centroids in the two CRM wings are calculated. A third order polynomial curve is created by fitting to the optimized panel thicknesses and corresponding Y-coordinates of panel centroids of the CRM wing with 37 ribs. Then the initial panel thickness in the CRM wing with 20 ribs can be calculated using the corresponding Y-coordinates of panel centroids and the fitted polynomial.

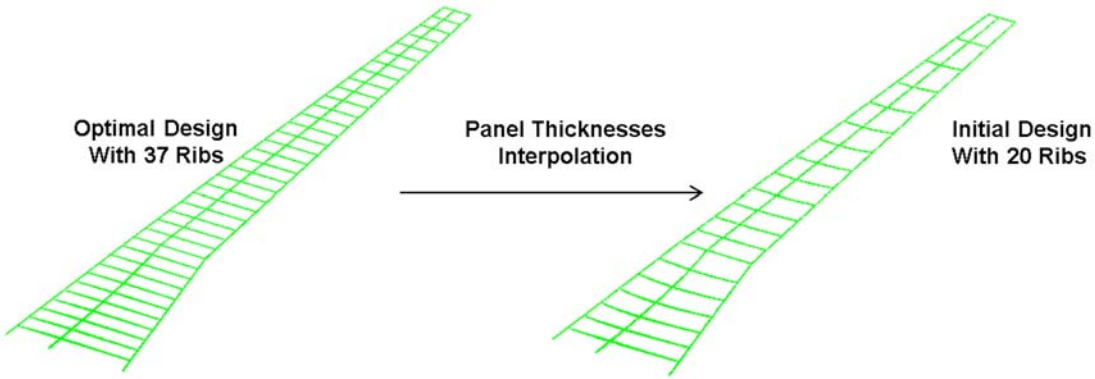

Figure 5.25: Initial Panel Thickness Calculation of Stiffened Panel Design

5.8.4 Results of Integrated Global-Local Optimization

The integrated global-local optimization is performed for the CRM wing. In this optimization case, the three spars of the CRM wing are fixed. Considering the relatively poor bucking performance of large size local panels, the number of ribs in inner wing and outer wing are given independently and subject to the following constraints:

$$6 \leqslant \text{Number of Ribs in Inner Wing} \leqslant 12$$

$$10 \leqslant \text{Number of Ribs in Outer Wing} \leqslant 30 \qquad (5.4)$$

The finite element model of CRM designs are created in global wing module ***EBF3WingOpt*** using the global wing design variables, and are optimized by the approximate stiffened panel optimization to evaluate the optimal weight of the CRM wing. As presented in Figure 5.20, the integrated global-local optimization is organized using a two-step approach. The first step of the

global-local optimization procedure is performed for the CRM wing with three spars. The number of ribs in each wing box is optimized using particle swarm method. Five design particles are created and analyzed in each optimization cycle. A converged optimal design is obtained in the fifth iteration. The minimum wing weight obtained in each iteration is presented in Figure 5.26.

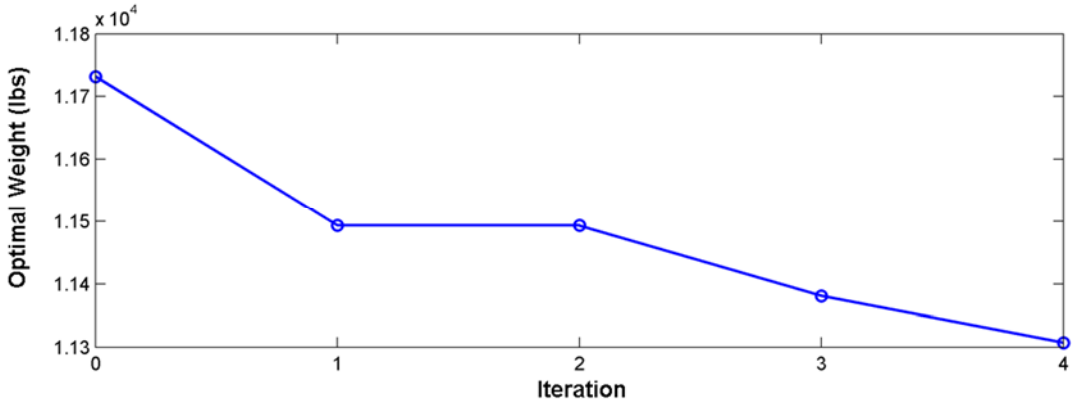

Figure 5.26: Convergence History of Optimal Wing Weight

The optimal wing weights of the 25 CRM designs optimized by the approximate stiffened panel optimization are shown in Figure 5.27. The CRM wing with less than 20 or more than 40 ribs are much heavier than the optimal design. The reason is a wing structure with too less ribs also has large size skin panels, which is usually relatively poor in buckling resistance. That means the thicknesses of those large size panels have to be increased to resist the panel buckling.

The minimum wing weight 11,307 lb is observed in the CRM wing with 9 inner wing ribs and 17 outer wing ribs. The details of the optimal CRM wing, including the local panels and stiffeners, are shown in Figure 5.28. Different numbers of blade stiffeners are placed on the wing skin panels along the spanwise direction. Figure 5.29 presents the optimal panel thicknesses of the wing skins, spars and ribs. The thicknesses of the panels close to wing tip have approached the

lower bound of 0.05 inch. The mid-spar panel that is close to the wing root has the highest thickness which of 0.43 inch.

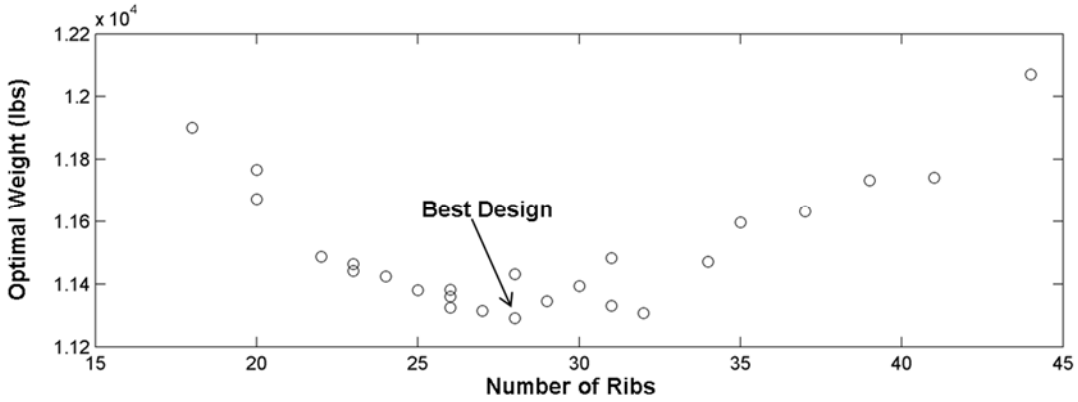

Figure 5.27: Approximate Optimal Weight of CRM Wing with Stiffened Panels

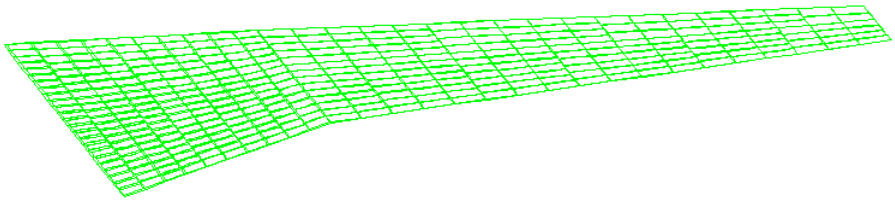

Figure 5.28: Geometry of CRM Wing with 9 Inner Wing Ribs and 17 Outer Wing Ribs

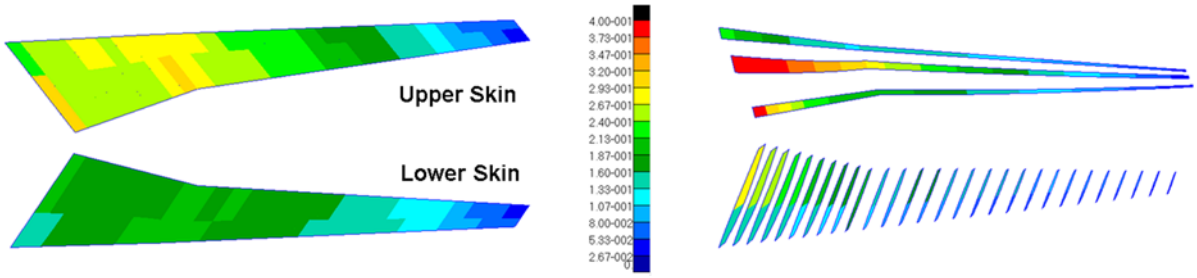

Figure 5.29: Thickness Distribution of Optimal CRM Design

The buckling and flutter analyses are performed for the optimal CRM design to check the buckling and dynamic flutter constraints. The static aeroelastic stress is evaluated using Kreisselmeier- Steinhauser (KS) criteria [85]. The dynamic pressure of the onset of flutter is also calculated and presented in Table 5.5. The optimal CRM wing satisfies all the constraints. Because of the complex design space of shape variables, the computational cost of the second step optimization, which optimizes the shape variables of spars and ribs, is very expensive. Currently, the second step optimization of the global-local framework is not performed for the CRM wing. Parallel computing has been implemented in the stiffened panel optimization using MATLAB programming. The drawback of the MATLAB parallel computing is only 12 processors can work simultaneously. In future, the parallel computing will be developed in Python environment to improve the computational efficiency.

Table 5.5: Constraints of Optimal CRM Design

Constraints	**Optimal Design**	**Low Bound**	**Up Bound**
M0.85 AOA -2 Degree KS	0.253	NA	1
M0.85 AOA 6 Degree KS	0.842	NA	1
1st Buckling Eigenvalue AOA -2 Degree	1.041	1.0	NA
1st Buckling Eigenvalue AOA 6 Degree	1.027	1.0	NA
Flutter Dynamic Pressure (psi)	9.68	2.1	NA

5.9 Optimization of Panel with Curvilinear Stiffeners

In the stiffened panel optimization described previously, the quasi-straight stiffeners are evenly distributed on the wing panels. In order words, the shape of stiffeners is not optimized in the optimization process. Most of the previous research studies about the stiffener topology optimization focus on a single stiffened panel and typical load cases, such as uniform compressive, tensile or shear loads, as shown in Figure 5.30. For the local panels in the CRM wing, the actual loads applied on the panel edges are non-uniform and more complicated. Computationally expensive evolution algorithms, such as genetic algorithm and particle swarm optimization, are widely used in the shape optimization of stiffeners. The common situation is that thousands of stiffened panel analyses are required to find the optimal design of the single stiffened panel. Considering there are hundreds wing panels in the CRM wing, an efficient optimization tool is needed to optimize the panel with curvilinear stiffeners at an acceptable computational cost.

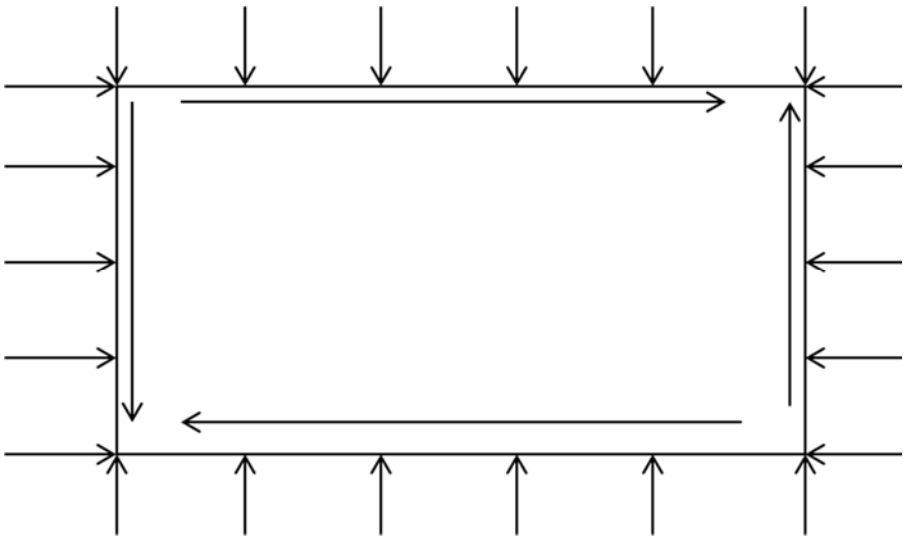

Figure 5.30: Typical Load Cases of Panels

In this section, the wing panels are optimized using curvilinear stiffeners to improve the buckling performance and minimize panel weight. The curvilinear stiffeners are parameterized using *Linked Shape Method* so as to reduce the number of design variables. As illustrated in Figure 5.31, three parameters are used to define a set of curvilinear stiffeners on a wing panel. The locations of starting points are determined by the ratio of the two spacing *Space_1_s* and *Spar_9_s*. The control point line is the mid-line between the top edge and the bottom edge of that panel. The control points are determined by the ratio of *Space_1_c* and *Spar_9_c*. The locations of ending points are computed using the end points ratio. As shown in Table 5.6, only five design variables are required to define the curvilinear stiffeners on one panel. The height and thickness of the stiffeners are uniform.

Table 5.6: Design Variables in Curvilinear Stiffener Optimization

DV1	Stiffener Height
DV2	Stiffener Thickness
DV3	Start Points Ratio
DV4	Control Points Ratio
DV5	End Points Ratio

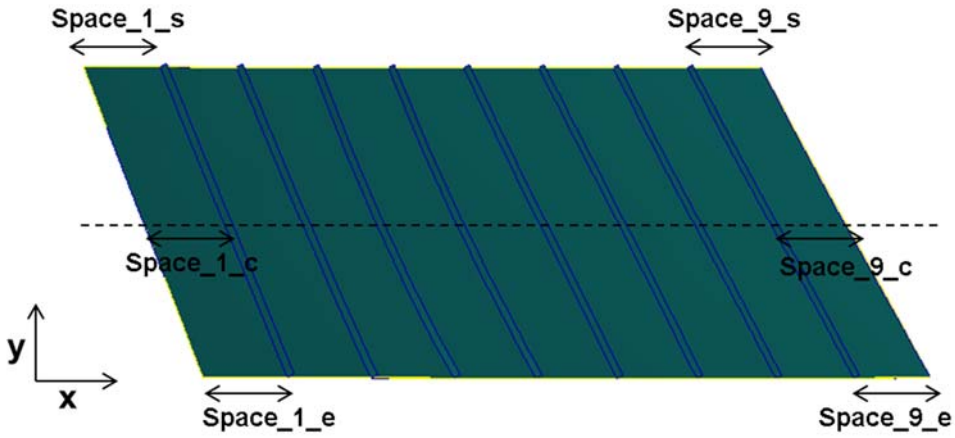

Figure 5.31: Geometry Parameterization of Curvilinear Stiffeners

The optimization procedure for the curvilinear stiffener optimization is presented in Figure 5.32. Two flight conditions are considered for the CRM wing: angle of attack is -2 degrees or 6 degrees. The shape design variables of curvilinear stiffeners are generated for creating the geometry of stiffened panel. The size design variables of curvilinear stiffeners are created to define the height and thickness of stiffeners. The panel thickness is optimized using the panel thickness optimization process described earlier in this chapter. The response values, such as panel weight, fundamental buckling eigenvalue, maximum von Mises stress are sent to the optimizer for generating the new design variables for the next optimization cycle. The curvilinear stiffened panel optimization is implemented using two optimization schemes: particle swarm optimization, and a two-step gradient optimization method. The particle swarm optimization is carried out with 20 particles. The convergence history of the first 200 iterations is shown in Figure 5.33. The optimal weight of the stiffened panel is 157.4 lbs, which is much heavier than the initial stiffened panel with evenly distributed quasi-straight stiffeners.

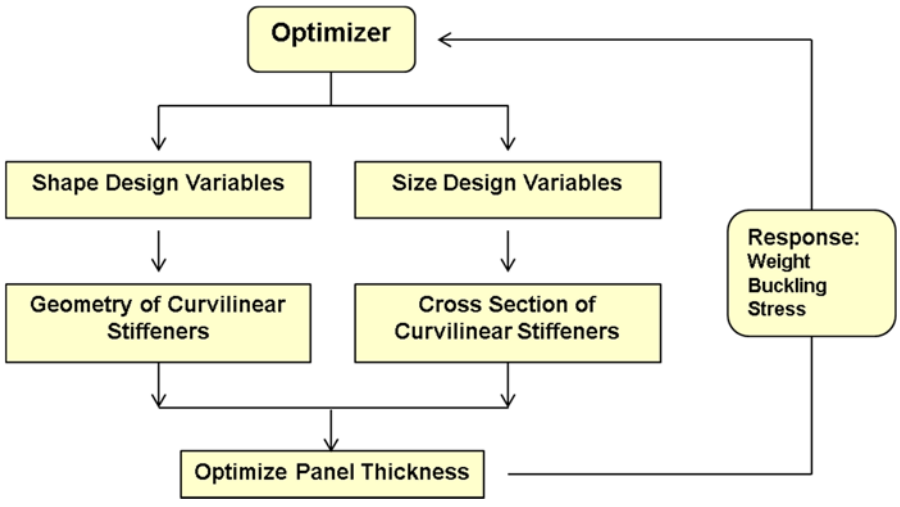

Figure 5.32: Optimization Procedure of Curvilinear Stiffeners

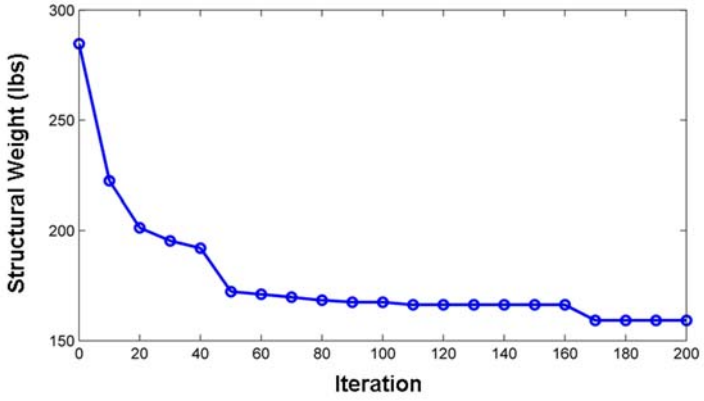

Figure 5.33: History of Curvilinear Stiffeners Optimization Using PSO

The stiffened panel is also optimized using a two-step method based on the initial design. In the first step, the spacing between those stiffeners is optimized using gradient method to minimize the panel weight subject to the stress and buckling constraints. The stiffener shape is not optimized in this step. Then the shape variables of stiffeners are optimized in the second step to obtain curvilinear stiffeners, also using gradient optimization method. The optimal panel weight and computational time are presented in Table 5.7. It shows that the panel weight has been reduced by the two-step method at about 10% computational cost compared to the PSO method.

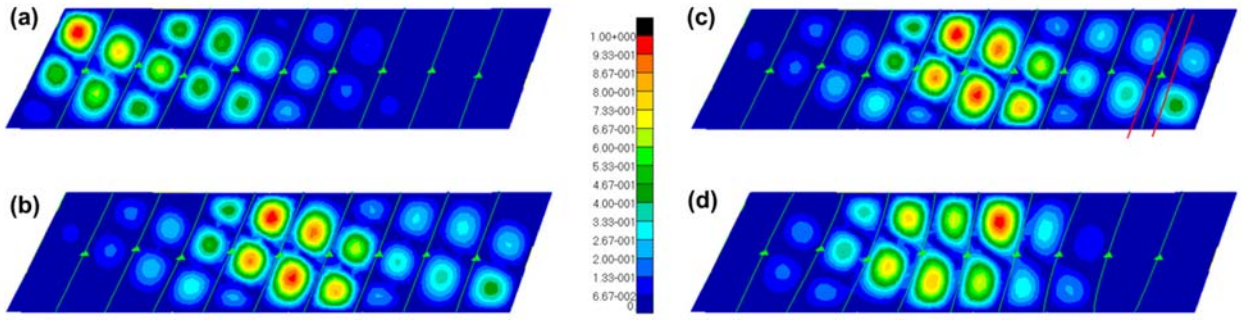

Figure 5.34: Curvilinear Stiffener Optimization Using Two-Step Approach

Table 5.7: Optimization Results of Curvilinear Stiffened Panel

	Initial Design	PSO	1st Step Optimum	2nd Step Optimum
Panel Weight (lbs)	105.5	157.4	103.1	101.9
1st Buckling Eigenvalue	1.003	1.005	1.003	1.001
CPU Time(min)		615	37	26

In the optimal stiffened panel, it is observed that the stiffeners are not very curved. Some stiffened panels obtain by PSO method have very curved stiffeners but much poorer buckling performance. As we know, the optimal placement of stiffeners depends on the stress distribution in the panel. In order to study this problem, a static analysis is carried out for an example local panel with spanwise stiffeners. As shown in Figure 5.35, the X and Y stress components of the stiffened panel are compressive, in which case the stress in the Y component is dominant. The Y component dominant compressive stress distribution is also observed in most of other wing skin panels. This phenomenon can explain the optimal curvilinear stiffeners locate along the spanwise direction.

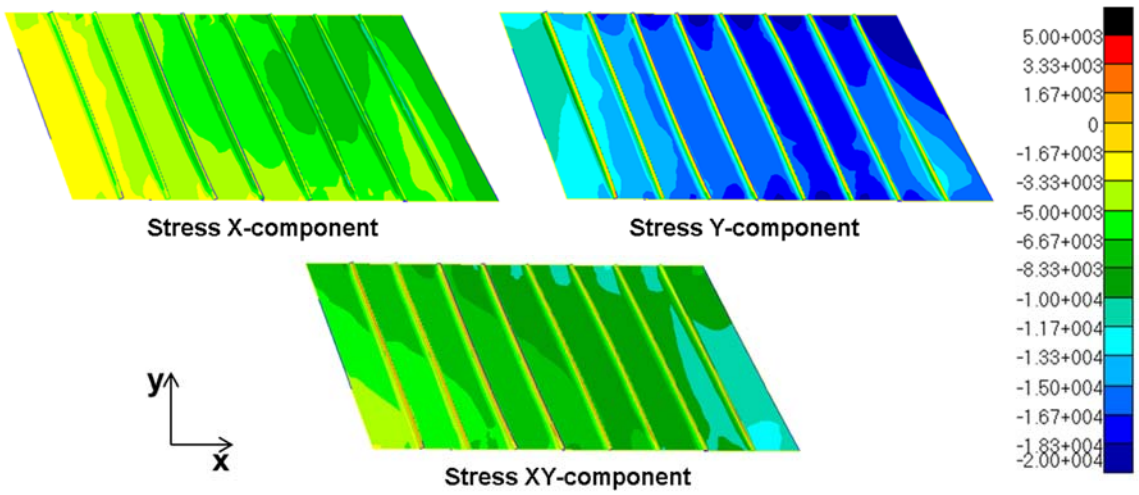

Figure 5.35: Stress Resultant of an Example Stiffened Panel

We have known that the optimal shapes and positions of curvilinear stiffeners depend on the stress distribution in that stiffened panel. The stress distribution computed in the static analysis is not used in the previous optimization process. There is potential to improve the efficiency of stiffener optimization by incorporating the stress distribution in the optimization process. The analytic solution of critical buckling stress of a rectangular stiffened plate has been described in the previous chapters, as shown in Eq. 5.5. Therefore, the Eq. 5.6 can be derived to describe the relation between the spacing between two adjacent stiffeners and the longitudinal compressive stress in the pocket bordered by the two stiffeners.

$$\sigma_{CR} = \frac{k\pi^2 E}{12(1-v^2)}\left(\frac{t_{skin}}{b_{stiff}}\right)^2 \tag{5.5}$$

$$\frac{spacing_i}{spacing_j} = \left(\frac{\sigma_j}{\sigma_i}\right)^{1/2} \tag{5.6}$$

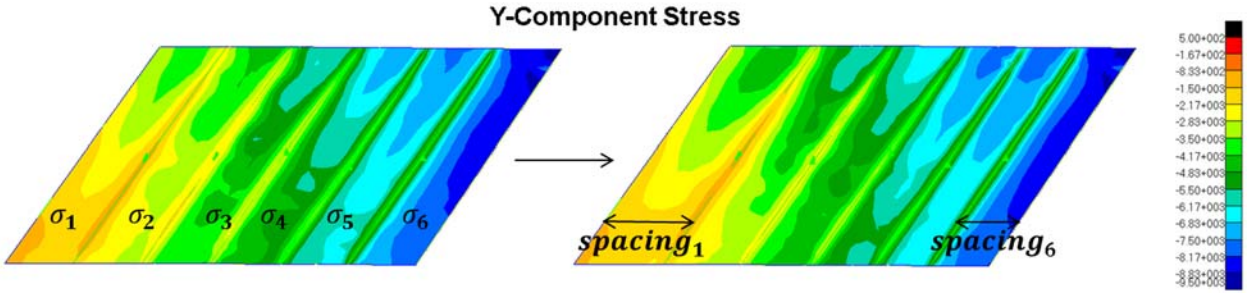

Figure 5.36: Stiffener Optimization Using Y-Component Stress

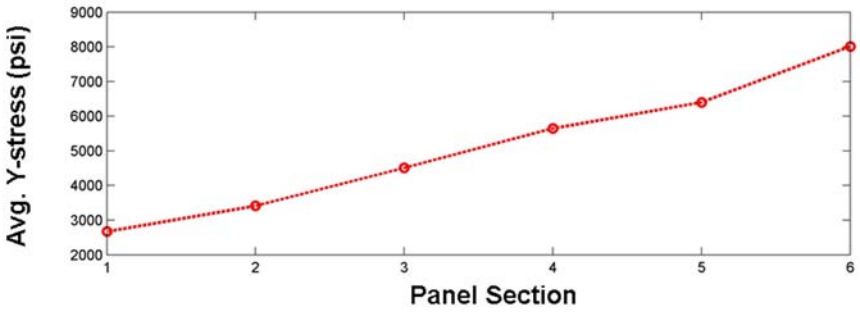

Figure 5.37: Average Y-Component Stress in Panel Sections

A stiffened panel with five evenly distributed stiffeners, which is extracted from the upper wing skin, is studied. As shown in Figure 5.36, the Y-component stress resultant distribution of the stiffened panel is computed using MSC.NASTRAN. The stiffened panel is divided into six sections by the five stiffeners. The average Y-component stress in each panel section is calculated and presented in Figure 5.37. It shows that the Y-component compressive stress in the left side of the panel is much less than the Y-component stress in the right side of the panel. According to Eq. 5.10, the panel buckling performance can be improved by reducing the stiffener spacing in the high compressive stress region. Therefore, the stiffener locations are updated using the spacing calculated by the Eq. 5.11. The right picture in Figure 5.36 shows the Y-component stress in the new stiffened panel. In that panel design, the $spacing\_1$ is about 70% greater than the $spacing\_6$. The plate thicknesses of the two stiffened panel are optimized to minimize the panel weight subject to the stress and buckling constraints. The optimal weight of the initial stiffened panel with evenly distributed stiffeners is 59.2 lbs. The optimal weight of the panel with non-uniform spacing is reduced to 53.7 lbs, or 9.3% weight reduction.

In order to compare the efficiency of different optimization schemes, three curvilinear stiffener optimization methods are compared. In the optimization scheme 1, the stiffeners are optimized

using the Eq. 5.11 in the first step. In the second step, the gradient optimization method is used to optimize the shape and size variables of the curvilinear stiffeners. The fundamental buckling mode shape of optimal stiffened panel obtained by scheme 1 is shown in Figure 5.38. In the optimization scheme 2, the stiffeners are optimized using the gradient method to minimize the panel weight. Particle swarm optimization is used in the optimization scheme 3 to optimize the shape and size variables of the stiffeners. The boundary conditions are the same in the three optimization schemes. The three optimization schemes are compared in Table 5.8. The minimum panel weight is obtained using scheme 1 at a much less computational time than the other two optimization schemes. It shows the advantage of incorporating the stress information for the stiffened panels into the optimization of curvilinear stiffeners.

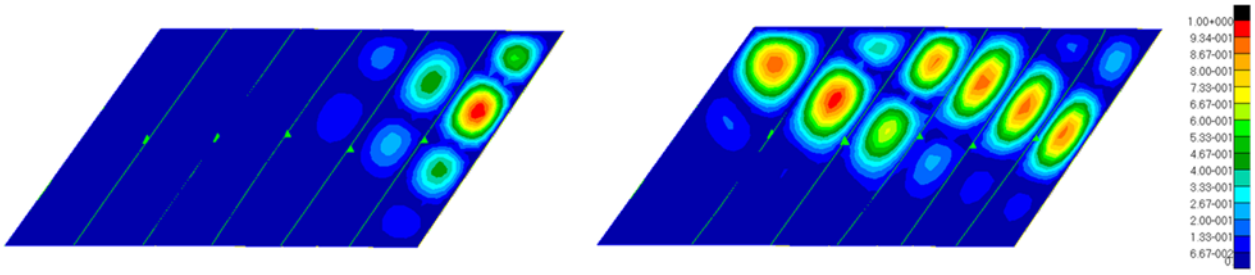

(a) Initial Panel with Evenly Distributed Stiffeners **(b) Optimized Panel using Scheme 1**

Figure 5.38: Fundamental Buckling Mode Shape of Stiffened Panel

Table 5.8: Comparison of Stiffener Optimization Schemes

	Initial Panel	Scheme 1	Scheme 2	Scheme 3
Optimal Weight (lbs)	59.2	50.7	51.6	52.4
1st Buckling Eigenvalue	1.002	1.001	1.003	1.002
CPU Time (min)	N.A.	23	65	331

5.10 Summary

A stiffened panel optimization procedure has been developed and applied to the structural design of the subsonic NASA CRM wing. Local panel optimization has been carried out for un-stiffened or stiffened panels to reduce the panel weight considering stress and buckling constraints. The results of the stiffened panel optimization have shown that the structural weight can be reduced by about 40%, compared to the results of un-stiffened panel optimization.

The interaction between global wing optimization and local panel optimization is studied to integrate the ***EBF3WingOpt*** and ***EBF3PanelOpt*** into a global-local optimization framework. The computational time of the stiffened panel optimization is reduced about 60% using an approximate panel optimization technique.

The integrated global-local optimization is implemented using a two-step approach and parallel computing. The optimization of global wing design variables and local panel design variables are integrated in the integrated global-local optimization. The minimum wing weight is observed in a CRM wing with 3 spars, 9 inner wing ribs and 17 outer wing ribs, subject to strength, buckling and flutter constraints. The optimization of stiffened panel with curvilinear stiffeners is also studied to exploit the advantage of curvilinear stiffening design. The comparison of three different optimization schemes shows that the computational time can be significantly saved by integrating the stress resultants information in the optimization process.

Chapter 6

Future Research

In this research, the optimization module ***EBF3WingOpt*** has been applied to the Boeing N+2 supersonic aircraft concept and NASA common research model. The fact that the optimal design has a significant weight reduction and all the constraints are satisfied shows the efficiency of the multidisciplinary optimization process and the advantage of the use of curvilinear *SpaRibs* and non-linear thickness fields. However, some further improvements are still required for the wing optimization. The aerodynamic loads calculation is implemented using the Doublet-Lattice method or ZONA51 method, in which the influence of thickness and viscosity is neglected. High fidelity aerodynamic and aeroelastic solutions can be obtained using CFD analysis. Considering the large amount of computational time of CFD analysis, it is not recommended to incorporate it in the computationally expensive optimization process. The CFD analysis can be used to check the multidisciplinary constraints for the optimal aircraft wing.

In the local panel optimization software package ***EBF3PanelOpt***, the size and shape design variables, which determine the panel thickness, cross-section and curvature of stiffeners, are

optimized in the stiffened panel optimization. At present, all the local panels are perfect without damages. In future, the damage tolerance of the panels with local damages (crack) will be integrated in the ***EBF3PanelOpt***.The interaction between local damages and stiffeners will be studied.

For a complex structural model, such as the Boeing HSCT wing and the NASA CRM wing, the computational cost of global-local multidisciplinary optimization is very high because of the large number of design variables and complex finite element model. The integrated global-local optimization is implemented using a two-step approach and parallel computing. The optimal number of ribs of the CRM wing is obtained in the first step optimization. The shape optimization of curvilinear spars and ribs will be carried in the second step optimization based on the optimal CRM design obtained in the first step optimization. The optimization of curvilinear stiffeners will be performed based on the optimal CRM wing with curvilinear *SpaRibs* which is obtained in the second step optimization.

The complex design space of shape variables forces the computational cost of the second step optimization to be very high. In this research, the optimization package of ***EBF3WingOpt*** and ***EBF3PanelOpt*** is developed using MATLAB and Python programming. Parallel computing can be implemented using MATLAB programming very easily. However, the maximum number of processors in the MATLAB parallel computing toolbox currently is mere *12*, which limits the potential efficiency of the application of the global-local optimization. That problem can be solved by implementing the parallel computing on multi-processor computers using Python programming. Massively parallel processing architectures Graphics Processing Units (GPU) is widely used in parallel computing. Improving the computational efficiency using GPU will also be considered in future work.

Bibliography

[1] Schmit, L. A., "Structural Design by Systematic Synthesis", *Second Conference on Electronic Computation, ASCE*, Pittsburg, 105-132, 1960.

[2] Schmit, L. A., and Ramanathan, R. K., "Multilevel Approach to Minimum Weight Design including Buckling Constraints", *AIAA Journal*, Vol. 16, No. 2, 1978, pp. 97-104.

[3] Schmit, L. A., "Structural Synthesis: Its Genesis and Development," *AIAA Journal*, Vol. 19, No. 10, 1981, pp. 1249–1263.

[4] Haftka, R. T., Starnes, J. H., Jr., Barton, F. W., and Dixon, S. C., "Comparison of Two Types of Optimization Procedures for Flutter Requirements," *AIAA Journal*, Vol. 13, No. 10, 1975, pp. 1333–1339.

[5] Haftka, R. T., "Optimization of Flexible Wing Structures Subject to Strength and Induced Drag Constraints," *AIAA Journal*, Vol. 14, No. 8, 1977, pp. 1106–1977.

[6] Starnes, J. H, and Haftka, R. T., "Preliminary design of composite wings for buckling, strength, and displacement constraints," *Journal of Aircraft*, Vol. 16, No. 8, 1978, pp. 564-570.

[7] Sobieszczanski-Sobieski, J., "Application of Computer-Aided Aircraft Design in a Multidisciplinary Environment", *Journal of Aircraft*, Vol. 11, No. 7, 1974, pp. 369-370.

[8] Miettinen, K., *Nonlinear Multiobjective Optimization*. Springer. 1999.

[9] Seeger, J. and Wolf, K., "Multi-objective Design of Complex Aircraft Structures Using Evolutionary Algorithms," *Journal of Aerospace Engineering*, October, 2011, vol. 225, No.10, 1153-1164.

[10] Mastroddi, F. and Gemma, S., "Analysis of Pareto Frontiers for Multidisciplinary Design Optimization of Aircraft", *Aerospace Science and Technology*, Volume 28, Issue 1, July 2013, 40–55.

[11] Marin, L., Trisa, D. and Badallo, P., "Optimization of Composite Stiffened Panels Under Mechanical and Hygrothermal Loads Using Neural Networks and Genetic Algorithms," *Composite Structures*, 2012, 3321-3326.

[12] Sobieszczanski-Sobieski, J., and Haftka, R. T., "Multidisciplinary Aerospace Design Optimization: Survey of Recent Developments," *Structural Optimization*, Vol. 14, 1997, pp. 1-23.

[13] Rabeau, S., Depince P., Bennis, F., and Janiaut, R., "Comparison of Global and Local Treatment for Coupling Variables into Multidisciplinary Problems", *11th AIAA/ISSMO Multidisciplinary Analysis and Optimization Conference*, No. AIAA 2006-7066, Portsmouth, Virginia, 6 - 8 September 2006.

[14] Martins, J. R. R. A., and Lambe, A. B., "Multidisciplinary Design Optimization: A Survey of Architectures", *AIAA Journal*, Vol. 51, No. 9, 2013, pp. 2049-2075.

[15] Locatelli, D., Mulani, S. B. and Kapania, R. K., "Wing-Box Weight Optimization Using Curvilinear Spars and Ribs (SpaRibs)," *Journal of Aircraft*, Vol. 48, No. 5, September-October 2011, pp. 1671–1684.

[16] Liu, S., Hou, Y., Sun, X. and Zhang, Y., "A Two-step Optimization Scheme for Maximum Stiffness Design of Laminated Plates Based on Lamination Parameters," *Composite Structures*, Vol. 94, June, 2012, pp. 3529-3537.

[17] Sobieszczanski-Sobieski, J., James, B. B., and Dovi, A. R., "Structural Optimization by Multilevel Decomposition", *AIAA Journal*, Vol. 23, No. 11, 1985, pp. 1775–1782.

[18] Sobieszczanski–Sobieski, J., "Optimization by Decomposition: A Step from Hierarchic to Non- Hierarchic Systems," *NASA Langley Research Center TR-CP-3031*, Hampton, VA, September, 1988.

[19] Ragon, S. A., Gürdal, Z., and Starnes, J. H., "Optimization of Composite Box-Beam Structures Including the Effects of Subcomponent Interaction", *AIAA/ ASME/ASCE/AHS/ASC 35th SDM Conference*, Hilton Head, SC, April 18-20, 1994.

[20] Ciampa, P. D. and Nagel, B., "Global Local Structural Optimization of Transportation Aircraft Wings," *51st AIAA/ASME/ASCE/AHS/ASC Structures, Structural Dynamics and Materials Conference*, No. AIAA-2010-3098, Orlando, Florida, 12-15 April 2010.

[21] Castellini, F., Riccardi, A., Lavagna, M., and Buskens, C., "Global and Local Multidisciplinary Design Optimization of Expendable Launch Vehicles," *52nd AIAA/ASME/ASCE/AHS/ASC Structures, Structural Dynamics and Materials Conference*, No. AIAA-2011-1901, Denver, Colorado, 4-7 April 2011.

[22] Haftka, R. T., and Watson, L. T., "Decomposition Theory for Multidisciplinary Design Optimization Problems with Mixed Integer Quasiseparable Subsystems," *Optimization and Engineering*, Vol. 7, No. 2, 2006, pp. 135–149.

[23] Dillinger, J. K. S., Abdalla, M. M., Klimmek, T., and Gurdal, Z., "Stiffness Optimization of Composite Wings with Aeroelastic Constraints", *Journal of Aircraft*, Vol.50, No. 4, 2013, pp. 1159-1168.

[24] Sobieski, I., and Kroo, I., "Aircraft Design Using Collaborative Optimization," *34th Aerospace Sciences Meeting and Exhibit*, No. AIAA-96-0715, Jan. 15-18, 1996.

[25] Braun, R., Cage, P., Kroo, I., and Sobieski., I., "Implementation and Performance issues in Collaborative Optimization," *6th AIAA/NASA/ISSMO Symposium on Multidisciplinary Analysis and Optimization*, Vol. 1, 1996, pp. 295–305.

[26] Kuhn, H. W., and Tucker, A. W., "Nonlinear programming". *Proceedings of 2nd Berkeley Symposium. Berkeley: University of California Press*, 1951, pp. 481–492.

[27] Schmit, L. A., and Chang, K. J., "Optimum Design Sensitivity Based on Approximation Concepts and Dual Methods," *International Journal for Numerical Methods in Engineering*, Vol. 20, Issue 1, pp. 39–75, January 1984

[28] Canfield, R. A., "High Quality Approximation of Eigenvalues in Structural Optimization," *AIAA Journal*, Vol. 28, No. 6, 1990, pp.1116-1122.

[29] Renner, G. and Ekárt, A., "Genetic algorithms in computer aided design," *Computer-Aided Design*, Vol. 35, Issue 8, July 2003, pp. 709-726.

[30] Venter, G. and Sobieszczanski-Sobieski, J., "Particle Swarm Optimization," *AIAA Journal*, Vol. 41, No. 8, 2003, pp. 1583–1589.

[31] Singh, G., Viana, F. A. C., Subramaniyan, A. K., Wang, L., DeCesare, D. G., Khan, G., and Wiggs, G., "Multimodal Particle Swarm Optimization: Enhancements and Applications," *12th AIAA Aviation Technology, Integration, and Operations (ATIO)*

Conference and 14th AIAA/ISSMO Multidisciplinary Analysis and Optimization Conference, No. AIAA 2012-5570, 17 - 19 September 2012, Indianapolis, Indiana

[32] Ahuja, V. and Hartfield, R. J., "Optimization of UAV Designs for Aerodynamic Performance Using Genetic Algorithms," *51st AIAA/ASME/ASCE/AHS/ASC Structures, Structural Dynamics and Materials Conference*, No. AIAA-2010-2759, Orlando, Florida, 12-15 April 2010.

[33] Venter, G. and Sobieszczanski-Sobieski, J., "Multidisciplinary Optimization of a Transport Aircraft Wing Using Particle Swarm Optimization," *9th AIAA/ISSMO Symposium on Multidisciplinary Analysis and Optimization*, No. AIAA-2002-644, Atlanta, Georgia, 4-6 Sep. 2002.

[34] Marin, L., Trisa, D., and Badallo, P., "Optimization of Composite Stiffened Panels Under Mechanical and Hygrothermal Loads Using Neural Networks and Genetic Algorithms", *Composite Structures*, 2012, 3321-3326.

[35] Zingg, D. W., Nemec, M., and Pulliam, T. H., "A Comparative Evaluation of Genetic and Gradient-Based Algorithms Applied to Aerodynamic Optimization," *European Journal of Computational Mechanics*, Vol. 17, Nos. 1–2, Jan. 2008, pp. 103–126.

[36] Plevris, V. and Papadrakakis, M., "A Hybrid Particle Swarm—Gradient Algorithm for Global Structural Optimization," *Computer-Aided Civil and Infrastructure Engineering*, Vol. 26, Issue 1, 48–68, January 2011.

[37] Hajikolaei1, K. H., Safari, A., Wang, G. G., and Lemu, H. G., "Surrogate-assisted Self-accelerated Particle Swarm Optimization", *10th AIAA Multidisciplinary Design Optimization Conference*, January 2014, National Harbor, Maryland.

[38] Goel, T., Vaidyanathan, R., Haftka, R. T., Shyy, W, Queipo, N. V., and Tucker, K., "Response Surface Approximation of Pareto Optimal Front in Multi-objective Optimization," *Computer Methods in Applied Mechanics and Engineering*, Vol. 196, Issues 4–6, 1 Jan. 2007, pp. 879-893

[39] Sunny, M. R., Mulani, S. B., Sanyal, S., Pant, R. S. and Kapania, R. K., "An Artificial Neural Network Residual Kriging Based Surrogate Model for Shape and Size Optimization of a Stiffened Panel," *54th AIAA/ASME/ASCE/AHS/ASC Structures, Structural Dynamics and Materials Conference*, No. AIAA-2013-1689, Boston, Massachusetts, 8-11 April, 2013.

[40] Box, G. E. P. and Wilson, K.B., "On the Experimental Attainment of Optimum Conditions". *Journal of the Royal Statistical Society* Series B13 (1), pp. 1–45.

[41] Liu, B., Haftka, R. T., and Watson, L. T., "Global-local Structural Optimization Using Response Surfaces of Local Optimization Margins", *Structural Multidisciplinary Optimization*, Volume 27, 2004, pp. 352–359.

[42] Paiva, R. M., Crawford, C., and Suleman, A., "Robust and Reliability-Based Design Optimization Framework for Wing Design," *AIAA Journal*, Vol. 52, No. 4, pp. 711-724.

[43] Jones, D. R., "A Taxonomy of Global Optimization Methods Based on Response Surfaces," *Journal of Global Optimization*, 21: 345–383, 2001

[44] Chandila, P. K., Agarwal, H., and Renaud, J. E., "An Effcient Strategy for Global Optimization Using Local Kriging Approximations," *45th AIAA/ASME/ASCE/AHS/ASC Structures, Structural Dynamics & Materials Conference*, 19 - 22 April 2004, Palm Springs, California.

[45] Shimizu, Y. and Kawamoto, H., "An Implementation of Parallel Computing for Hierarchical Logistic Network Design Optimization Using PSO," *Computer Aided Chemical Engineering*, Vol. 25, 2008, pp. 605-610.

[46] Mussi, L., Daolio, F., and Cagnoni, S., "Evaluation of Parallel Particle Swarm Optimization Algorithms within the CUDA™ Architecture," *Information Sciences*, Vol. 181, Issue 20, 15 October 2011, pp. 4642-4657.

[47] Lundquist, E. E. and Stowell, E. Z., "Critical Compressive Stress for Flat Rectangular Plates Supported Along All Edges and Elastically Restrained Against Rotation Along the Unloaded Edges", Report 733, National Advisory Committee for Aeronautics.

[48] Timoshenko, S., Theory of Elastic Stability, McGraw-Hill Book Company, 1936.

[49] Vescovini, R. and Bisagni, C., "Buckling Analysis and Optimization of Stiffened Composite Flat and Curved Panels", *AIAA Journal*, Vol. 50, No. 4, April 2012, pp. 904-915.

[50] Block, D., Card, M., and Mikulas, M., "Buckling of Eccentrically Stiffened Orthotropic Cylinders", *NASA TN D-2960*, Aug. 1965.

[51] Megson, T. H. G., *Aircraft Structures for Engineering Students*, Arnold, 1999.

[52] Ratzersdorfer, J., "Rectangular Plates with Stiffeners: The Buckling of Simply Supported Plates under Compressive Stress", *Aircraft Engineering and Aerospace Technology*, Volume 14, Issue 9, 1942, pp. 260-264.

[53] Gerard, G., *Introduction to Structural Stability Theory*, McGraw-Hill Book Company, New York, 1962.

[54] Mittelstedt, C., "Closed-form Analysis of the Buckling Loads of Uniaxially Loaded Blade Stringer-stiffened Composite Plates Considering Periodic Boundary Conditions", *Thin-Walled Structures*, Vol. 45, No. 4, April 2007, pp. 371-382.

[55] Coburn, B. H., Wu, Z., and Weaver, P. M., "Local Buckling of Blade Stiffened Variable Angle Tow Panels," *55th AIAA/ASMe/ASCE/AHS/SC Structures, Structural Dynamics, and Materials Conference*, 13-17 January 2014, National Harbor, Maryland.

[56] Loos, A. C. and MacRae, J. D., "A Process Simulation Model for the Manufacture of a Blade-Stiffened Panel by the Resin Film Infusion Process," *Composites Science and Technology,* Vol. 56, Issue 3, 1996, pp. 273–289.

[57] Herencia, J. E., Weaver, P. M., and Friswell, M. I., "Optimization of Long Anisotropic Laminated Fiber Composite Panels with T-Shaped Stiffeners," *AIAA Journal*, Vol. 45, No. 10, 2007, pp. 2497–2509.

[58] Williams, J. and Stein, M., "Buckling Behavior and Structural Efficiency of Open-section Stiffened Composite Compression Panels," *AIAA Journal*, Vol. 14, May 1976, pp. 1618-1626.

[59] Bisagni, C. and Vescovini, R., "Fast Tool for Buckling Analysis and Optimization of Stiffened Panels," *Journal of Aircraft*, Vol. 46, No. 6, 2009, pp. 2041–2053.

[60] Vitali, R., Park, O., Haftka, R. T., and Sankar, B. V., "Structural Optimization of a Hat-Stiffened Panel Using Response Surfaces," *Journal of Aircraft*, Vol. 39, No. 1, 2002.

[61] Bedair, O., "Analysis and Limit State Design of Stiffened Plates and Shells: A World View," *Applied Mechanics Reviews*, Vol. 62, No. 2, 2009, pp. 16.

[62] Jaunky, N., Knight, N. F., and Ambur, D. R., "Optimal Design of Grid-Stiffened Composite Panels Using Global and Local Buckling Analyses," *Journal of Aircraft*, Vol. 35, No. 3, 1998, pp. 478–486.

[63] Dang, T. D., Kapania, R. K., Slemp, W. C. H., Bhatia, M. and Gurav, S. P., "Optimization and Postbuckling Analysis of Curvilinear-Stiffened Panels Under Multiple-Load Cases," *Journal of Aircraft*, Vol. 47, No. 5, September–October 2010, pp. 1656-1671.

[64] Zheng, Y. and Dasb, P. K., "Improved Response Surface Method and its Application to Stiffened Plate Reliability Analysis," *Engineering Structures*, Vol. 22, Issue 5, May 2000, pp. 544–551.

[65] Walch, D., Tetreault, S. and Dervault, F., "Smeared Stiffeners in Panel for Mesh Simplification at Conceptual Design Phase", *54th AIAA/ASME/ASCE/AHS/ASC Structures, Structural Dynamics and Materials Conference*, No. AIAA-2013-1809, Boston, Massachusetts, 8-11 April 2013.

[66] Locatelli, D., Mulani, S. B., and Kapania, R. K., "A Multidisciplinary Analysis Optimization Environment for Wings Having SpaRibs", *53rd AIAA/ASME/ASCE/AHS/ASC Structures, Structural Dynamics and Materials Conference*, Honolulu, Hawaii, 23 - 26 April 2012.

[67] Mulani, S. B., Locatelli, D., and Kapania, R. K., "Algorithm Development for Optimization of Arbitrary Geometry Panels using Curvilinear Stiffeners," *51st AIAA/ASME/ASCE/AHS/ASC Structures, Structural Dynamics and Materials Conference*, No. AIAA-2010-2674, Orlando, Florida, 12-15 April 2010.

[68] Nicholas, E. D., "Developments in the Friction-Stir Welding of Metals," *ICAA-6: 6th International Conference on Aluminium Alloys*, 1998.

[69] Caseiro, J. F., Valente, R.A.F., Andrade-Campos, A. and Yoon, J. W., "On the elasto-plastic buckling of Integrally Stiffened Panels (ISP) joined by Friction Stir Welding (FSW): Numerical simulation and optimization algorithms," *International Journal of Mechanical Sciences*, Vol. 76, November 2013, pp. 49–59.

[70] Taminger, K. M. B. and Hafley, R. A., "Electron Beam Freeform Fabrication: A Rapid Metal Deposition Process", *Proceedings of 3rd Annual Automotive Composites Conference*, 9-10 Sept. 2003, Troy, MI. Society of Plastics Engineers, 2003.

[71] Locatelli, D., Liu, Q., Tamijani, A. Y., Mulani, S., and Kapania, R. K., "Multidisciplinary Optimization of Supersonic Wing Structures Using Curvilinear Spars and Ribs (SpaRibs)", *54th AIAA/ASME/ASCE/AHS/ASC Structures Conference*, Boston, Massachusetts, April 8-11, 2013.

[72] Mulani, S. B., Slemp, W. C. H. and Kapania, R. K., "EBF3PanelOpt: An Optimization Framework for Curvilinear Blade-Stiffened Panels", *Thin-Walled Structures*, Vol. 63, 2013, pp. 13-26

[73] Mulani, S. B., Locatelli, D. and Kapania, R. K., "Grid-Stiffened Panel Optimization using Curvilinear Stiffeners", *52th AIAA/ASME/ASCE/AHS/ASC Structures, Structural Dynamics and Materials Conference*, No. AIAA-2011-1895, Denver, Colorado, 4-7 April 2011.

[74] Bhatia, M. and Kapania, R. K., "Stiffener Effectiveness Approach for Optimal Stiffener Placement on Curvilinear Stiffened Panel", *50th AIAA/ASME/ASCE/AHS/ASC Structures, Structural Dynamics and Materials Conference*, No. AIAA-2009-2640, Palm Springs, California, 4-7 April 2009.

[75] Albano, E. and Rodden, W. P., "A Doublet_Lattice Method for Calculating Lift Distributions on Oscillating Surfaces in Subsonic Flows," *AIAA Journal*, Vol. 7, NO. 2, February 1969, pp. 279-285.

[76] Rodden, W. P., Giesing, J. P., and Kalman, T. P., "Refinement of the Nonplanar Aspects of the Subsonic Doublet-Lattice Lifting Surface Method," *Journal of Aircraft*, Vol. 9, NO. 1, January 1972, pp. 69-73.

[77] Chen, P. C. and Liu, D. D., "A Harmonic Gradient Method for Unsteady Supersonic Flow Calculations," *Journal of Aircraft*, Vol. 22, No. 15, May 1985, pp. 371-379.

[78] *MSC Nastran Version 68, Aeroelastic Analysis User's Guide*, MSC.Software Corporation, 2010.

[79] Strong, D. D., Kolonay, R. M., Huttsell, L. J., and Flick, P. M., "Flutter Analysis of Wing Configurations Using Pre-Stressed Frequencies and Mode Shapes," *46th AIAA/ASME/ASCE/AHS/ASC Structures, Structural Dynamics & Materials Conference*, No. AIAA 2005-2173, Austin, Texas, 18 - 21 April 2005

[80] Locatelli, D., Mulani, S. B., and Kapania, R. K., "Parameterization of Curvilinear Spars and Ribs (SpaRibs) for Optimium Wing Structural Design," *53rd AIAA/ASME/ASCE/AHS/ASC Structures, Structural Dynamics and Materials Conference*, Honolulu, Hawaii, April 23-26 2012.

[81] Schumaker, L. L., *Spline Functions: Basic Theory*, Cambridge Mathematical Library, 2007.

[82] "N+2 Supersonic Concept Development and System Integration", Technical Report, Contract NNL08AA16B, Submitted by Boeing Company, Final Draft, July 2009

[83] Chen, D., Britt, R. T., Roughen, K., and Stuewe, D. "Practical Application of Multidisciplinary Optimization to Structural Design of Next Generation Supersonic

Transport", *13th AIAA/ISSMO Multidisciplinary Analysis Optimization Conference*, 13-15 September 2010, Fort Worth, Texas.

[84] Locatelli, D., *Optimization of Supersonic Aircraft Wing-Box Using Curvilinear SpaRibs*, Ph.D. thesis, Virginia Polytechnic Institute and State University, 24061, Blacksburg, VA, 2012.

[85] Kreisselmeier, G. and Steinhauser, R., "Systematic Control Design by Optimizing a Vector Performance Index," *Proceeding IFAC Symposium on Computer-aided Design of Control Systems*, Zurich, Switzerland; 1979. pp. 113–7.

[86] Vassberg, J., DeHaan, M., Rivers, S., and Wahls, R., "Development of a Common Research Model for Applied CFD Studies", *AIAA Applied Aerodynamics Conference*, Honolulu, HI, August, 2008.